FIELD AND LABORATORY STUDY OF THE FLÁAJÖKULL GLACIER, ICELAND

by

William R. Jacobson Jr.

A Dissertation Submitted in

Partial Fulfillment of the

Requirements for the Degree of

Doctor of Philosophy

in Geosciences

at

The University of Wisconsin-Milwaukee

December 2015

ABSTRACT

FIELD AND LABORATORY STUDY OF THE FLÀAJÖKULL GLACIER, ICELAND

by

William R. Jacobson, Jr.

University of Wisconsin-Milwaukee, 2015
Under the Supervision of Professor Thomas Hooyer and Professor John Isbell

The increased surface melting of the outlet glaciers of the Vatnajökull Ice Cap has a profound affect on the dynamics of the ice-bed couple and landform genesis. Soft-bedded glaciers are largely inaccessible, which creates a problem. One challenge is to understand the complex interactions of the glacier bed and its resultant depositional and deformational landform systems. This study investigates an outlet glacier from the Vatnajökull Ice Cap, described herein as the Fláajökull glacier system. To circumvent some of these problems, three separate projects were conducted in this dissertation: (1) magnetic fabric study of effective pressure (difference between the ice-overburden pressure and pore-water pressure) and shear rate (glacier velocity) using a laboratory ring-shear device; (2) glaciological analysis of magnetic fabrics and c-axis orientations of dirty ice veins; and (3) investigation of drumlin formation using magnetic till fabrics and field relationships. Several hypotheses were addressed for each of these studies, which include: (1) to determine if fabric strength is independent of shear rate and effective pressure. This hypothesis was tested and the results confirmed that the fabric strength (S_1 eigenvalue) was independent of shear rate and effective pressure. Based on these results, effective pressure and shear rate cannot be interpreted from fabric strength evidence from glacial deposits; (2) in the glaciological study, I hypothesized that the dirty ice veins were sub-vertically sheared from the bed near the ice front, but then moderately deformed. Results from the

magnetic fabrics indicate that the maximum K_1 susceptibility axis (77º plunge) is approximately parallel to the vein margins verify that the injection was sub-vertical. The long axes of the recrystallized ice grains (parallel to foliation plane defined by K_1 - K_2) appeared to show a good correlation with the plunge of the maximum K_1 susceptibility. Also, the eigenvector plunge of the c-axes was approximately normal to the shear plane, which supports previous theory that c-axes rotate away from the shear plane toward the vertical. Multi-maximum girdle fabrics from the c-axes and associated textures from thin sections (e.g. nucleated grains, bulging of grain boundaries and slips band) suggest that some deformation likely occurred after emplacement; and (3) the Boulton hypothesis was tested using magnetic till fabrics and field relationships. According to this idea, drumlins form due to hydrologic heterogeneity (permeability differences in granular materials) causing a solid nucleus to form in the bed where sediment is accreted and sheared in the direction of ice flow. At Fláajökull, the magnetic fabrics from sites B and C mimicked the glacier flow direction with the longitudinal flow plane (K_1 - K_3) approximately parallel to the NNW-SSE drumlin long axis. The drumlin cores consisted of outwash sand and gravels which likely acted as rigid obstacles in the bed. Ice overriding resulted in heterogeneous deformation of the drumlin cores following the deposition of the upper basal till carapace. These results support the Boulton hypothesis.

These studies demonstrate significant progress toward understanding fabric strength development of soft-bedded glaciers. In linking studies (1) and (3) the ring-shear device was used to provide insights into fabric strength development upon shear rate and effective pressure. In the third study previous ring-shear experiments, magnetic till fabrics and field relationships were used to understand modern drumlin genesis.

TABLE OF CONTENTS

LIST OF FIGURES

LIST OF TABLES

ACKNOWLEDGEMENTS

I would like to express my gratitude to Dr. Thomas Hooyer for his helpful suggestions during the completion of this dissertation. A portion of this project was supported through Dr. Hooyer's start-up funds, Geological Society of America and the Department of Geosciences at UWM. I would also like to thank the committee members Dr. Richard Alley (Penn State University), Dr. John Isbell, Dr. William Kean, Dr. Dyanna Czeck, and Dr. Rani Elhajjar for critically reading the dissertation and providing helpful comments. In addition, I thank Dr. Richard Alley for his continuing support and mentorship in the absence of Dr. Thomas Hooyer, due to a serious medical condition.

This project could not have been completed without the hospitality of the people of Iceland. I thank Kjarton Màsson for his kind discussions and his logistical support for transporting dry ice from Reykjavik to Höfn. I also greatly appreciate the Vatnajökull Hotel for utilizing their freezer for accommodating the ice core specimens. In addition, I would like to thank Ivàr Benediktsson for his helpful suggestions.

Over the duration of this project both field and laboratory work was undertaken. I would like to give special thanks to the Health Care Division at *General Electric (GE)* and the Institute of Rock Magnetism (IRM) at the University of Minnesota for use of their laboratories. I thank Mark Woodford at *GE* and Julie Bowles at the IRM. Furthermore, I am extremely grateful for my two field assistants, James Amato and Emily Joynt. This work could not have been done without their hardworking and relentless efforts while conducting field work in Iceland.

CHAPTER 1: INTRODUCTION

The dynamics of the glacier bed (defined here as a soft bed) has important implications for sediment transport and the creation of various landforms, including drumlins, eskers, crevasse-squeeze-ups and moraines. The overlying ice near the glacier bed may creep (e.g. ice grains move under their own weight due to gravity), but a large proportion of the movement occurs in the underlying substrate. Ice can also decouple from its bed and slide along a pressurized film of meltwater (Hooke et al., 1997). The complexity of the ice/bed interface is affected by many factors but the effective pressure is of primary importance because it controls the shear strength of the till (Clarke, 2005).

One overarching problem is our understanding of the coupled ice dynamics and glacial depositional and deformational landform systems. Observations of soft-bedded glaciers are largely inaccessible; although some opportunities have been made in subglacial tunnels (e.g. Boulton at Breiðamerkurjökull, Iceland) and along ice-margins. Limited exposure of this environment ultimately has hampered progress.

Modeling deformations in the laboratory is an alternative (e.g. using a ring-shear apparatus) vehicle for understanding processes at the glacier bed. Two salient variables examined in this dissertation include: effective pressure (difference between the ice-overburden pressure minus the pore-water pressure) and shear rate (glacier velocity) upon magnetic particle fabrics. These variables were analyzed using anisotropy of magnetic susceptibility (AMS) technique. One important hypothesis that was tested in these experiments was: Will an increase in the effective pressure affect the critical state porosity and constrain particle rotation causing the K_1 fabric strength to increase. Hypothesis two relates to the shear rate. I hypothesized that the K_1 fabric strength might increase monotonically with glacier velocity suggesting a possible

dependence on the shear rate. These experimental tests are described more thoroughly in Chapter 2.

In chapter 3 AMS and c-axis fabrics were applied to samples collected from dirty ice veins on the glacier margin. Based on the vein characteristics and field relationships and comparisons to other studies (Ensminger et al., 2001; Lovell et al., 2015), the debris was likely injected from the bed near the ice front, but then moderately deformed. This hypothesis is supported by the magnetic and c-axis fabric data which are included in this dissertation.

In chapter 4 the Boulton hypothesis of drumlin formation was tested on the drumlins at Fláajökull. According to the Boulton hypothesis, the fabric within the drumlin carapace should mimic the direction of sediment deformation with a strong fabric throughout the drumlin with a potentially weak fabric defining the core. This hypothesis was tested and the fabrics were interpreted using results from ring-shear experiments (Hooyer et al., 2008).

In the following sections I will discuss soft bed deformation and experimental work using the ring-shear device, drumlin formation, and the physical properties of ice related to creep or deformation.

1.1 Soft bed deformation beneath glaciers

For some time it has been known that glaciers can shear their basal sediments resulting in increased glacier flow rates and sediment transport (MacClintock and Dreimanis, 1964). It has also been suspected that shearing of basal sediments leads to a preferred orientation of debris or a fabric in that sediment (Harrison, 1957; Evenson, 1971). Sheared fabrics have been recognized through field investigation and experimental work (Benn, 1995; Larsen and Piotrowski, 2003; Shumway and Iverson, 2009; Gensoto, et al., 2011) using a variety of

techniques including measuring clast and sand particle orientations and the use of magnetic fabrics. Many of these methods have confirmed the same general conclusion: Particles align parallel to the direction of shear and plunge mildly upglacier (Gensoto, et al., 2011).

Other than studying sheared glacial fabrics, it is also important to study the boundary conditions at glacier beds. It is imperative to investigate conditions at glacier beds because of global climate warming. Climate warming may cause instability in glacier flow which could lead to changes in sea-level-rise. Mechanisms of glacier movement have been based on numerous measurements (e.g. tilt meters and transducers) of glacier beds obtained through boreholes (Blake et al., 1997; Kamb, 2001). The accuracy of these measurements is somewhat limited by range of the instruments and positioning within the bed geometry making deformation extrapolations difficult. Glacier movement may result from a combination of processes (e.g. internal ice deformation, sliding along the ice/bed interface, ploughing of particles gripped in the ice also referred to as lodgement, and deformation of the bed which may be either fault-like or pervasive shear) (Fig. 1). The activation of these mechanisms is modulated by the water pressure between the ice and the till bed. Hook et al. (1997) found that decreases in the water pressure (higher effective stresses) increased the coupling between the glacier and the bed whereas increased water pressures (lower effective stresses) weakened the coupling between the glacier and the bed, allowing the glacier to move over the bed faster while deforming the bed less. Measurements were collected from tilt meters embedded in the till and water pressures were measured from boreholes and within the till. The surface velocity of the glacier was also recorded from frequent surveys of a stake network (Hooke et al., 1997).

In addition to collecting field measurements on bed deformation and or sliding, these processes can be modeled through experimentation. Explicitly these studies may focus on debris

entrainment within the basal ice and its impact on sliding and bed erosion (Byers et al., 2002; Emerson, 2007; Iverson and Petersen, 2011; Zoet and Iverson, 2015). Empirical relationships for estimating sliding speed, basal drag, effective pressure and ice/bed separation is achieved by shearing a ring of ice over a sinusoidal bed with a mechanical device. Zoet and Iverson (2015) found an important relationship indicating that drag (e.g. resistance from bed obstacles) decreases up to 50% at steady glacier speeds (up to 350 m $year^{-1}$) if cavity formation on the lee side of an obstacle covers 93% of the bed. This drag relationship is not accounted for in ice-sheet models and has implications for changes in glacier boundary conditions driven by climate variability (e.g. decreases in effective pressure due to surface melt-water input), which may increase glacier sliding speeds. With the introduction of new technology, simulation of glacier bed dynamics will be modeled more accurately through empirical relationships.

1.2 Experimental studies of soft bed deformation

Laboratory ring-shear experiments have been used most commonly to model soft bed deformation (Iverson et al., 1997). Most of these experiments have focused on basal sediment related to glacier flow (Iverson, 1999); grain fracturing (Hooke and Iverson, 1995), diffusive mixing between till contacts (Hooyer and Iverson, 2000a), and more recently magnetic fabric characterization (Iverson et al., 2008).

Experimental studies of magnetic fabric strength with the ring-shear device were used as a basis for shear strain estimates on basal tills from the geologic record; however, only within the shear strain window of 7-25 (Hooyer et al., 2008). Application of ring-shear results to field situations are problematic because quantitative knowledge of shear strain at most field sites is

always poorly known, and the exact processes that formed the basal till are ambiguous, making it difficult to estimate glacier motion and strain in the bed.

Clarke (2005) suggested that glacial investigators have inferred that the fabric strength of a till decreases with increasing cumulative strain. Hooyer and Iverson (2000) disproved this conjecture by experimentation using magnetic particle fabrics with the ring-shear apparatus. They found that shearing actually strengthens the particle fabric at shear strains of 7-30; however, once a steady state is achieved shear strain is no longer viable for interpreting fabric (Fig. 2).

One criticism of the magnetic fabric work described in Figure 2 is that the fabric strength might vary as a function of ice thickness (effective pressure) and shearing rate. To test this hypothesis, we performed ring-shear experiments in order to isolate the effects of the effective pressure (ice load minus the bed porewater pressure) and shearing rate on fabric development.

Ring-shear experiments have been useful for modeling fabric at the glacier bed; however Hart (2009) proposed that these experiments do not accurately model the glacier bed. Hooyer et al. (2008) strongly advocated "that we are not attempting to simulate the natural system which is most likely impossible, but simplifying the system whereby we can observe the effect of individual parameters while controlling other variables."

1.3 Magnetic Fabrics-Anisotropy of Magnetic Susceptibility (AMS)

Anisotropy of magnetic susceptibility is an important technique which depicts preferred orientation of magnetic minerals in unconsolidated sediments and or rocks. In this dissertation, however, it was applied to temperate glacial ice and glacial sediments. The AMS technique determines the three-dimensional state of strain, fabric strength and direction from the magnetic

ellipsoids. The technique provides an excellent spatial resolution because of its averaging effect of many magnetic grains compared to traditional fabric techniques where only the long axis of clasts are measured in outcrop with a compass. As discussed by Hooyer et al. (2008), in deformed sediments such ellipsoids commonly arise from the shaped-preferred orientations of magnetite, maghemite or other strongly magnetic particles which have magnetic fields aligned with their shape elongations.

1.4 Drumlin formation

Drumlins are prominent landforms in glacial landscapes and cover between 15 to 70% of the terrain in Canada, Ireland, Scandinavia, and Britain (Knight, 2010). Drumlins are tear-dropped shaped landforms that form beneath the ice and typically have a long axis that is parallel to the ice flow direction. Even though hundreds of papers have been written about drumlins, there has been a lack of definitive hypotheses for their genesis simply because they form hidden from view tens to hundreds of meters beneath the ice. Many ideas have been proposed about drumlin genesis. One of the more popular ideas is that of Boulton (1987) who suggested that drumlins may form where the effective normal stress (ice load minus the bed porewater pressure) is high, which strengthens the sediment and inhibits deformation (Fig. 3). These areas of strong till form the nucleus of a drumlin where sediment is subsequently accreted and sheared in the prevailing direction of ice flow. Sediment is eroded between drumlins, where presumably the effective stress is low. Hydrologic heterogeneity in the sediment allows the drumlins to nucleate where the sediment is strong. Drumlins are important because they have been used to infer bed conditions and flow dynamics of former glaciers and ice streams.

Another idea for the formation of drumlins is motivated by their association with

longitudinal crevasses. This has been recently observed at a small valley glacier named Mùlajökull in Iceland (Johnson et al., 2010). Johnson et al. hypothesized that deviations in effective normal stress under and between the crevasses would have caused differences in erosion at the glacier bed. For example, areas under the crevasses would have a lower effective normal stress (higher pore water pressure) due to the smaller ice mass there. In this case a lower effective normal stress protects the bed from erosion by preventing ice from infiltrating into the sediment during basal sliding, which is thought to be the primary mechanism of glacier motion at Mùlajökull. In between the drumlins; however, the effective normal stresses would be higher (greater mass) resulting in a stronger ice/bed coupling and hence greater erosion. Drumlins would then be erosional remnants of a preexisting till layer.

Finally, drumlin growth may be effected by crevasse development at the glacier bed. This was documented by Sharp (1985) where till was squeezed upward into the fractures at the base of the ice at Eyjabakkajökull, Iceland. This process is driven by pressure gradients in the till whereby the till is squeezed into areas of lower pressure. Evidence of this is based on diapir-like structures within drumlin cores (Stanford and Mickelson, 1985). Despite these and many other ideas not presented herein, it is still unclear how drumlins form.

1.5 Physical properties of ice

This section gives a brief discussion on the literature on deformation or creep of ice. Here I discuss important terms such as *basal plane*, *c-axis*, *dislocation*, and *creep*. I will introduce the flow law for ice and some of its flaws as well as improvements. Additionally, I will briefly discuss ice crystal fabrics and their potential link to climate (Diprinzio et al., 2005).

1.5.1. Ice crystal structure

The water molecule consists of one oxygen and two hydrogen atoms. Our attention will focus on terrestrial ice, ice Ih (known as ice-phase-one) because it is stable within the pressures and temperatures within glaciers found on earth. The other eight forms of ice are stable only at pressures in excess of about 200 MPa which are not achieved under glacial conditions and therefore will not be considered here (Hooke, 2005). The crystal structure of ice Ih viewed normal to the c-axis is shown in Figure 4. A tetrahedron is formed when each oxygen atom is surrounded by four other oxygen atoms. This tetrahedron is joined in a manner that the hexagonal rings form with the two oxygen bonds migrating slightly up and down around the hexagonal ring (Fig. 5). The plane of these rings is defined as the basal plane (0001) of the crystal structure. The axis normal to the basal plane is referred to as the c-axis.

1.5.2 Polycrystalline ice

Ice is a marvelous material due to its plastic behavior. Different types of ice may form depending on its environment. For example, ice at the base of an ice sheet is distinctly different from the overlying ice and may range from 0.2 m at Breiðamerkurjökull, Iceland to >70 m at Thule, Greenland. The overlying ice is a product of the firnification process (pressure burial of successive snow layers) and is generally cleaner whereas ice at the base is dirty and contains more chemical solutes and gases due to its interaction with the bed (Hubbard and Sharp, 1989). On the other hand, dirty ice may also form by injection of debris-laden water within a crevasse at the glacier bed (Bennett et al., 2000; Ensminger et al., 2001).

Ice is an assemblage of many crystals, known as a polycrystal. The orientation of ice grains (c-axes) in a polycrystal is termed *fabric*. The grain size and shape (*texture*) are also used

to infer the stress state of the polycrystal and the *microstructure* refers to the grain boundary network. The grain size varies from tenths of millimeters up to several centimeters in diameter. Other authors have pointed out (Durand et al., 2006; Eichler, 2013), that no terminology convention exists for the use of *texture*, *fabric* and *microstructure* in crystalline ice. In materials science or geology these expressions (*texture*, *fabric*, and *microstructure*) may refer to different features.

1.5.3 Glen's flow law

Glen (1955) described a constitutive relationship for the deformation of polycrystalline ice. He described the behavior of ice as a non-linear viscous fluid. The following relationship was experimental derived in the laboratory and is called *Glen's flow law*:

$$\dot{\gamma} = A\tau^n$$

$\dot{\gamma}$ - strain rate

A - fluidity, depending on temperature, impurity content, crystal orientation, revised as the strain rate enhancement factor *E*.

τ - shear stress

n - stress exponent, typically varies from 1 to 3.

Glen's creep experiments were formulated at stresses 10^2 and 10^3 times higher than those in nature. These experiments did not address any micro-related processes (e.g. subgrain rotation and migration recrystallization), which are important when attempting to model the system accurately. Thus, a current challenge in glaciology is to develop a constitutive flow law that incorporates recrystallization processes under natural ice conditions (Eichler, 2013).

1.5.4 Recrystallization

Recrystallization occurs in all crystalline materials, e.g. rocks, glaciers as well as in metals. Recrystallization during deformation is referred to as dynamic recrystallization. Poirier (1989) emphasized two types of recrystallization processes: subgrain rotation recrystallization and migration recrystallization.

1.5.5. Subgrain rotation recrystallization

Subgrain rotation recrystallization (also polygonization) involves the formation of new grain boundaries resulting from the subdivision of older grains. This occurs when a stress is applied to an ice grain. This process is depicted in Figure 6. These new neighboring grains have a small angle of misorientation; however, high angles may develop with progressive stress. As indicated by Cuffey and Paterson (2010) polygonization may have little effect on c-axis fabrics with only slight deviations probably in the range of ±5 degrees between neighboring grains. Figure 7 shows an example of a thin section undergoing subgrain rotation recrystallization.

1.5.6. Migration recrystallization

Migration recrystallization is an important mechanism in fabric development and is common in many temperate glaciers. This style of recrystallization is associated with high temperature (close to the melting point, T> -12° C) which allows the nucleation of new, strain-free grains (low density of defects) and the rapid migration of grain boundaries (Schulson and Duval, 2009). These boundaries migrate because of the differences in free energy (Gibbs energy) between crystals (Schulson and Duval, 2009) resulting from their curved boundaries (pressure difference). The primary fabrics are destroyed while the strain-free grains form to the

new stress and strain regime (Petersen, 2012). These new strain free grains typically have large orientation gradients near their grain boundaries and often exhibit a c-axis girdle or multi-clustered pattern (Alley, 1995, Diprinzio et al., 2005). An example of migration recrystallization is shown in Figure 8.

1.5.7. Microinclusions and soluble impurities

Grain growth and migration of boundaries may be inhibited by the presence of solid inclusions (microparticles) and soluble impurities. The concentration of debris and soluble impurities significantly impacts the mechanical properties, recrystallization, grain growth, electrical conductivity, and fabric development in ice (Paterson, 1991, Budd and Jacka, 1989, Song et al., 2008, Taylor, 1992). The microstructural properties of the ice have been used to infer patterns of deformation and provide clues to paleoclimate (Faria et al., 2010). In addition, fabric measurements provide inputs for ice flow laws (Thorsteinsson et al., 1999) and for testing fabric models (Alley, 1988; Faria et al., 2003).

The data within this dissertation pertain to the effect of the insoluble particles on the physical properties of ice and its influence on fabric. The chemical component (soluble ions such as Na^+, Cl^-) was not inspected.

1.5.8 Creep of polycrystalline ice

Plastic deformation of an ice body under the influence of stress is referred to as *creep*. Even under the application of very low stress, single ice crystals can deform plastically. Creep is characterized by the movement of dislocations (migration of linear defects) within a crystal lattice. Movement may occur along grain boundaries or within individual crystals. Dislocations

are linear defects or imperfections that develop during crystal growth or develop when crystals are stressed (Poirier, 1985).

Two fundamental linear defects are edge and screw dislocations (Figure 9). In dislocation theory, a Burgers vector (represents the magnitude and direction of a distortion in the crystal lattice) is often used to describe the path of these dislocations (Weertman and Weertman, 1992). Migration of these defects ultimately causes slip of the two parts of the lattice against each other causing deformation. Grain boundaries have been shown to restrict the propagation of dislocations and hence creep (Richeton et al., 2005b). Most ice creep occurs along the basal plane (dislocation glide) however, non-basal (prismatic) slip has been reported (Duval et al., 1983). The coefficient of resistance along the non-basal planes is ~60 times higher than on the basal planes.

New experimental investigations on ice plasticity have also revealed that dislocation avalanches, resulting from dislocation "pile ups" (impediment of dislocations at grain boundaries), are fundamental to understanding the development of stress heterogeneities inside grains and the polycrystal (Duval et al., 2010). Furthermore, the study of ice rheology and structure has helped parameterize models of glacier flow. According to Alley et al. (1992) there may not be a simple flow rule that can characterize deformation of ice in glaciers. This assertion largely stems from the fact that deformation processes compete against each other such as dislocation glide (basal slip), dislocation climb and grain boundary diffusion; this presents a problem with predicting a given process under certain ice conditions.

Ice exhibits three stages of creep: an initial decelerating primary creep, a stationary secondary creep and finally a tertiary steady state creep. Figure 10 shows a typical creep curve for polycrystalline ice under a constant stress (Petrenko and Whitworth, 1999). One ongoing

problem with creep experiments is that it is difficult to reach steady state (tertiary stage) because of the long time scales necessary, which are difficult to attain in the laboratory (century to millennia).

1.5.9 C-axis development with creep

The evolution of ice fabrics has been investigated in the laboratory with artificial ice (Wilson and Peternell, 2012; Azuma and Higashi, 1985) and likewise from natural cores obtained from ice sheets or glaciers. C-axis fabrics record the deformational history in the ice.

In ice the orientation of a crystal is defined by the crystallographic axis (c-axis) that is perpendicular to the basal plane. Ice with a random orientation of c-axes is considered isotropic, while ice with a preferred orientation of c-axes is anisotropic (Kennedy et al., 2013). At the base of an ice sheet, horizontal shear becomes more dominant than vertical compression and the ice is strongly anisotropic favoring a "soft" orientation. The crystals tend to align with their basal planes oriented horizontally and their c-axes oriented vertically, this fabric is referred to as single-maximum (Alley, 1988). Ice fabrics (e.g. single-maximum and multi-maximum girdle) develop by grain rotation combined with glide on their basal planes. In addition, dynamic recrystallization processes may significantly contribute to fabric development (described in the sections below). The rate at which crystals rotate (how quickly fabric evolves) depends primarily on strain rate (on the order of 300 seconds per year for temperate valley glaciers) which is a function of stress, temperature, impurity content and crystal orientations (Kennedy et al., 2013; Paterson, 1991). During grain rotation, the c-axis in ice always rotates toward the compressional axis and away from the tensional axes (Alley, 1992 see Figure 1 page 249). This occurs because ice grains are constrained laterally by their neighbors.

1.6.0 Ice crystal fabrics and their link to climate

It has been suggested that ice fabrics may provide a link for paleoclimate reconstruction. Kennedy et al. (2013) highlights several important studies from Paterson (1991), Gusmeroli et al. (2012) and Pettit et al. (2011). I will briefly summarize the salient information from these studies which imply that fabric may have a link to climate. The first hint of this connection was proposed by Paterson (1991). He showed that there were differences in texture and fabric at an important boundary in an ice core from Greenland-Dye 3 (Ice Age/Holocene boundary). The Ice Age ice at this boundary revealed smaller crystal size and stronger fabric than the Holocene ice. Moreover, sonic velocities taken from profiles from Dome C, East Antarctica, Gusmeroli et al. (2012) has shown transitions in the fabric (e.g. speed of compressional-waves are faster along the c-axes providing a measure for fabric strength, strong fabric = high p-wave speed) that correlate to glacial-interglacial transitions through the depth of the ice sheet. Finally, Pettit et al. (2011) showed a strong correlation between O^{18} (an isotope of oxygen) and fabric data suggesting that fabric records climate information. In the future, it may be possible for fabric to be utilized as climate proxy.

I also propose that it may be beneficial to measure the magnetic anisotropy of susceptibility on the dirty basal ice (GISP2 core) to aid in climate reconstruction. In chapter 3, I discuss how this technique can be used to help locate unknown sheared layers in the ice core and its importance to climate history.

2. Glaciological Setting

Iceland is located in a climatically variable area. The glaciers of Vatnajökull including Flàajökull have been losing mass during the last century (Vaughan, et al., 2013). According to

detailed models of ice dynamics and hydrology, Flowers et al. (2005) suggested that these glaciers of southeast Vatnajökull are most sensitive to future warming of all outlet glaciers.

The Fláajökull glacier was an ideal location to conduct these investigations since it was easily accessible off the main highway. In some cases a cross-section of the bed of the glacier was visible along the ice margin yielding some insight into deformation processes. Moreover, the drumlins at Fláajökull have been sculpted by the overriding glacier providing a good test of the Boulton hypothesis. In addition, a commercialized freezer was available within a reasonable distance (Foss Hotel Vatnajökull) for the preservation of the specimens.

3. Dissertation Objectives

1. I performed laboratory experiments using the ring-shear apparatus (we thank Neal Iverson for allowing the use of this device) to test the hypotheses that shearing rate and effective pressure do not impart a signature on fabric strength. A thorough knowledge of soil mechanics and hydraulics was useful while working with the fabric device. Fabric measurements included: anisotropy of magnetic susceptibility (AMS) methods, hysteresis and high temperature susceptibility to determine grain size and magnetic mineralogy.

2. I conducted a detailed glaciological investigation of two dirty ice veins located on the margin of Fláajökull using a suite of analytical measurements including: anisotropy of magnetic susceptibility (AMS) of dirty ice cores, high temperature susceptibility and hysteresis measurements, c- axis orientations using the four axis Rigsby stage, thin section analysis of grain scale processes, and ice core CT scans at *General Electric.*

As I discussed in the introduction, the vein characteristics and field relationships and

comparisons to other studies (Ensminger et al., 2001; Lovell et al., 2015), the debris was likely injected from the bed near the ice front, but then moderately deformed. This hypothesis is supported by the magnetic and c-axis fabric data which are included in this dissertation.

3. Lastly, AMS till fabrics were also collected from newly formed drumlins to test the Boulton hypothesis. The premise of this hypothesis states that the fabric within the drumlin carapace should mimic the direction of sediment deformation with strong fabric throughout the drumlin with a potentially weak fabric defining the core.

4. Significance of Research

This work presents new information on fabric development using a ring shear apparatus, magnetic particle fabrics and their relationship to c-axis orientations and also new details on drumlin formation. To my knowledge, only one study using magnetic fabrics on polar ice has been undertaken by Fleming et al. (2013); however, magnetic particle fabrics applied to debris charged temperate ice has not been researched. In addition, there are no data comparing magnetic fabrics to c-axis crystal orientations. Therefore, this dissertation will hopefully improve and provide valuable instruction to scientists working in the glaciological community and perhaps help characterize the magnetic fabric properties of ice cores for climate change purposes (e.g. help locate unrecognized folds that have been sheared in ice cores). In addition, magnetic till fabrics from ring-shear studies may provide a reference frame for estimating shear strain (7-25) in glacial deposits. Both of these spectra will potentially contribute to improving our understanding of internal ice processes (e.g. microstructual processes related to magnetic fabrics in dirty basal ice) and the formation of glacial deposits.

5. Dissertation Structure

This dissertation consists of three manuscripts written for publication in scientific journals. The formatting style of these manuscripts will consist of three journals: *Geomorphology (Chapter 2*, published), Journal *of Glaciology (Chapter 3, resubmitted to journal with improved revisions)* and *Quaternary Science Reviews (submitted)*. A final chapter will summarize the most important findings of these manuscripts at the end of this dissertation. I also co-authored on a manuscript entitled, "Submarginal drumlin formation and late Holocene history of Fláajökull", southeast Iceland which is located in the appendix. My contribution to this manuscript incorporated the analysis of magnetic anisotropy of basal tills from several drumlins and its impact on drumlinization.

Figures

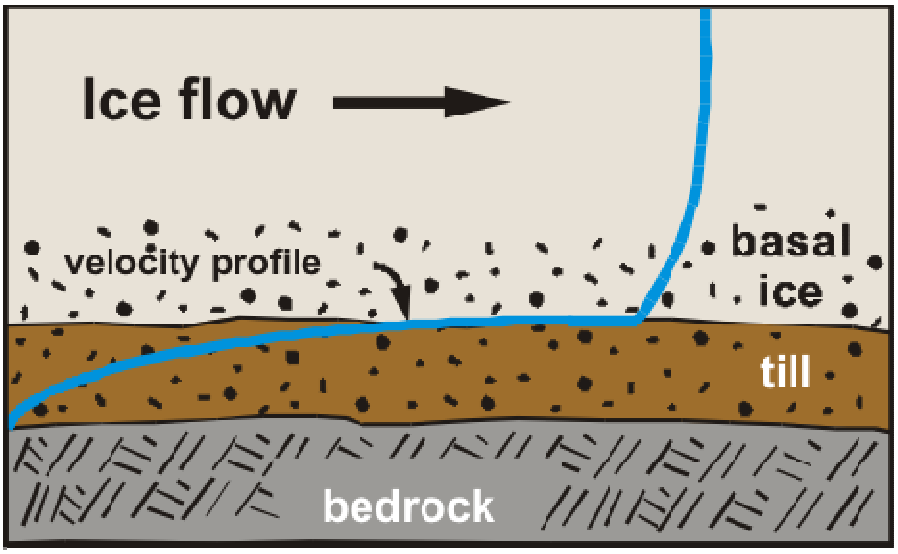

Figure 1. Schematic diagram showing a velocity profile through a longitudinal transect of a glacier underlain by till. Glacier motion may occur by internal ice deformation, basal sliding, or deformation of subglacial sediment. (diagram courtesy of Thomas S. Hooyer).

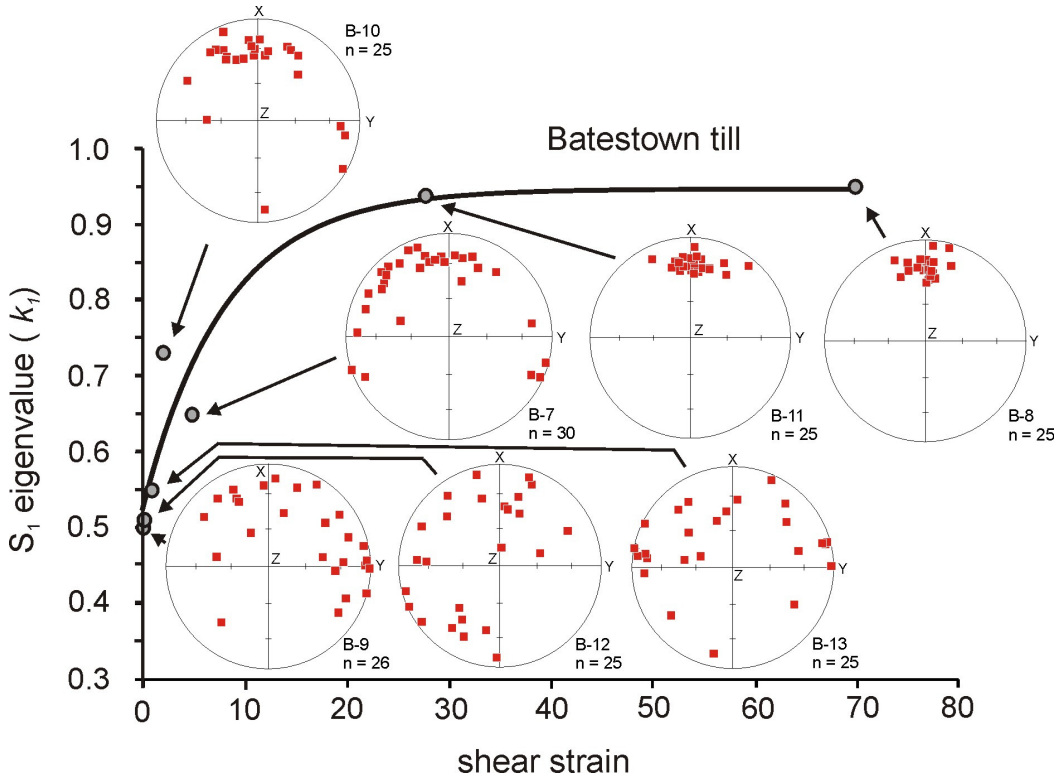

Figure 2. AMS fabric strength, based on K_1 orientations (maximum principal susceptibility), as a function of shear strain. A steady state fabric develops at a shear strain of >~25 and remains strong to high strains. Experiments were conducted at an effective stress of 65 kPa and a shearing rate of 400 m year^{-1}. Diagram acquired from Iverson et al. (2008). Experiments are labeled B-7 to B-13.

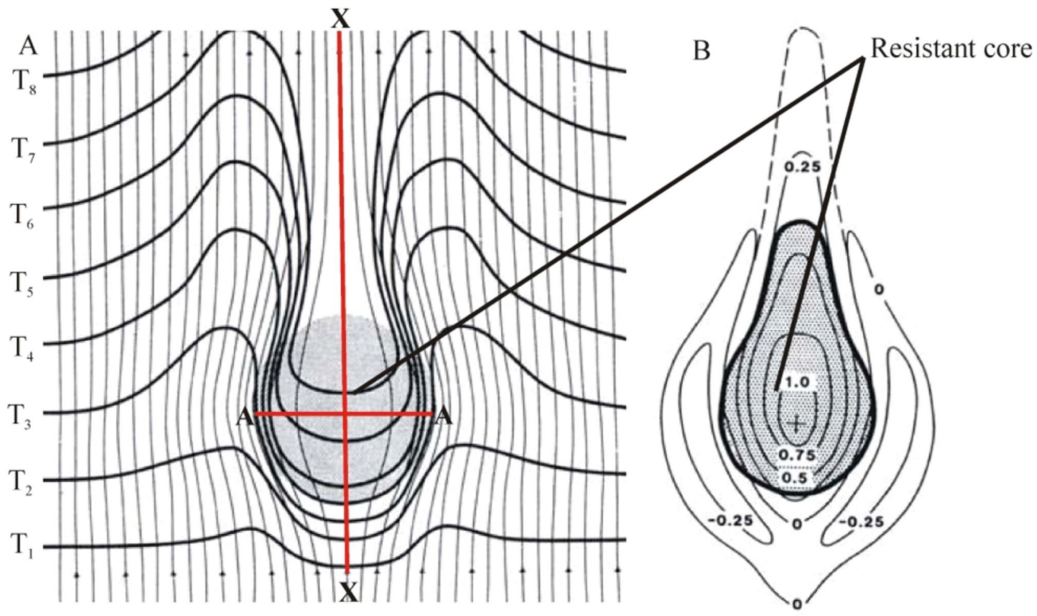

Figure 3. Boulton (1987) model of drumlin formation. (A) Streamlines in till deforming around a better drained (e.g. zones of high effective stress) and less deformable core (shaded). Thick lines labeled $T_{1\text{-}8}$ indicate the deformation of initially straight markers in the till as it passes the core. (B) Growth of drumlin by peripheral erosion (negative values) and accretion to core (positive values) (acquired from Boulton, 1987).

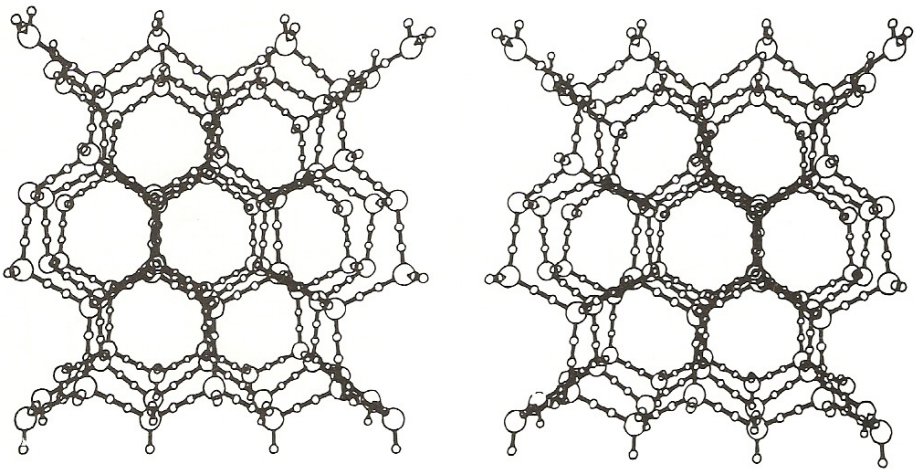

Figure 4. Examples of ice structures [Ih] viewed down the c-axis. Small circles indicate hydrogen sites. Diagram acquired from Hooke (2005).

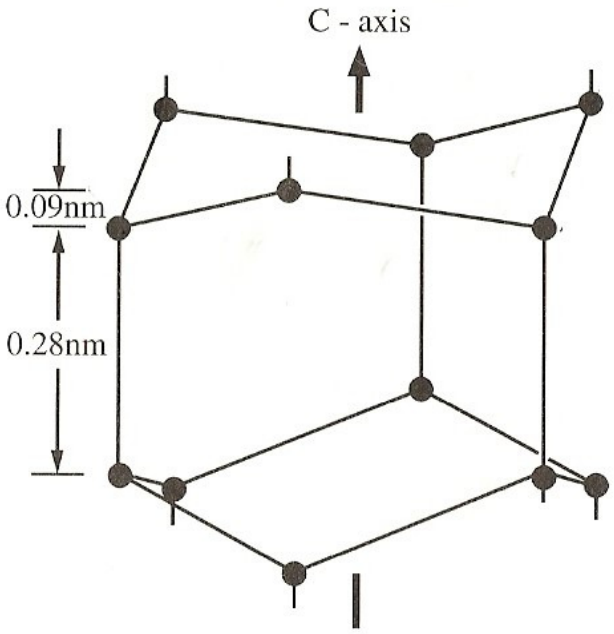

Figure 5. Illustrates the structure of ice [Ih] showing the two hexagonal rings (above and below) and associated bonds migrating upward and downward. Ice structure is viewed normal to the c-axis. Diagram acquired from Hooke (2005).

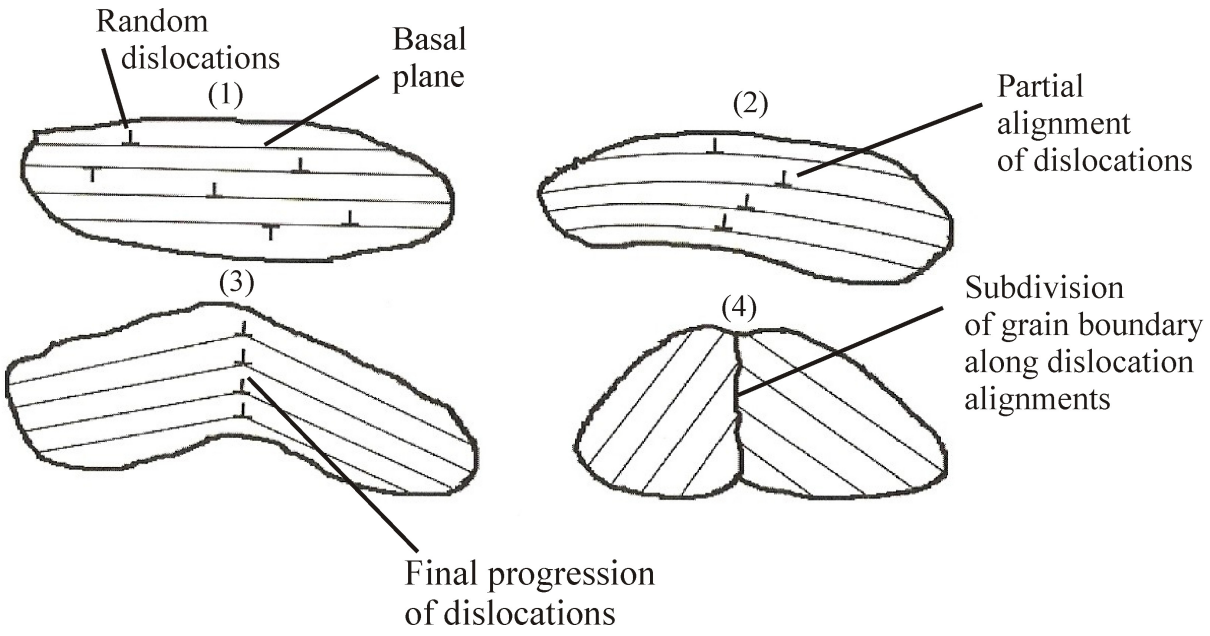

Figure 6. An example of subgrain rotation recrystallization occurring in four steps. (1) All dislocation types are at random, lines represent basal planes. Steps (2)-(4) demonstrate through a successive stress the alignment of one type of dislocation forming a new grain boundary (modified from Eichler, 2013).

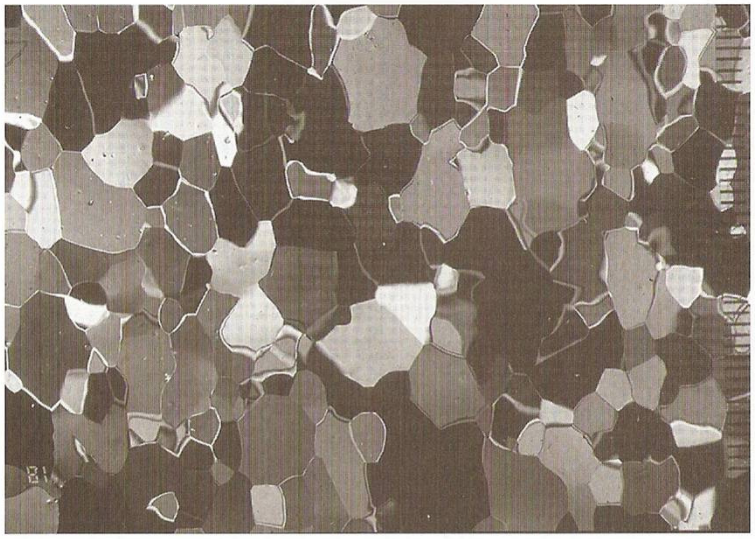

Figure 7. Ice thin section from the Vostok ice core, East Antarctica photographed under cross polarizers. Sample collected at depth 2351 m; scale in mm. Note the uniformly sized crystals resulting from polygonization (from Schulson and Duval, 2009).

Figure 8. Ice thin section from Terre Adélie, East Antarctica, photographed under crossed polarizers. Note the interlocking grain structure and serrated boundaries representative of migration recrystallization. Sample collected at 70 m depth. Finest division on scale is 1mm (from Duval and Castelnau, 1995).

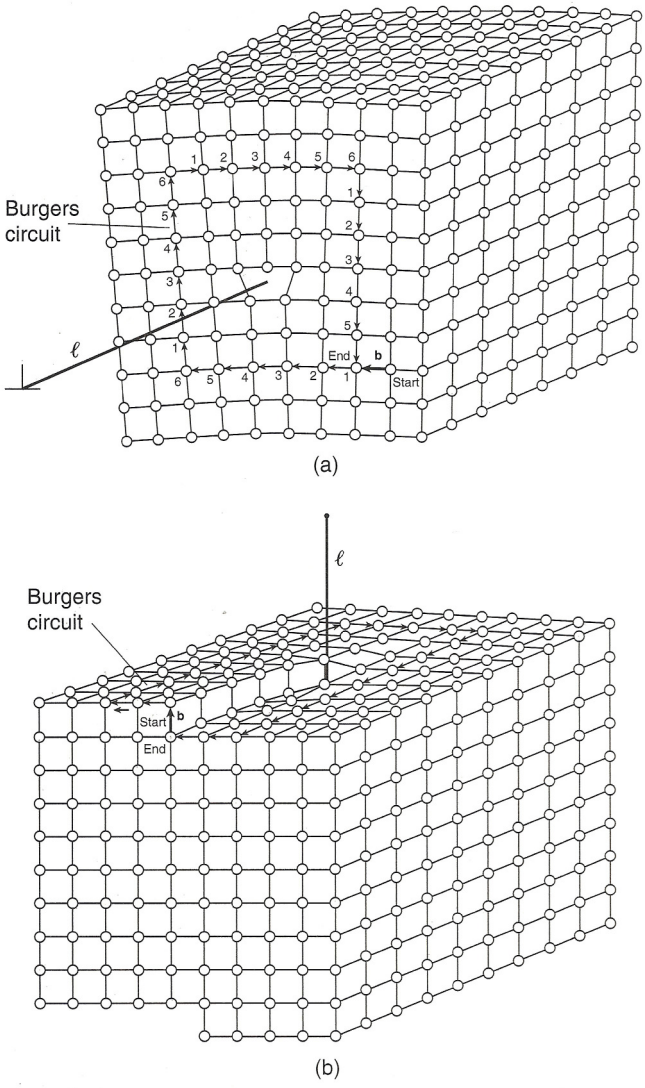

Figure 9. Examples of dislocations defects (a) edge and (b) screw types with Burgers vector, **b**, in a cubic lattice using a Burgers circuit. (a) The Burgers circuit around an edge dislocation (extra half-plane of atoms) marked with dislocation line l. In the edge dislocation **b** ⊥ l. (b) A Burgers circuit with a screw dislocation (circuit steps up or down to another plane). In the screw dislocation **b//**l. Diagram from van der Pluijm and Marshak (1997).

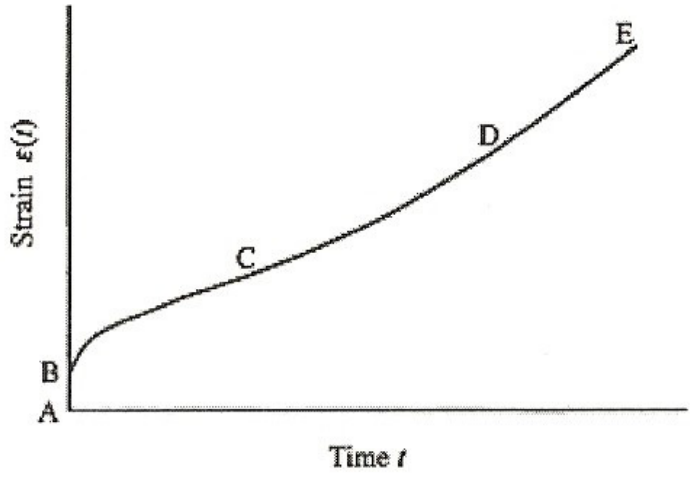

Figure 10. Creep curve of laboratory prepared polycrystalline ice with random grain orientations. AB: elastic deformation; BC: primary creep; C: secondary creep; CD: deformation acceleration due to dynamic recrystallization; DE: Steady state (tertiary creep) (from Petrenko and Whitworth, 1999).

References

Alley, R.B., 1988. Fabrics in polar ice sheets: development and prediction. Science, v. 240, 493-495.

Alley, R.B., 1992. Flow-law hypotheses for ice-sheet modeling. Journal of Glaciology, v. 38, 245-256.

Alley, R.B., Gow, A.J., Meese, D.A., 1995. Mapping c-axis fabrics to study physical processes in ice. Journal of Glaciology, v. 41, 197-203.

Alley, R.B., Cuffey, K.M., Evenson, E.B., Strasser, J.C., Lawson, D.E., Larson, G.J., 1997. How glaciers entrain and transport basal sediment: Physical constraints. Quaternary Science Reviews, v. 16, 1017-1038.

Azuma, N., and Higashi, A., 1985. Formation processes of ice fabric pattern in ice sheets. Annals of Glaciology, v. 6, 130-134.

Bennett, M.R., Huddart, D., Waller, R.I., 2000. Glaciofluvial crevasse and conduit fills as indicators of supraglacial dewatering during a surge, Skeiðaràrjökull, Iceland. Journal of Glaciology v. 46, 25-34.

Benn, D.I., 1995. Fabric signature of subglacial till deformation, Breidamerkurjökull, Iceland. Sedimentology v. 42, 735-747.

Blake, E.W., Clarke, G.K.C., Gerin, M.C., 1992. Tools for examining subglacial bed deformation. Journal of Glaciology v. 38, 388-396.

Boulton, G.S., 1987. A theory of drumlin formation by subglacial sediment deformation. In Menzies, J., and J., Rose, eds., Drumlin Symposium, A.Balkema, Rotterdam, 25-80.

Budd, W.F., Jacka, T.H., 1989. A review of ice rheology for ice sheet modeling. Cold Region Science Technology v. 16, 107-144.

Byers, J., Cohen, D., Iverson, N.R., 2012. Subglacial clast/bed contact forces. Journal of Glaciology v. 58, 89-98.

Clarke, G.K.C., 2005. Subglacial processes. Annual Review of Earth Planetary Science v. 33, 247-276.

Cuffey, K.M., Paterson, W.S.B., 2010. The physics of glaciers. Fourth edition. Oxford, Butterworth-Heinemann. 704 pp.

Diprinzio, C.L., Wilen, L.A., Alley, R.B., Fitzpatrick, J.J., Spencer, M.K., Gow, A.J., 2005. Fabric and texture at Siple Dome, Antarctica. Journal of Glaciology v. 51, 281-290.

Durand, G., Weiss, J., Lipenkov, V., Barnola, J.M., Krinner, G., Parrenin, F., Delmonte, B., Ritz, C., Duval, P., Röthlisberger, R., Bigler, M., 2006. Effect of impurities on grain growth in cold ice sheets. Journal of Geophysical Research v. 111, 1-18.

Duval, P., Ashby, M.F., Anderman, I., 1983. Rate-controlling processes in the creep of polycrystalline ice. Journal of Physical Chemistry v. 87, 4066-4074.

Duval, P., Montagnat, M., Grennerat, F., Weiss, J., Meyssonnier, J., and Philip, A., 2010. Creep and plasticity of glacier ice: a material science perspective. Journal of Glaciology v. 56, 1059-1068.

Eichler, J., 2013. C-axis analysis of the NEEM ice core. Alfred-Wegener-Institut für Polar-und Meeresforschung in der Helmholtz-Gemeinschaft. Freie Universität Berlin, Unpublished Diploma Thesis. 63 p.

Emerson, L.F., Rempel, A.W., 2007. Thresholds in the sliding resistance of simulated basal ice. The Cryosphere v. 1, 11-17.

Ensminger, S.L., Alley, R.B., Evenson, E.B., Lawson, D.E., Larson, G.J., 2001. Basal-crevasse-fill origin of laminated debris bands at Matanuska Glacier, Alaska, U.S.A. Journal of Glaciology v. 47, 412-422.

Evenson, E.B., 1971. The relationship of macro-and microfabric of till and the genesis of glacial landforms in Jefferson County, Wisconsin. In Goldthwaite, R.P. (ed.): Till: A symposium, 345-364.

Faria, S.H., Kremer, G.H., and Hutter, K., 2003. On the inclusion of recrystallization processes in the modeling of induced anisotropy in ice sheets: a thermodynamicists's point of view. Annuals of Glaciology v. 37, 29-34.

Faria, S.H., Freitag, J., Kipfstuhl, S., 2010. Polar ice structure and the integrity of ice-core paleoclimate records. Quaternary Science Reviews v. 29, 338-351.

Fleming, E.J., Lovell, H., Stevenson, C.T.E., Petronis, M.S., Benn, D.I., Hambrey, M.J., Fairchild, I.J., 2013. Magnetic fabrics in the basal ice of a surge-type glacier. Journal of Geophysical Research: Earth Surface v. 118, 2263-2278.

Flowers, G. E., Marshall, S. J., Björnsson, and Clarke, G. K. C., 2005. Sensitivity of Vatnajökull ice cap hydrology and dynamics to climate warming over the next 2 centuries, Journal of Geophysical Research: Earth Surface v. 110, 1-19.

Glen, J.W., 1955. The creep of polycrystalline ice. Proceeding Royal Society of London v. 228, 519-538.

Gentoso, M.J., Evenson, E.B., Kodama, K.P., Iverson, N.R., Alley, R.B., Berti, C. and Kozlowski, A., 2011. Exploring till bed kinematics using AMS magnetic fabrics and pebble fabrics: the Weedsport drumlin field, New York State, USA. Boreas v. 41, 31-41.

Gusmeroli, A., Pettit, E.C., Kennedy, J.H., Ritz, C., 2012. The crystalline fabric of glacial ice from full-waveform borehole sonic logging. Journal of Geophysical Research, v. 117, 1-13, (doi:10.1029/2012JF002343).

Harrison, P.W., 1957. A clay-till fabric: Its character and origin. Journal of Geology v. 65, 275-308.

Hart, J.K., 1994. Till fabric associated with deformable beds. Earth Surface Processes and Landforms v. 19, 15-32.

Hart, J.K., Rose, K.C., Martinez, K., Ong, R., 2009. Subglacial clast behaviour and its implications for till fabric development: new results derived from wireless subglacial probe experiments. Quaternary Science Reviews, v. 28, 597–607.

Hooke, R. LeB., Iverson, N.R., 1995. Grain-size distribution in deforming subglacial tills: Role of grain fracture. Geology v. 23, 57-60.

Hooke, R. LeB., Hanson, B., Iverson, N.R., Jansson, P., Fischer, U.H., 1997. Rheology of till beneath Storglaciären, Sweden. Journal of Glaciology v. 43, 172-179.

Hooke, R. Leb., 2005. Principles of glacier mechanics, Second Edition. Cambridge University Press, Cambridge. 248 pp.

Hooyer. T.H., Iverson, N.R., 2000a. Diffusive mixing between shearing granular layers: constraints on bed deformation from till contacts. Journal of Glaciology v. 46, 641-651.

Hooyer, T.H., Iverson, N.R., 2000. Clast-fabric development in a shearing granular material: implications for subglacial till and fault gouge. Geological Society of America Bulletin v. 112, 683-692.

Hooyer, T.S., Iverson, N.R., Lagroix, F., Thomason, J.F., 2008. Magnetic fabric of sheared till: A strain indicator for evaluating the bed deformation model of glacier flow. Journal of Geophysical Research-Earth Surface v. 113, 1-15.

Hubbard, B., Sharp, M., 1989. Basal ice formation and deformation: a review. Progress in Physical Geography, v. 13, 529-558.

Iverson, N.R., Baker, R.W., Hooyer, T.S., 1997. A ring-shear device for the study of till deformation: test on tills with contrasting clays contents. Quaternary Science Reviews, v. 16, 1057-1066.

Iverson, N.R., Baker, R.W., Hooke, R., LeB., Hanson, B., Jansson, P., 1999. Coupling between a glacier and a soft bed: I. A relation between effective pressure and local shear stress determined from till elasticity. Journal of Glaciology v. 45, 31-40.

Iverson, N.R., Hooyer, T.S., Thomason, J.F., Graesch, M., Shumway, J.R., 2008. The experimental basis for interpreting particle and magnetic fabrics of sheared till. Earth Surface Processes and Landforms v. 33, 627-645.

Johnson, M.D., Schomacker, A., Benediktsson, Í. Ö., Geiger, A., Ferguson, J. A., and Ingólfsson, Ó., 2010. Active drumlin field revealed at the margin of Múlajökull, Iceland: A surge-type glacier. Geology, v. 38, 943-946.

Kennedy, J.H., Pettit, E.C., Di Prinzio, C.L., 2013. The evolution of crystal fabric in ice sheets and its link to climate history. Journal of Glaciology, v. 59, 357-373.

Knight, J., 2010. Drumlins and the dynamics of the subglacial environment, Sedimentary Geology, v. 232, 91-97, (doi: 10.1016/j.sedgeo.2010.10.001.).

Larsen, N.K., Piotrowski, J.A., Kronborg, C., 2004. A multiproxy study of a basal till: a time-transgressive accretion and deformation hypothesis. Journal of Quaternary Science v. 19, 9-21.

MacClintock, P., and Dreimanis, A., 1964. Orientation of till fabric by an overriding glacier in the Saint Lawrence Valley. American Journal of Science v. 262, 133-142.

Paterson, W.S.B., 1991. Why ice-age is sometimes “soft”. Cold Regions Science and Technology v. 20, 75-98.

Petersen, B.B., 2012. An experimental study of ice-bed separation during glacial sliding. Iowa State University, Unpublished thesis.

Pettit, E.C., Waddington, E., Thorsteinsson, Gusmeroli, A., Kennedy, J., Ritz, C., Carns, R., 2011. Using borehole sonic logging to infer ice microstructure and climate history. Geophysical Research Abstracts, v. 13, EGU2011-1460

Poirier, J.P., 1985. Creep of crystals: High-temperature deformation processes in metals, Ceramics and minerals. Cambridge University Press. 258 p.

Richeton, T.J., Weiss, J., Louchet, F., 2005b. Dislocation avalanches: role of temperature, grain size and strain hardening. Acta Materialia v. 53, 4463-4471.

Schulson, E.M., Duval, P., 2009. Creep and fracture of ice. Cambridge University Press. 391 p.

Schumway, J.R., Iverson, N.R., 2009. Magnetic fabrics of the Douglas Till of the Superior lobe: exploring bed-deformation kinematics. Journal of Glaciology v. 28, 107-119.

Sharp, M.J., 1985. “Crevasse fill” ridges-A landform type characteristic of surging glacier? Geografiska Annaler, v. 67A, 213-220.

Song, M., Baker, I., Cole, D.M., 2008. The effect on particles of creep rate and microstructures of granular ice. Journal of Glaciology v. 54, 533-537.

Standford, S.D., Mickelson, D.M., 1985. Till fabric and deformational structures in drumlins near Waukesha, Wisconsin, U.S.A. Journal of Glaciology, v. 31, 220-228.

Taylor, K., Alley, R.B., Fiacco, J., Grootes, P., Lamorey, G., Mayewski, P.A., Spencer, M.J., 1992. Ice-core dating and chemistry by direct-current electrical conductivity. Journal of Glaciology v. 38, 325-332.

Thorsteinsson, T., Waddington, E.D., Taylor, K.C., Alley, R.B., Blankenship, D.D., 1999. Strain-rate enhancement at Dye 3, Greenland. Journal of Glaciology v. 45, 338-345.

Tulaczyk, S., Kamb, W.B., Engelhardt, H.F., 2000. Basal mechanics of Ice Stream B, Antarctica 1. Till mechanics. Journal of Geophysical Research v. 105, 463-481.

Van der Pluijm, B.A., Marshak, S., 1997. Earth Structure: An Introduction to Structural Geology and Tectonics. The McGraw-Hill Companies. 495 p.

Vaughan, D.G., Comiso, J. C., Allison, I., Carrasco, J., Kaser, G., Kwok, R., Mote, P., Murray, T., Paul, F., Ren, J., Rignot, E., Solomina, O., Steffen, K., Zhang, T., 2013. Observations: Cryosphere, in: Climate Change 2013: The Physical Science Basis. Contribution of Working Group I to the Fifth Assessment Report of the Intergovernmental Panel on Climate Change. Cambridge University Press. UK and New York, NY, USA. 317-382 p.

Weertman, J., Weertman, J.R., 1992. Elementary Dislocation Theory. Oxford University Press. 211 p.

Wilson, C.J.L., Peternell, M., 2012. Ice deformed in compression and simple shear: control of temperature and initial fabric. Journal of Glaciology, v. 58, 11-22.

Zoet, L.K., Iverson, N.R., 2015. Experimental determination of a double-valued drag relationship for glacier sliding. Journal of Glaciology v. 61, 1-7

Chapter 2: Laboratory Study of Fabric Development in Shearing Till: The Importance of Effective Pressure and Shearing Rate

William R. Jacobson Jr.[*a] and Thomas S. Hooyer[a]

[a]Department of Geosciences, University of Wisconsin--Milwaukee, Milwaukee, 53201, USA

Abstract

Herein we present data on the shearing rate (glacier velocity) and effective pressure (difference between the ice-overburden pressure and pore-water pressure) in the development of magnetic fabric (anisotropy of magnetic susceptibility) using a rotary ring- shear device. A Wisconsin-age basal till was used in the experiments and deformed to its critical state at shear strains as high as 93. We also present data from hysteresis and high temperature susceptibility experiments to identify the magnetic carrier in the basal till. Results showed little change in fabric strength when varying the shearing rate in the speed range of 110 to 860 m/y^{-1}. Moreover, the effective pressure tests also showed an inconsistency in fabric between 30 and 150 kPa; however, a slight strengthening effect was documented. Thus, the K_1 magnetic fabric strength is independent of the shearing rate and effective pressure. This suggests that the fabric strength upon these variables cannot be used as a benchmark for estimating shear deformation to the geological record. The K_1 fabric strength in this study, however, remained consistent with respect to other till particle fabric methods (e.g., sand and pebble) in which the same conclusion was drawn: all particles align parallel to the direction of shear and plunge mildly upglacier.

[*a] Corresponding author.
Email addresses: wrjjr@uwm.edu (W.R. Jacobson Jr.), hooyer@uwm.edu (T.S. Hooyer)

Keywords: magnetic till fabrics; subglacial processes; laboratory ring-shear apparatus

1. Introduction

The effective pressure and the shearing rate are important glaciological variables that affect the distribution of deformation and flow on soft beds (Clarke, 2005; Rempel, 2009; Cuffey and Paterson, 2010). In certain circumstances, these variables may have a bearing on fabric development and genesis of subglacial landforms (Larsen et al., 2006b; Johnson et al., 2010; Gentoso et al., 2011). Moreover, low effective pressure (difference between the ice-overburden pressure and pore-water pressure) has been shown to inhibit deep bed deformation as well as reduce vertical regelation (Alley et al., 1997; Iverson et al., 2007). Numerous laboratory studies (Kamb, 1991; Iverson et al., 1998; Tulaczyk et al., 2000) have indicated that till strength is insensitive to its deformation rate and varies directly with effective pressure, consistent of a Coulomb-plastic rheology. These findings are also consistent with classical soil mechanics (e.g., Lambe and Whitman, 1979). Consequently, debate still exists as to whether till is best characterized as a *viscous* rheology or a plastic rheology (Hindmarsh, 1997; Fowler, 2003; Rathbun et al., 2008). Furthermore, some field measurements (devices inserted in till) beneath modern glaciers suggest a Mohr-Coulomb plastic rheology rather than a viscous rheology (Clarke, 1987; Fischer and Clarke, 1994; Hooke et al., 1997; Truffer et al., 2001).

Despite these exciting developments, the effect on steady state fabric (referred to herein as where the specimen reaches a critical value in porosity and strength) in response to changes in effective pressure and shearing rate (glacier velocity) remains unknown.

Hooyer et al. (2008) implied that an increase in effective pressure (pore-water pressure reduction) will affect the critical state porosity, which may constrain particle rotation and increase the fabric strength. Benn and Evans (1996) also suggested a similar argument upon the fabric strength and effective pressure. Furthermore, Larsen and Piotrowski (2003) found that the

size of the particles had no affect on fabric strength. On the other hand, Carr and Rose (2003) proposed that a particle size dependence on fabric orientations that is driven by effective pressure. These assertions were largely based upon microstructures observed in thin section and on clast macrofabrics from a till sequence in central Scotland. Other geological investigations (Dowdeswell and Sharp, 1986; Hart, 1994; Benn, 1995; Hart et al., 2009) have postulated that the fabric orientation and strength varies as a result of changes in thickness of the deforming layer, which is dependent on the applied stress (glacier velocity) and water pressure (matrix strength). However, we argue that the assumptions from Carr and Rose (2003) on till fabric is uncertain because of insufficient data pertaining to key variables such as the effective pressure, shearing rate, and till deformation state (e.g., in a transient behavior or steady state condition). These variables have an impact on particle fabric development. Nonetheless, these inferences can be evaluated systematically in the laboratory to determine whether the shearing rate (glacier velocity) and effective pressure influence till fabric strength.

These new ring-shear experiments differ from Hooyer et al. (2008) wherein the shearing rates and effective pressures were varied as opposed to keeping these variables constant. This experimental setup was necessary to confirm the effects on fabric development and to either prove or disprove the above conjectures.

Herein, we present new findings on till particle fabrics using a customized ring-shear apparatus. The fabrics were analyzed using the anisotropy of magnetic susceptibility (AMS) technique that measures the orientation of magnetic minerals. The orientations of these minerals are portrayed as an ellipsoid, where three-dimensional strain and magnitude are evaluated.

2. Methodology

A ring-shear device was constructed to study the mechanical properties of till at high strains (Iverson et al., 1997). The device shears sediment that is saturated between two horizontal plates (Fig. 11). The shearing rate can be varied through nearly the full glacial range (0 to 1000 m/y^{-1}) and normal stress (30 to 200 kPa). Pore water movement within the till can enter or exit the sample chamber that is open to the atmosphere.

2.1 Experimental Procedure

A total of 12 experiments were performed with the Ozaukee till, a late Wisconsin-age basal till that was deposited beneath the Lake Michigan Lobe. This till is light brown in color and has a matrix grain-size distribution of 13% sand and 87% silt and clay. Six experiments, S1 through S6, were performed where the shearing rate was varied from 110 to 860 m/y^{-1} covering the full range of glacier speeds while maintaining a constant effective pressure of 85 kPa. The remaining six experiments, E7 through E12, were performed where we varied the effective pressure between 30 and 150 kPa and held the shearing rate constant. This till was chosen because of its high clay and silt content, which is representative of many soft-bedded glaciers.

To begin the experiment, the till was initially saturated with distilled water and disaggregated. In all experiments, particles <8 mm in diameter, one-tenth of the smallest dimension of the annulus, were removed from the till specimen in accordance with geotechnical procedures (Head, 1989). The saturated sediment was then loaded into the sample chamber of the ring-shear device to a thickness of about 80 mm. Prior to applying the normal stress to the till, three vertical columns of displacement markers consisting of plastic beads 5 mm in diameter were placed across the width of the till to ultimately assess the distribution of strain. Upon

completion of the test, the shear strain was calculated by dividing the total shear displacement at the sample centerline by the shear zone thickness.

Prior to shearing, the normal-load plate and upper platen were positioned and a normal stress of 85 kPa was applied to the till. Consolidation was measured by recording the change in specimen thickness as a function of time, which typically occurred over a 24-h period. Once the sample was finished consolidating, the yoke was adjusted to minimize the intrusion of sediment along the sliding interface between the upper and lower walls. Vacuum grease was also applied there to reduce friction while the base was rotating. The motor driving the ring-shear device was then turned on, and the till was sheared to a predetermined displacement.

Following shearing, the ring-shear device was disassembled and strain markers were located to define the shear zone. The upper portion of the till specimen, where no shearing occurred, was removed to expose the top of the shear zone. A minimum of 50 plastic boxes (8 cm^3) were then collected from the chamber. Unsheared samples have been examined in prior ring-shear experiments and were not deemed relevant to this project.

Each box was measured for the anisotropy of magnetic susceptibility (AMS) with an MF*K1*-FA Multi-Function Kappabridge system. This system measures magnetic susceptibility many times while rotating it through three orientations. The strength of the induced magnetization of a given till sample, *M*, is given by kH, where the constant of proportionality *k* is called the susceptibility and *H* is the magnetic field strength (Jelinek, 1978). In materials in which the shapes or crystallographic orientations of mineral grains have become aligned, *k* varies with direction such that a second-rank tensor is required to characterize it (Tarling and Hrouda, 1993). This tensor is visualized with a susceptibility ellipsoid that has lengths of its long, intermediate, and short axes equal to the principal susceptibilities K_1, K_2, and K_3, (Fig. 12). In

addition, the AMS method reflects the volume-averaged effect of many magnetic particles and provides excellent spatial resolution compared to macroscale pebble fabrics.

The shape of the AMS ellipsoid was also determined using equations provided by Borradaile and Jackson (2004) that have been used in the past to characterize deformed rocks. The percent total anisotropy (*P%),* where k_v represents the volume susceptibility, represents the mean of principal susceptibilities:

$$P\% = 100\left(\frac{k1 - k3}{kv}\right) \quad (1)$$

Two other important parameters provided by Jelinek (1981) that describe the AMS ellipsoid include the shape parameter (T_j) and the corrected degree of anisotropy (P_j). The ellipsoid is prolate if $-1 \leq T_j < 0$ and oblate if it is $0 < T_j \leq 1$. If the ellipsoid is a sphere, $P_j = 1$ and the value of P_j will increase with increasing anisotropy.

$$T_j = \frac{\ln\left(\frac{k2}{k3}\right) - \ln\left(\frac{k1}{k2}\right)}{\ln\left(\frac{k2}{k3}\right) + \ln\left(\frac{k1}{k2}\right)} \quad (2)$$

$$P_j = \exp\left(\sqrt{2\left[\left(\ln\left(\frac{k1}{k}\right)\right)^2 + \left(\ln\left(\frac{k2}{k}\right)\right)^2 + \left(\ln\left(\frac{k3}{k}\right)\right)^2\right]}\right) \quad (3)$$

High temperature susceptibility (HTS) experiments were also conducted to determine the mineralogy of the particles (Evans and Heller, 2003). The HTS system included a CS-2 furnace apparatus linked to the Kappabridge. The mineralogy of magnetic particles was conducted on fine-grained particles (clay and silt) that were <65 μm. The sample was heated from 25 to 700°C and cooled back to 25°C while measuring the magnetic susceptibility. During the HTS experiments, the unblocking temperature was usually reached (destabilization of magnetic moments from the input of thermal energy). The unblocking temperature never exceeded the Curie temperature and was used to identify the mineralogy of the magnetic particles.

Hysteresis experiments were performed to estimate the grain sizes responsible for the anisotropy imparted on the sheared till. In these experiments an alternating magnetic field B was applied to the fine fractions in opposing directions of magnetization (±800 mT). The variation in the magnetization as a function of the applied magnetic field B was typically plotted (Fig. 13). The shape of the loop depends on the mineralogy and sizes of magnetic particles (Iverson et al., 2008). Several loop parameters were defined including the saturation magnetization M_S, the maximum magnetization attainable, the remanent saturated magnetization M_{RS}, the magnetization under no applied field, and the coercivity of remanence B_C, the reverse applied field required to reduce the saturation magnetism to 0 (Fig. 3). Day diagrams were used to assess particle size where M_{RS}/M_S were plotted as a function of B_{CR}/B_C (Dunlop, 2002) and parameters were determined by analyzing the hysteresis data. Plotting the data on Day plots helped constrain particle size.

The fabric strength and direction were determined using eigenvectors (V_1, V_2, and V_3) and corresponding eigenvalues (S_1, S_2, and S_3), respectively (Mark, 1973). The S_1 eigenvalue represents the degree of clustering of K_1 orientations around the V_1 eigenvector. An S_1 eigenvalue

of 0.33 indicates random alignment of K_1 orientations; whereas an S_1 eigenvalue of 1.0 indicates K_1 orientations that are perfectly aligned. The magnetic fabric was analyzed using the software package *SpheriStat3* from Pangaea Scientific.

3. Results

3.1 Strain Distribution

Locations of the marker beads excavated at the ends of experiments demonstrated that the shear strain was distributed across the central portion of the till specimen (Fig. 14). The thickness of this shear zone varied from 17 to 33 mm, with an average thickness of 22 mm for the first series of experiments and 25 mm for the second set. Shear strains were calculated by taking the displacement and dividing it by the shear zone thickness. Shear strains varied for the experiments and ranged from 51 to 93. The parameters describing shear deformation from experiments is summarized in Table 1.

3.2 Magnetic Mineralogy and Grain Size

Magnetite dominates the mineralogy of the Ozaukee till as indicated by the dependence of magnetic susceptibility on temperature (Fig. 15). An abrupt reduction in susceptibility occurs at temperatures around ~580 to 600°C, which is consistent with a magnetite Curie temperature (Bertotti, 1998). In light of this finding, magnetite is a good petrofabric indicator (Fuller, 1964) because it is morphologically controlled (e.g. magnetization is induced along the long axes of the grains).

More information on the sizes of magnetic grains can be determined from the high temperature susceptibility data. A marked peak in susceptibility occurred at 480°C (Fig. 15),

which represents the so-called *Hopkinson* peak confirmed by Dunlop and Özdemir (1997). This peak implies that some of the grains of the Ozaukee till are <0.1μm (single-domain magnetite particles). Therefore, this suggests that some of the finer grains are possibly contained within larger rock fragments and do not contribute to the magnitude of anisotropy (Hooyer et al., 2008).

Figure 16 illustrates the shape of the hysteresis loop for the Ozaukee till. Hysteresis parameters derived from the loop may provide further data for estimating particle sizes (Table 2). The ratios of M_{RS}/M_S and B_{CR}/B_C have commonly been used to estimate grain size. Moreover, the ratios indicate a mean magnetite grain size of ~15 μm (see Dunlop, 2002; Figs 8C, 8D, and 8E) and plot within the pseudo-single domain range. Considering both of the size fractions (a remnant single and pseudo domain), there are some magnetite grains >15 μm. An estimation of the mass fraction of magnetic grains contained in these larger fragments was not analyzed; only the fine fraction (<63 μm) was measured.

Tentatively, given the HTS and hysteresis results, the principal magnetic mineral in these tills is magnetite and it is generally silt sized or smaller.

3.3 Anisotropy of Magnetic Susceptibility

The principal susceptibilities of the individual samples did not vary systematically with either shearing rate and or effective pressure. The AMS ellipsoids were close to being spheres as indicated by P_j. Moreover, the mean volume susceptibility of the Ozaukee till was 712 ± 156 μSI. Average percent anisotropy for samples from all experiments was 8.4 ± 2.0% for the Ozaukee till. Similarly, mean values of the shape parameter and the corrected degree of anisotropy were near 0 and 1 (Table 3). Contrary to the shape parameter and corrected degree of anisotropy, all K_1 axes (parallel to the long axes of the magnetite grains) show a strong

correlation with the shearing direction. Our results further suggested that the magnetic grains <63 μm were mainly responsible for the anisotropy imparted on the till during shearing.

The orientations of principal magnetic susceptibilities plotted on the lower hemisphere stereonets detail the development of the microfabric from both experiments (Figs. 17 and 18). We hypothesized that the K_1 fabric strength might increase monotonically with glacier velocity, suggesting a possible dependence on the shearing rate. However, strong unimodal K_1 clusters resulted regardless of changes in the shearing rate, which varied from 110 to 860 m/y^{-1} (Fig. 17). The S_1 eigenvalues ranged from 0.93 to 0.98 (Table 4). In this case, in experiment S3 with a shearing rate of 342 m/y^{-1}, 3 of the 50 samples had K_1 orientations outside the cluster, which explains a reduction in S_1. Conversely, the S_1 eigenvalue remained strong at 0.93. Fabric directions, as indicated by eigenvectors computed from K_1 orientations, were relatively consistent trending N-S (Table 4) with a mean *upglacier* plunge of 23°. The K_2 orientations were roughly parallel to the shear plane and transverse to the shear direction; whereas, K_3 orientations plunged steeply downglacier.

Figure 18 shows the results of test segments at different effective pressures (30 to 150 kPa) with a constant shearing rate of 400 m/y^{-1}. Interestingly, these tests did not show any change with respect to the orientation of the magnetic principal susceptibilities which was illustrated in the shearing rate experiments. According to the regressed data, the fabric strength variability was high ($0.85 < S_1 < 0.99$) (Fig. 16). The mean *upglacier* plunge was 20°. The S_1 eigenvalues ranged from 0.91 to 0.96.

A strengthening affect over the given effective pressures is another important qualification. The change in slope, the line defined by the data, represents a slight compaction or a decrease in dilatancy; likewise, after inspection it appeared small (Fig. 18).

4. Discussion

4.1 Laboratory Results

The magnetic fabric data from our experiments were similar and consistent with the work of Iverson et al. (2008) in that their fabric was also controlled by silt-sized magnetite particles in the till matrix; however, in their analysis the shear strain magnitude was varied.

4.2 Effective Pressure

Perhaps the most interesting result from this study is that the K_1 magnetic fabric is insensitive to the effective pressure. Changes in effective pressure beneath soft-bedded glaciers can cause unsteady deformation resulting in increased glacier flow (Iverson, 1999; Iverson et al., 1999; Truffer and Harrison, 2006). In these latter studies it was reported that the till was not in its critical state suggesting transient bed conditions (fluctuations in water pressure). In our study the fabric coincides with a steady strength (shear resistance) and porosity (Skempton, 1985). We hypothesize that the lack of dependence on the effective pressure on fabric may be linked in part to its low diffusivity and permeability. Although, we did not measure the hydraulic diffusivity, the Ozaukee till is relatively clay-rich. As pointed out by Iverson (2010), tills with low hydraulic diffusivity are most susceptible to dilatant strengthening. These clay-rich tills are least likely to consolidate significantly in response to an increase in effective pressure. In general, increases in the effective pressure at the critical state will cause the rate of shear to decrease (e.g., shearing a till in its critical state probably requires a greater shear stress than a till that is not in its critical state or in its dilatant state). Again, this may be relevant because we observed a slight strengthening effect (possible pore-water pressure decline) with increasing effective pressures

(Fig. 18). Typically, we would suspect this to occur as the effective pressure increases (Reynolds, 1885).

4.3 Ring-Shear Experiments

Previous test experiments by Iverson et al. (2008) indicated that the fabric strength was dependent on shear strain at ~6-25, whereas the fabric strength stabilized when the shear strain reached a magnitude >~25. These results are significant in that they can be used to identify weak till fabrics in the geologic record that have been sheared to strains too small (<~6-25 for the ring-shear tests) to be relevant to the pervasively high strains (10^3 - 10^5) needed for most shearing of glacier beds. Larsen et al. (2006a) came to similar conclusions when they showed that their calibrated microstructures and microshears were also limited in strain reconstruction. They concluded that the microstructures cannot be used as a proxy for strain because the fabric strength becomes steady at strains above ~18.

The work conducted by Carr and Rose (2003) provided some merit; however, the application of a stress-dependence on particle size for field interpretations may not be appropriate. Our results using the magnetic fabric technique demonstrate a consistent orientation in fabric and strength through various shear rates, effective pressures, and particle sizes (typically silt to sand). A stress dependence on different size fractions is negligible. Moreover, results from other ring-shear studies on sand particle fabrics (Thomason and Iverson, 2006) and pebble-sized fabrics (Hooyer and Iverson, 2000) all confirm similar characteristics in fabric orientations and strength, despite shape and particle size.

4.4 Till Rheology

The rotational behavior of granular materials is often considered in till deformation studies. The Jeffery model (1922) or March model (1932) is usually invoked to characterize particle rotation in till. The Jeffery model is based on viscous assumptions of shearing a fluid with the no-slip criteria. Comparatively, in the March model, slip occurs between the individual grains and particles do not rotate through the shear plane, which is one requisite of maintaining stronger fabrics. Strong field evidence for slip along clast surfaces (striated faces) has been observed in sheared till (Benn, 2002). The March model has become increasingly favored as a result of field and experimental studies on sediment deformation (Benn and Evans, 1996; Hooyer and Iverson, 2000; Larsen and Piotrowski, 2003), although the Jeffery model also has been suggested (Hicock, 1991; Hart, 1994).

5. Conclusions

The results of these experiments indicate that the fabric strength is independent of effective pressure and shearing rate. Regardless of varying the shearing rate and effective pressure, S_1 eigenvalues remained strong (0.91 to 0.98). Clustering of the maximum K_1 susceptibilities in the direction of shear is controlled by magnetite particles that are silt sized or smaller.

The observed strengthening effect over the pressure range may be a result of a small decrease in critical state porosity with fabric strength; however, this could not be confirmed in these experiments because it was not directly measured. In addition, our data suggest that the sheared sediments behaved like a Coulomb plastic material and that the magnetic fabric developed according to the *March model*. Furthermore, the ring-shear data cannot be used as

proxies for interpreting fabric strength in basal tills of the geologic record.

From a soil mechanics perspective, these results are consistent with the fact that once steady state is achieved (constant void ratio and volume) little variance occurs in fabric strength.

Acknowledgements

This work was supported by the University of Wisconsin-Milwaukee, Geosciences Department. We would like to thank the Institute of Rock Magnetism (IRM) at the University of Minnesota for providing the facilities for gathering the magnetic data; Julie Bowles was helpful at the IRM. We thank Neal Iverson for allowing us to use the ring-shear device. Constructive reviews by Nicolaj K. Larsen and one anonymous referee have improved this manuscript.

Tables

Table 1. Parameters Describing Shear Deformation

Experiment	Shearing Displacement at Sample Centerline (mm)	Shear Zone Thickness *h* (mm)	Shear Strain γ
	Ozaukee Till		
S1	1666	26	64.0
S2	1624	24	67.6
S3	1622	19	85.3
S4	1633	22	74.2
S5	1592	20	79.6
S6	1628	23	70.7
E7	1580	17	92.9
E8	1650	27	61.1
E9	1625	23	70.6
E10	1856	26	71.3
E11	1672	33	50.6
E12	1628	23	70.7

Table 2. Hysteresis Loop Parameters for Fine (<63μm) Fractions of the Ozaukee Tills

	M_{RS} (mAm^2/kg)	M_s (mAm^2/kg)	B_C (mT)	B_{CR} (mT)	M_{RS}/M_s	B_{CR}/B_C
Fine-116	0.011	0.088	13.5	36.7	.125	2.71
Fine-144	0.008	0.075	13.7	37.6	.106	2.74

Table 3. AMS Data From Experiments (Ordered by Shearing Rate and Normal Stress)

Experiment	n	Shearing Rate (m/a)	Normal Stress (kPa)	Shear Strain	K_v[a] (μ SI)	K_1[a] (μ SI)	K_2[a] (μ SI)	K_3[a] (μ SI)	P_j[a]	T_j[a]	P%[a](%)
Ozaukee Till											
S1	50	860	85	64.0	710±123	734±124	720±148	678±116	1.107±.224	0.36±0.22	8.0±1.8
S2	50	680	85	67.6	697±116	726±122	698±117	667±109	1.089±.152	0.08±0.24	8.5±2.1
S3	50	500	85	85.3	736±214	766±220	736±216	706±207	1.087±.151	0.01±0.22	8.3±1.8
S4	50	342	85	74.2	684±113	713±118	684±114	654±108	1.090±.152	0.06±0.19	8.6±1.6
S5	50	193	85	79.6	754±127	787±133	753±127	720±122	1.093±.153	-0.01±0.20	8.9±1.9
S6	50	110	85	70.7	740±169	768±174	740±169	711±169	1.082±.012	0.01±0.18	7.8±1.5
E7	50	420	85	92.9	630±147	651±151	632±148	608±141	1.071±.151	0.14±0.28	6.8±2.6
E8	50	420	30	61.1	696±116	731±117	687±148	696±116	1.088±.154	0.02±0.23	8.5±2.1
E9	50	420	150	70.6	694±163	722±166	695±163	663±160	1.091±.153	0.11±0.16	8.6±2.2
E10	50	420	115	71.3	748±327	781±335	748±326	715±321	1.095±.157	0.07±0.20	8.9±3.7
E11	50	420	70	50.6	715±106	749±111	717±107	680±101	1.102±.153	0.09±0.19	9.6±1.8
E12	50	420	55	70.7	740±152	773±114	739±151	709±148	1.092±.152	-0.03±0.17	8.8±1.7

[a]Values represent the mean and ±1 standard deviation.

Table 4. AMS Fabric Data

Sample Group	*n*	Shear Strain	S_1	S_2	S_3	Eigenvector V_1 (°) Trend	Eigenvector V_1 (°) Plunge	Eigenvector V_3 (°) Trend	Eigenvector V_3 (°) Plunge
S1	50	64.0	0.97	0.02	0.01	3	23	185	67
S2	50	67.6	0.96	0.03	0.01	1	28	172	62
S3	50	85.3	0.93	0.06	0.01	355	23	188	66
S4	50	74.2	0.98	0.01	0.01	360	23	182	67
S5	50	79.6	0.97	0.02	0.01	360	20	191	70
S6	50	70.7	0.97	0.02	0.01	358	23	186	67
E7	50	92.9	0.96	0.03	0.01	354	20	191	70
E8	50	61.1	0.96	0.03	0.01	1	21	180	70
E9	50	70.6	0.91	0.08	0.01	350	22	183	69
E10	50	71.3	0.92	0.07	0.01	0	16	189	74
E11	50	50.6	0.96	0.03	0.01	359	19	191	71
E12	50	70.7	0.96	0.03	0.01	359	21	184	69

Figures

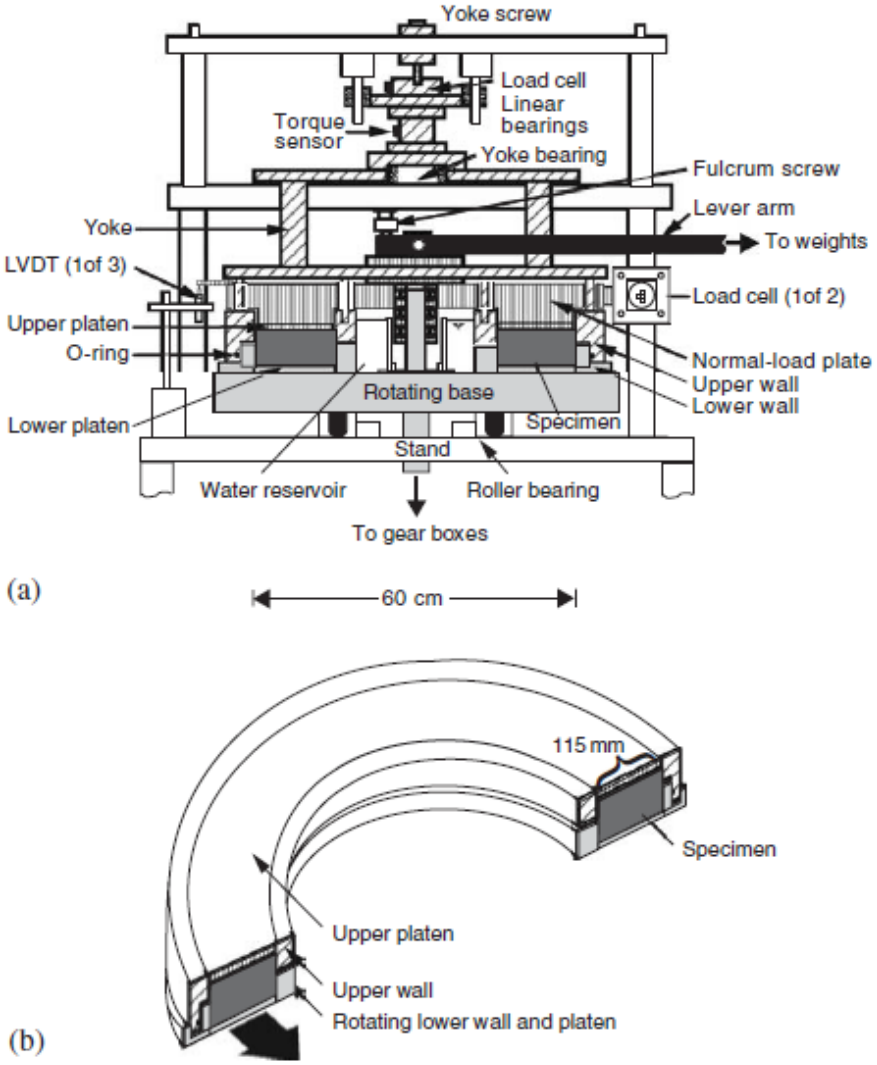

Figure 11. (a) Cross-section of ring-shear device and (b) detail of sample chamber. Solid light-gray components rotate (from Iverson et al., 1997).

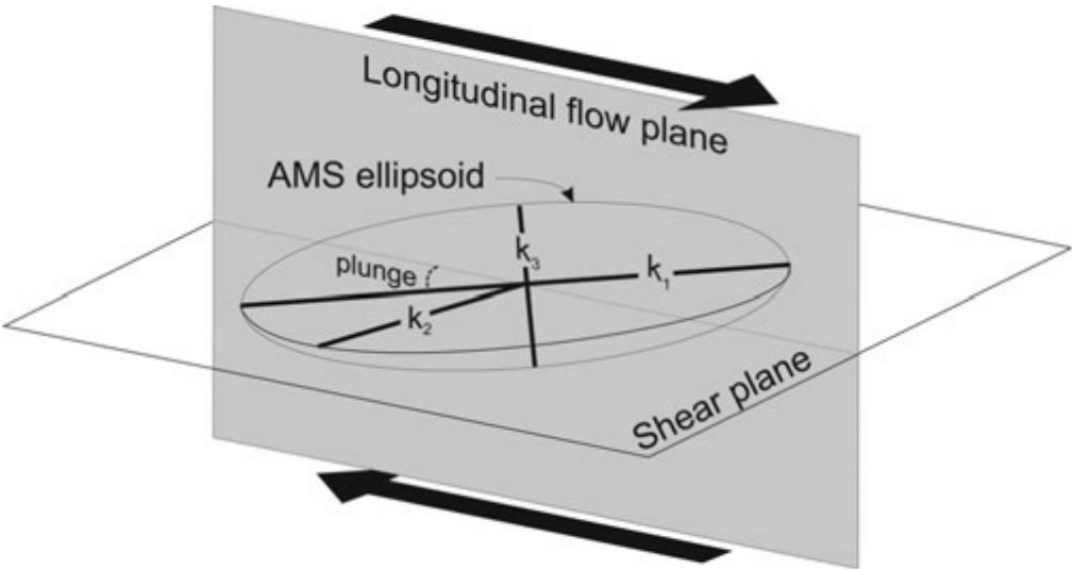

Figure 12. Anisotropy ellipsoid illustrating the three principal axes: maximum: K_1 , intermediate: K_2, and minimum: K_3 . In this case, the maximum axis of the ellipsoid is aligned parallel to the shear direction (from Shumway and Iverson, 2009)

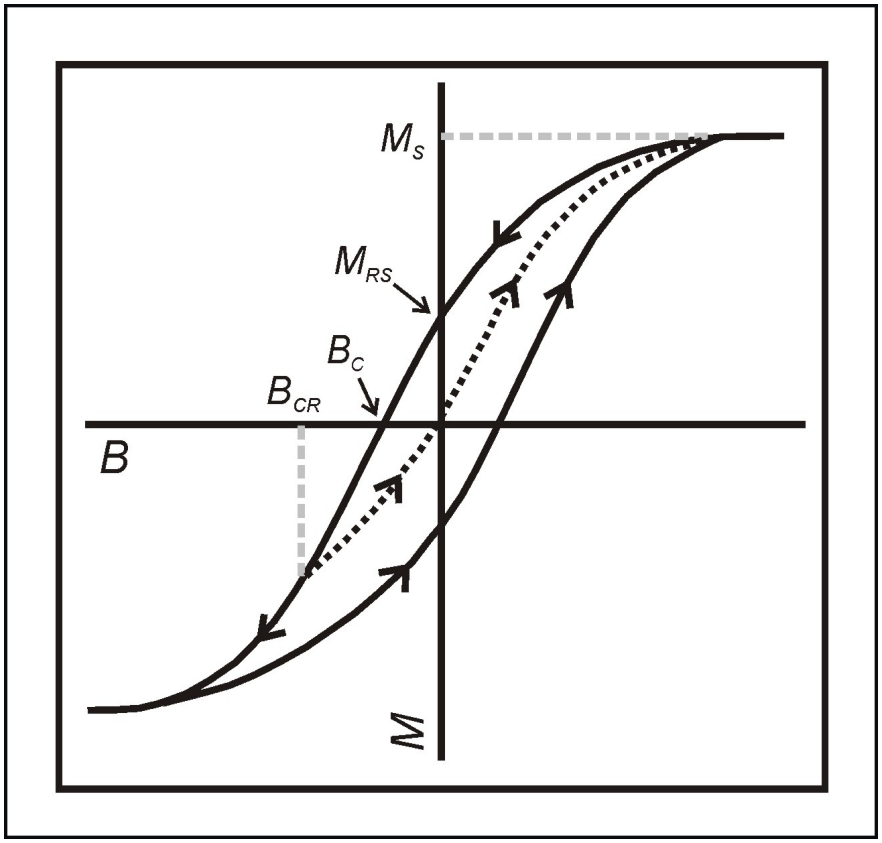

Figure 13. Idealized hysteresis loop where B and M are the applied and induced magnetic fields, respectively. M_S is the saturation magnetization, M_{RS} is the remanent saturation magnetization, B_{CR} is the coercivity of remanence, and B_C is the coercivity (from Hooyer et al., 2008.)

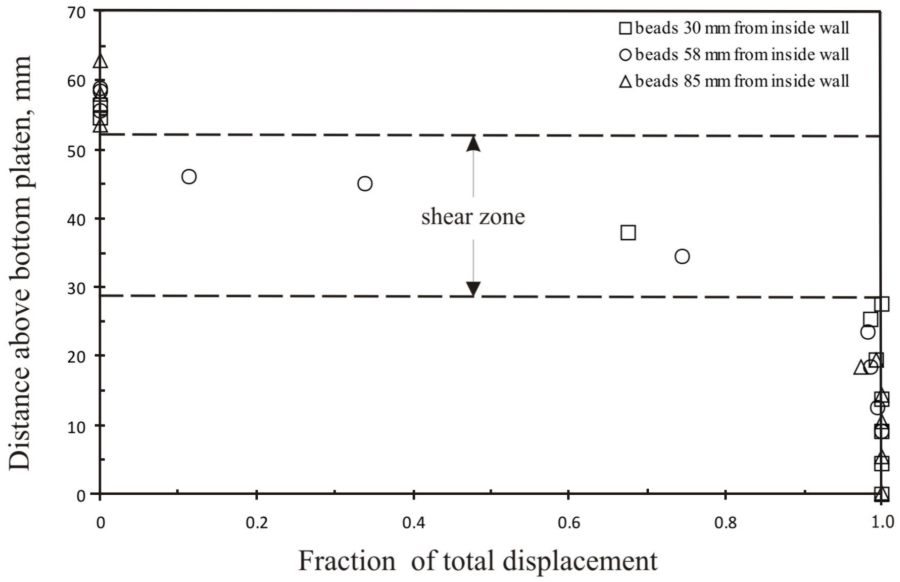

Figure 14. The vertical distribution of shearing displacement after an experiment, as determined by the displacement of beads, initially inserted in three vertical columns across the width of the till specimen.

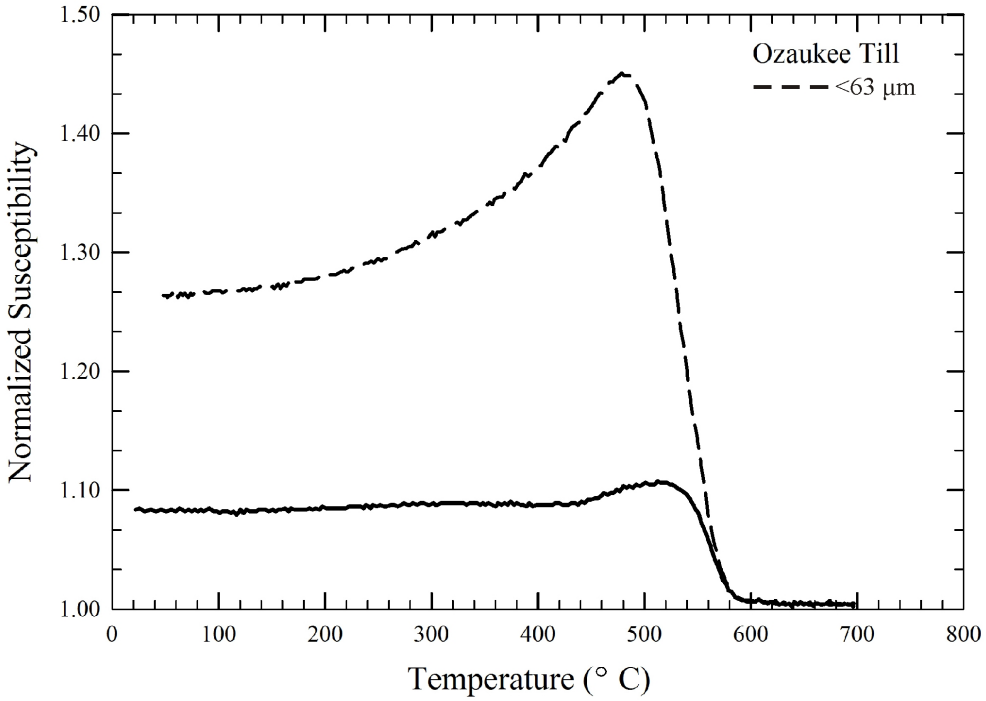

Figure 15. Magnetic susceptibility, normalized to susceptibility at 25° C, during heating of the fine fractions of the Ozaukee till. The dashed line represents the heating curve and solid line represents the cooling curve. Fine fractions were separated by mechanical sieving.

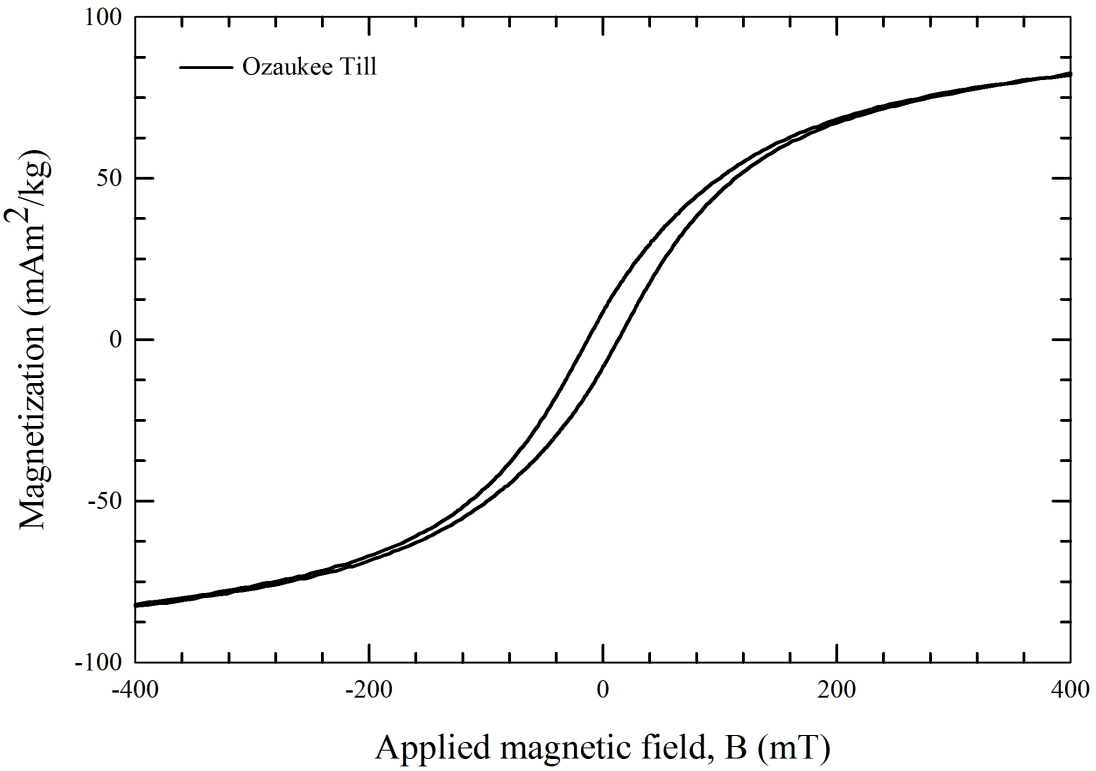

Figure 16. Hysteresis loop of representative sample of the Ozaukee till (high-field paramagnetic and diamagnetic contributions have been removed). The hysteresis parameters for fine fractions are listed in Table 2.

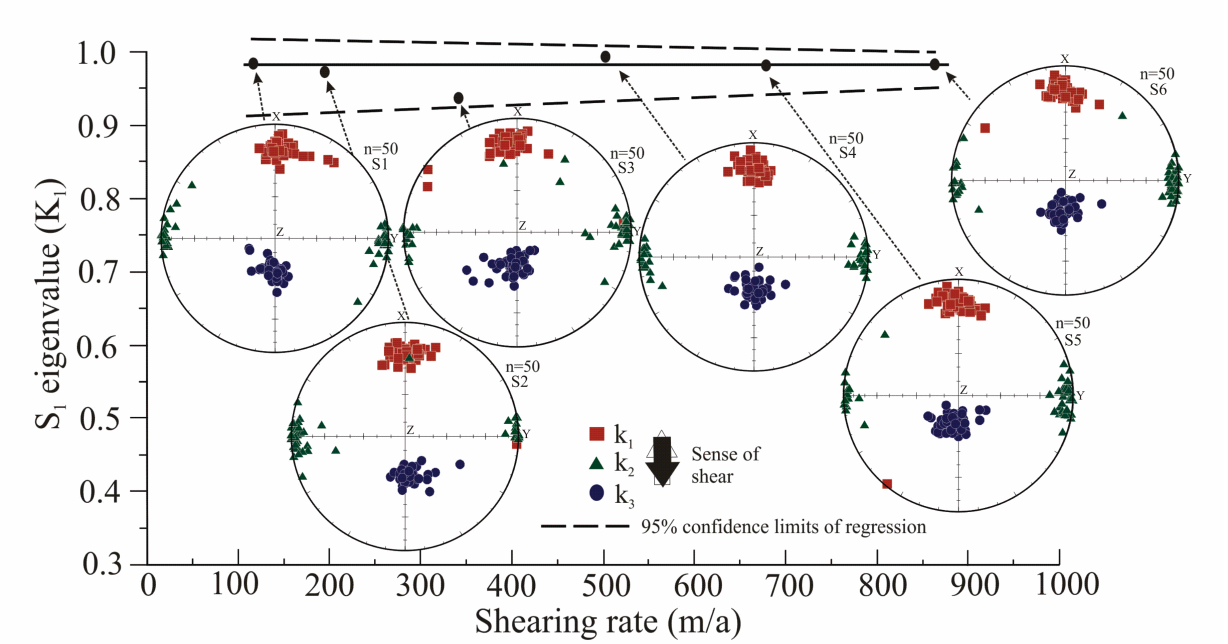

Figure 17. AMS fabric strength, based on K_1 orientations (maximum principal susceptibility), as a function of the shearing rate. Fabric strength, as characterized by S_1 values, has been fitted to a linear function and 95% confidence limits (dashed lines) computed on that basis. Lower hemisphere stereonets accompany each data point showing the maximum (squares), intermediate (triangles), and minimum (circles) principal susceptibilities. The direction of shearing is along the *x* axis and the sense of shearing in the stereonets is bottom north (white arrow) and top south (black arrow). Stereonet labels indicate experiment number (S1) and the number of samples (n).

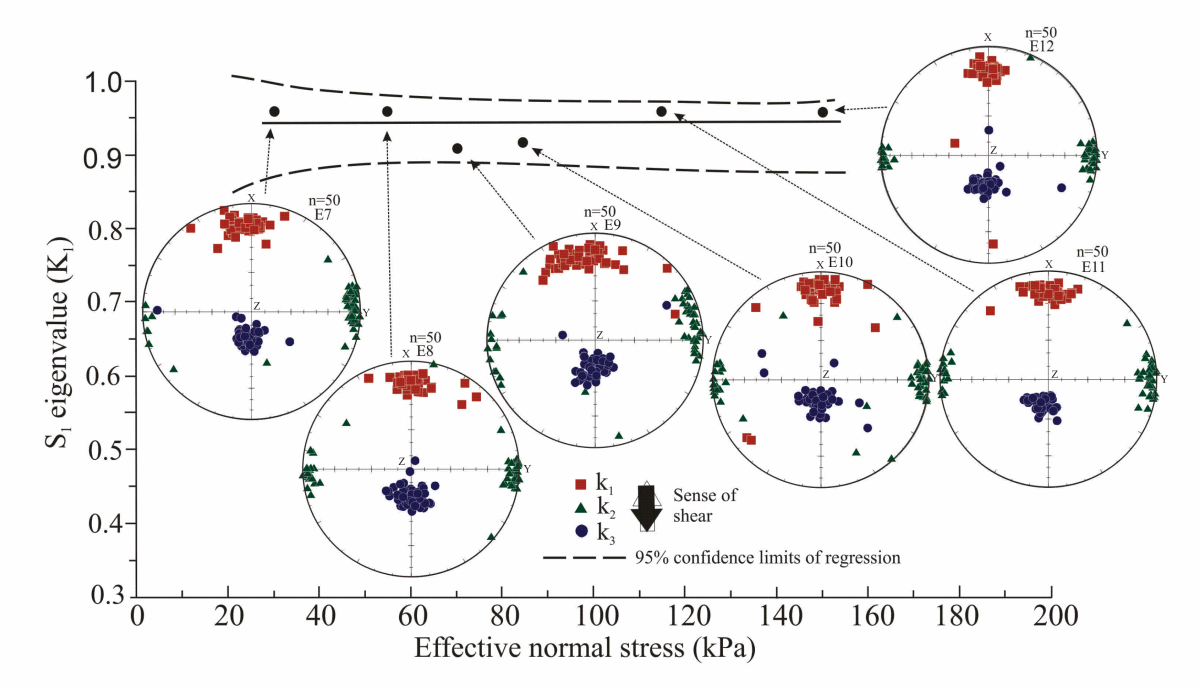

Figure 18. AMS fabric strength, based on K_1 orientations (maximum principal susceptibility), as a function of the effective normal stress. Fabric strength, as characterized with S_1 values, have been fitted to a linear function and 95% confidence limits (dashed lines) computed on that basis. Lower hemisphere stereonets accompany each data point showing the maximum (squares), intermediate (triangles), and minimum (circles) principal susceptibilities. The direction of shearing is along the *x* axis and the sense of shearing in the stereonets is bottom north (white arrow) and top south (black arrow). Stereonet labels indicate experiment number (E1) and the number of samples (n).

References

Alley, R.B., Cuffey, K.M., Evenson, E.B., Strasser, J.C., Lawson, D.E., Larson, G.J., 1997. How glaciers entrain and transport basal sediment: Physical constraints. Quaternary Science Reviews, v. 16, 1017-1038.

Benn, D.I., 1995. Fabric signature of subglacial till deformation, Breiðamerkurjökull, Iceland. Sedimentology, v. 42, 735-747.

Benn, D.I., 2002. Clast fabric development in a shearing granular material: implications for subglacial till and fault gouge-Discussion. Bulletin of the Geological Society of America, v. 114, 382-383.

Benn, D.I., Evans, D.J.A., 1996. The interpretation and classification of subglacially deformed materials. Quaternary Science Reviews, v. 15, 23-52.

Bertotti, G., 1998. Hysteresis in Magnetism: For Physicists, Material Scientists, and Engineers, Academic Press, Inc. 558 p.

Borradaile, G.J., Jackson, M., 2004. Anisotropy of magnetic susceptibility (AMS): Magnetic petrofabrics of deformed rocks in Magnetic Fabric: Methods and Applications, Geological Society of Publications, v. 238, 299-360.

Carr, S.J., Rose, J., 2003. Till fabric patterns and significance: particle response to subglacial stress. Quaternary Science Reviews, v. 22, 1415-1426.

Clarke, G.K.C., 1987b. Subglacial Till: a physical framework for its properties and processes. Journal of Geophysical Research, v. 92, 9023-9036. doi: 10.1029/JB092iB09p09023

Clarke, G.K.C., 2005. Subglacial Processes. Annual Review of Earth and Planetary Science. v. 33, 247-276.

Cuffey, K.M., Paterson, W.S.B., 2010. The Physics of Glaciers. Fourth edition. Oxford, Butterworth-Heinemann. pp. 255-269.

Dowdeswell, J.A., Sharp, M., 1986. Characterization of pebble fabrics in modern terrestrial glacigenic sediments. Sedimentology, v. 33, 699-710.

Dunlop, D.J., 2002. Theory and application of the Day plot (M_{rs}/M_s versus H_{cr}/H_c) 1. Theoretical curves and tests using titanomagnetite data. Journal of Geophysical Research, v. 107, 2056. doi:10.1029/2001JB000486.

Dunlop, D.J., Özdemir, D., 1997. Rock Magnetism: Fundamentals and Frontiers. Cambridge University Press, New York. 573 p.

Evans, M.E., Heller, F., 2003. Environmental Magnetism: Principles and Applications of Enviromagnetics, Elsevier, San Diego 295 p.

Fisher, U.H., Clarke, G.K.C., 1994. Ploughing of subglacial sediment. Journal of Glaciology, v. 40, 97-106.

Fowler, A.C., 2003. On the rheology of till. Annals of Glaciology, v. 37, 55-59.

Fuller, M.D., 1964. A magnetic fabric in till. Geological Magazine, v. 99, 233-237.

Gentoso, M.J., Evenson, E.B., Kodama, K.P., Iverson, N.R., Alley, R.B., Berti, C., Kozlowski, A., 2011. Exploring till bed kinematics using AMS magnetic fabrics and pebble fabrics: the Weedsport drumlin field, New York State, USA. Boreas, v. 41, 31-41. doi: 10.1111/j.1502-3885.2011.00221.x.

Hart, J.K., 1994. Till fabric associated with deformable beds. Earth Surface Processes and landforms, v. 19, 15-32.

Hart, J.K., Rose, K.C., Martinez, K., Ong, R., 2009. Subglacial clast behaviour and its implications for till fabric development: new results derived from wireless subglacial probe experiments. Quaternary Science Reviews, v. 28, 597-607.

Head, K.H. 1989. Soil Technician's Handbook. New York, etc., John Wiley and Sons. p. 83.

Hicock, S.R., 1991. On subglacial stone pavements in till. Journal of Geology, v. 99, 607-619.

Hindmarsh, R., 1997. Deforming beds: viscous and plastic scales of deformation. Quaternary Science Reviews, v. 16, 1039-1056.

Hooke, R. LeB., Hanson, B., Iverson, N.R., Jansson, P., Fischer, U.H., 1997. Rheology of till beneath Storglaciären, Sweden. Journal of Glaciology, v. 43, 172-179.

Hooyer, T.S., Iverson, N.R., 2000. Clast-fabric development in a shearing granular material: Implications for subglacial till and fault gouge. Geological Society of American Bulletin, v. 112, 683-692.

Hooyer, T.S., Iverson, N.R., Lagroix, F., Thomason, J.F., 2008. Magnetic fabric of sheared till: A strain indicator for evaluating the bed deformation model of glacier flow. Journal of Geophysical Research-Earth Surface, v. 113, 1-15. doi:10.1029/2001JF000757.

Iverson, N.R., 1999. Coupling between a glacier and a soft bed: II. Model results. Journal of Glaciology, v. 45, 41-53.

Iverson, N.R. 2010. Shear resistance and continuity of subglacial till: hydrology rules. Journal of Glaciology, v. 56, 1104-1114.

Iverson, N.R., Baker, R.W., Hooyer, T.S., 1997. A ring-shear device for the study of till deformation: Tests on a clay-rich and a clay-poor till. Quaternary Science Review, v. 16, 1057-1066.

Iverson, N.R., Hooyer, T.S., Baker, R.W., 1998. Ring-shear studies of till deformation: Coulomb-plastic behavior and distributed strain in glacier-beds. Journal of Glaciology, v. 44, 634-642.

Iverson, N.R., Hooyer, T.S., Fischer, H.S., Cohen, D., Moore, P.L., Jackson, M., Lappegard, G., Kohler, J., 2007. Soft-bed experiments beneath Engabreen, Norway: regelation infiltration, basal slip and bed deformation. Journal of Glaciology, v. 53, 323-340.

Iverson, N.R., Hooyer, T.S., Thomason, J.F., Graesch, M., and Shumway, J.R., 2008. The experimental basis for interpreting particle and magnetic fabrics of sheared till. Earth Surface Processes and Landforms, v. 33, 627-645.

Jeffery, G.B., 1922. The motion of ellipsoidal particles immersed in a viscous fluid. Proceedings of the Royal Society of London, v. 102, 169-179.

Jelinek, V., 1978. Statistical processing of anisotropy of magnetic susceptibility measured on groups of specimens. Studia Geophyisca Et Geodaetica, v. 22, 50-62.

Jelinek, V., 1981. Characterization of magnetic fabric of rocks, Tectonophysics, v. 79, 563-567.

Johnson, M.D., Schomacker, A., Benediktsson, I.O., Geiger, A.J., Ferguson, A., Ingólfsson, O., 2010. Active drumlin field revealed at the margin of Múlajökull, Iceland: A surge-type glacier. Geology, v. 38, 943-946.

Kamb, B. 1991. Rheological nonlinearity and flow instability in the deforming bed mechanism of ice stream motion. Journal of Geophysical Research, v. 96, 16585–16595. doi: 10.1029/91JB00946.

Lambe, T.W., Whitman, R.V., 1979. Soil mechanics. New York, John Wiley and Sons. p. 573.

Larsen, N.K., Piotrowski, J.A., 2003. Fabric pattern in a basal till succession and its significance for reconstructing subglacial processes. Journal of Sedimentary Research, v. 73, 725-734.

Larsen, N.K., Piotrowski, J.A., Christiansen, F., 2006a. Microstructures and microshears as proxy for strain in subglacial diamicts: implications for basal till formation. Geology, v. 34, 889-892.

Larsen, N.K., Piotrowski, J.A., Christoffersen, P., Menzies, J., 2006b. Formation and deformation of basal till during a glacier surge; Elisebreen, Svalbard. Geomorphology, v. 81, 217-234.

March, A., 1932. Mathematische theorie der regelung nach der korngestalt bei affiner deformation: Zeitschrift für Kristallographie, v. 81, 285-297.

Mark, D.M., 1973. Analysis of axial orientation data, including till fabrics. Geologic Society of American Bulletin, v. 84, 1369-1374.

Rathbun, A.P., Marone, C., Alley, R.B., Anandakrishnan, S., 2008. Laboratory study of the frictional rheology of sheared till. Journal of Geophysical, v. 113, 1-14, doi:10.1029/2007JF000815.

Rempel, A.W., 2009. Effective stress profiles and seepage flows beneath glaciers and ice sheets. Journal of Glaciology, v. 55, 431-443.

Reynolds, O., 1885. On the dilatancy of media composed of rigid particles in contact, with experimental illustrations. Philosophical Magazine, v. 20, 469-481.

Shumway, J.R., Iverson, N.R., 2009. Magnetic fabrics of the Douglas till of the Superior lobe: exploring bed-deformation kinematics. Quaternary Science Reviews, v. 28, 107-119.

Skempton, A.W., 1985. Residual strength of clays in landslides, folded strata, and the laboratory. Gétechnique, v. 35, 3-18.

Tarling, D.H., Hrouda, R., 1993. The Magnetic Anisotropy of Rocks, Chapman and Hall, London. 218 pp.

Thomason, J.F., Iverson, N.R., 2006. Microfabric and microshear evolution in deformed till. Quaternary Science Reviews, v. 25, 1027-1038.

Truffer, M., Harrison, W.D., 2006. In situ measurements of till deformation and water pressure. Journal of Glaciology, v. 52, 175-182.

Truffer, M., Echelmeyer, K.A., Harrison, W.D., 2001. Implications of till deformation on glacier dynamics. Journal of Glaciology, v. 47, 123-134.

Tulaczyk, S., Kamb, W.B., Engelhardt, H.F., 2000a. Basal mechanics of Ice Stream B, West Antarctica. Till mechanics, Journal of Geophysical Research, v. 105, 463-481. doi: 10.1029/1999JB900329.

Chapter3: Application of magnetic fabrics in dirty ice: a new fabric proxy for ice cores?

William R. Jacobson, Jr.*

Department of Geosciences, University of Wisconsin-Milwaukee, Milwaukee, 53201, USA

Abstract

Small cores of dirty ice obtained in veins near the terminus of the Flàajökull Glacier, Iceland have been investigated using two fabric methods, anisotropy of magnetic susceptibility (AMS) and ice c-axis fabrics. Differences between these two fabric proxies and their importance to the history of deformation are demonstrated. Results from these methods suggest that the magnetic properties of the insoluble impurities (solid mineral particles) in the ice may provide a better strain gauge than c-axis fabrics, which revealed a multi-maximum girdle, suggesting they have been reset by recrystallization. The magnetic proxy indicated a bulk three-dimensional strain signature (K_1, K_2, and K_3) of subvertical shear consistent with field relations. Moreover, variations in grain sizes and textural features (e.g. nucleated grains, bulging of grain boundaries, boundary pinning by particles and slip bands) imply that intracrystalline deformation was inhomogeneous and resulted from a combination of pure and simple shear. The veins were most likely formed by injection from an overpressured basal water system into crevasses followed by *in situ* freezing and deformation.

---

*Author.
Email address: wrjjr@uwm.edu (W.R. Jacobson, Jr.)

1. Introduction

The magnetic properties of microparticles in glacial ice commonly have been used as an indicator capable of documenting changes in dust sources and atmospheric transport processes (Steffensen, 1997; Lanci et al., 2004; ZongQi et al., 2011). However, research on magnetic particle *fabrics* (orientation of magnetic inclusions) in relation to glacier dynamics is limited (Fleming et al., 2013).

A comparison between two fabric methods is presented using the classical Rigsby stage technique for measuring c-axis fabrics as indicators of ice deformation (Langway, Jr., 1958; Rigsby, 1960; Lipenkov et al., 1989; Alley, 1992; Tison et al., 1994a; Alley et al., 1995; also see Diprinzio et al., 2005; Wilson and Peternell, 2011; Montagnat et al., 2014; Fitzpatrick et al., 2014), and magnetic fabrics as deformation indicators, applied to dirty-ice veins from a temperate glacier in southeast Iceland. Based on the vein characteristics and field relationships, and comparisons to other studies (Ensminger et al., 2001; Lovell et al., 2015), the debris was injected from the bed near the ice front, but then moderately deformed. This hypothesis is supported by the magnetic and c-axis fabric analyses. The area is well-suited to a study utilizing magnetic anisotropy owing to the terrane, which has an abundance of iron-bearing minerals.

2. Method and materials

Magnetic susceptibility measurements were performed on 84 samples from the terminus region of Flàajökull glacier in southeast Iceland (Fig. 19). The samples were taken from two veins enriched in debris (FL-1 and FL-2). Figures 20a and 20b show the vein *in situ* after sampling.

Samples were obtained with the use of a portable high torque hammer drill (Milwaukee Fuel M18 XC) with a 29 mm diameter x 25 mm long tungsten carbide-tipped hole cutter. Core sampling was completed by orienting the samples relative to magnetic north, and marking one side of each core with red dye prior to extraction from the vein. Core samples were drilled parallel to the foliation. Red dye was added to highlight the orientation mark after drilling of the core.

In addition to the core samples, a debris-laden block (18 cm x 15 cm x 20 cm from FL-1) was cut out via chainsaw for c-axis measurements. Several cavities were excavated in the glacier in which to store samples temporarily. The specimens were transported in a cooler packed with glacier ice to a local freezer ~13 km away. For transit from Iceland to the US, samples were packed in a high-quality cooler (YETI) with 34 kg of pelletized dry ice. Upon arrival in the US, the samples were immediately transported to the University freezer. The specimens arrived in ideal condition for evaluation.

For magnetic analyses, ice core specimens were cut while still in the laboratory freezer into pieces ~22 mm long (Fig. 21) (~10.5 cm^3) in order to fit them into the test harness of the susceptibility bridge (Fig. 21). Sawing was done manually, with a nonmagnetic beryllium-copper blade, and care was taken to avoid melting or contamination. No other cleaning or preparation was applied.

Debris concentrations were measured by cutting three relatively equal-sized blocks of dirty ice (18 cm x 15 cm x 20 cm), in the field, melting them in polyethylene bags, waiting several days to allow particle settling, and then decanting the water and measuring the volume using a conventional plastic graduated cylinder. The debris was later dried and weighed in the laboratory, before being used in the high-temperature susceptibility and hysteresis experiments.

Thin sections were prepared from the FL-1 vein with a conventional band saw, and manually shaved to ~0.5-1 mm (first-order to low second-order maximum birefringence colors). Owing to the debris content, the ice did not bond well to the slides by freezing. It was found through trial and error that chilled cyanoacrylate glue was the most effective technique for this purpose (Daley and Kirby, 1984; Tison, 1994b). Mean thin section dimensions were ~50 x 75 mm. Thin sections were both cut parallel (XZ plane) and normal to the foliation (YZ plane). Eleven were cut parallel to the foliation and five normal to it. C-axis orientations of a total 180 grains were measured in those sections cut parallel to the foliation, and 79 grains were measured normal to it. Thin sections were photographed using a point-and-shoot Fujifilm XP Freeze Proof camera for studying grain-scale features. The thin section slides were scanned, producing high-resolution images of each sample.

C-axis measurements were conducted on a Rigsby universal stage (Langway, Jr., 1958) and plotted on an equal-area net using 1 percent area contour with refraction corrections supplied by Kamb (1959). C-axis parameters such as the orientation strengths (*R*) and fabric shapes (eigenvalues) were calculated according to Adam (1989). When c-axes are randomly distributed, R = 0, and when they are clustered in a single maximum, R = 100%. The isotropy index of Hockey (1970) was also calculated based on ratios of eigenvalues; I = 0 indicates clustering while I = 1 indicates an isotropic distribution.

High-temperature susceptibility (HTS) and hysteresis experiments were conducted to determine the magnetic mineralogy and grain size. These experiments were performed on a bulk sample containing grain sizes ranging from clay and silt < 63 μm to sand > 63 μm. The high-temperature susceptibility was measured on an AGICO MF*K1*-FA Kappabridge coupled with a CS4 Furnace Apparatus. The debris was step-heated from 25 to 700° C and cooled back to 25°C

while measuring the bulk susceptibility. The susceptibility is typically reduced when the unblocking or Curie temperature is reached (destabilization of magnetic moments due to thermal energy); this helps in identifying the mineralogy of the magnetic particles. Hysteresis experiments were performed at the Institute for Rock Magnetism at the University of Minnesota using a 2 Hz vibrating sample magnetometer. Hysteresis loop parameters from these experiments were used to help constrain particle size (Dunlop, 2002 (see Bertotti, 1998 for more complete information on the theory of hysteresis of ferrimagnetic materials).

Principal directions of magnetic susceptibility K_1, K_2, and K_3 were measured using the AGICO MF*K1*-FA Automatic Kappabridge to determine. The magnetic susceptibility was determined by inserting the specimen into a compensating pick-up coil. Once the bride re-balanced itself, its pre-programmed algorithm combined the measurements in three-perpendicular planes plus one bulk value to complete the susceptibility measurement. The sensitivity of the pick-up coil at 976 Hz, 400 A/m peak is 2×10^{-8} (SI). For more detailed theory of the Kappabridge system, see Jelinek (1978). The measurements were carried out as quickly as possible (~ 90 s) to avoid warming the ice as this may cause a physical reorientation of the particles (Lanci et al., 2012).

The principal susceptibilities K_1, K_2, and K_3 typically are visualized with a susceptibility ellipsoid. As discussed by Hooyer et al. (2008), in deformed sediments such ellipsoids commonly are observed to arise from the shaped-preferred orientations of magnetite, maghemite or other strongly magnetic particles, which have magnetic fields aligned with their shape elongations. Figure 22 shows an example of a susceptibility ellipsoid in simple shear. The magnetic fabric in many cases can be measured more accurately and repeatably, and with higher spatial resolution, than the shape orientation of the particles.

The susceptibility ellipsoid was characterized following Tarling and Hrouda (1993) and Borradaile and Jackson (2004) with the percent total anisotropy $P\%$ (equation 1), the shape parameter T_j, (equation 2), and the corrected degree of anisotropy P_j, (equation 3; Jelinek, 1981).

$$P\% = 100\left(\frac{k1-k3}{kv}\right), \quad (1)$$

$$T_j = \frac{\ln\left(\frac{k2}{k3}\right) - \ln\left(\frac{k1}{k2}\right)}{\ln\left(\frac{k2}{k3}\right) + \ln\left(\frac{k1}{k2}\right)} \quad (2) \text{ and}$$

$$P_j = \exp\left(\sqrt{2\left[\left(\ln\left(\frac{k1}{k}\right)\right)^2 + \left(\ln\left(\frac{k2}{k}\right)\right)^2 + \left(\ln\left(\frac{k3}{k}\right)\right)^2\right]}\right) \quad (3)$$

The ellipsoid is prolate if $-1 \leq T_j < 0$, and oblate if $0 < T_j \leq 1$. If the ellipsoid is a sphere, $P_j = 1$, and the value of P_j will increase with increasing anisotropy.

The method of Mark (1973) was used to analyze the AMS fabric data. The fabric strength and direction were determined using eigenvectors (V_1, V_2, and V_3), and corresponding eigenvalues (S_1, S_2, and S_3), respectively. The S_1 eigenvalue represents the degree of clustering of K_1 orientations around the V_1 eigenvector. An S_1 eigenvalue of 0.33 indicates random alignment of K_1 orientations, whereas, an S_1 eigenvalue of 1.0 indicates K_1 orientations that are perfectly aligned.

3. Results

3.1 Magnetic Mineralogy and Grain Size

Debris concentrations and susceptibilities are given for FL-1 and Fl-2 in Tables 5 and 6. The volume susceptibilities are moderate despite low debris concentration, likely because of the high concentration of ferromagnetic minerals eroded from the surrounding volcanic terrane.

The dependence of magnetic susceptibility on temperature is shown in Figure 23; both samples show a reduction in susceptibility at a temperature of ~590-600° C, consistent with the Curie temperature of magnetite (Bertotti, 1998).

Hysteresis parameters also provide information on the magnetic mineralogy and grain size (Evans and Heller, 2003). The low coercivity of remanence (B_{CR}), (Table 7) and the field saturation (M_s) at 200 mT indicate that most of the particles are magnetite (Fig. 24). Lanci et al. (2008) showed that the corecivity of remanence and field saturation using Isothermal Remnant Magnetization (IRM) aid in differentiating magnetic minerals contained in polar ice (e.g. magnetite versus hematite) (see Figure 3). Typically, the saturation magnetization expected for magnetite is about 0.2T, versus the higher saturation of ~3T for hematite.

Particle size was evaluated based on hysteresis ratios (M_{RS}/M_s and B_{CR}/B_C) calibrated with experimental data from Dunlop (2002). The values of the ratios indicate a mean magnetite grain size of ~15 μm (see Dunlop, 2002-Figure 8), which falls within the pseudo single domain (PSD) range. Hooyer et al. (2008) found similar ratios for a Wisconsin-age basal till that they mechanically sheared in the laboratory.

In conclusion, the HTS and hysteresis experiments indicate that magnetite is the dominant magnetic mineral in the ice and that these particles are primarily silt-sized or smaller.

Other magnetic minerals and grain sizes might be present; however, they are secondary compared to the magnetite silt signal.

3.2 Anisotropy of Magnetic Susceptibility (AMS)

Calculations of the shape parameter (T_j) of the AMS ellipsoids indicate a triaxial shape for FL-1 and oblate for FL-2, following Hrouda (1982). The percent total anisotropy (*P%*) averaged 2.5 ± 1.9% and the shaped parameter (*Tj*) averaged 1(Table 6).

AMS fabrics from the specimens are plotted on equal area stereonets (Fig. 25). Fabrics from FL-1 clearly show triaxial ellipsoids. The magnetic ellipsoid is subvertically oriented, as shown by the plunge of 77° of the mean V_1 eigenvector (Table 8). In contrast, FL-2 shows oblate ellipsoids with a scattered pattern and with a mean plunge of 65° for the V_1 eigenvector. The FL-2 fabrics are not as strong, perhaps indicating smaller cumulative strain. The well-developed susceptibility clusters of FL-1 represent a bulk strain signature of subvertical shear, perhaps also with inheritance from emplacement, as discussed below.

4. Ice c-axes

Results of the fabric analysis from FL-1 vein are presented in Figure 26. Following Cuffey and Paterson (2010, and references therein) these fabrics and the associated textures are not completely diagnostic, but likely indicate that some deformation with recrystallization has occurred to create multi-maximum girdle fabrics. C-axis orientations from both planes (XZ // to foliation and YZ ⊥ foliation) exhibited similar eigenvector angles of 78º and 70º, respectively.

5. AMS relationships to c-axis development from FL-1 vein

The rate at which crystals rotate (how quickly fabric evolves) depends primarily on strain rate, which is a function stress, temperature, impurity content and crystal orientations (Kennedy et al., 2013). The strain rate (300 seconds per year for temperate valley glacier) has a strong influence on the how the c-axes and the K_1 susceptibility axes react under varying strain rate conditions over time. In this study sub-vertical shearing is clearly shown by eigenvector plunge of the maximum K_1 susceptibility axis (77º). The eigenvector plunge (78º) measured from the c-axis (e.g. YZ shear plane) rotated approximately toward the vertical. The relative orientation and strength of these eigenvectors depends on the history and state of deformation.

Fleming et al. (2013) showed that sub-horizontal shearing of cold dirty basal ice from a surging glacier in Svalbard develops a magnetic anisotropy pattern where the minimum susceptibility axes (K_3) are sub-vertical, defining the pole to the magnetic foliation and shear plane ($K_1 – K_2$) and the K_1 susceptibility axes plunge mildly up-glacier. Fleming et al. (2013) did not measure the c-axis orientations but it is likely that the c-axes would show a strong correlation with minimum susceptibility axes (K_3). Grain shape elongations also appeared to show a good correlation with the plunge of the maximum K_1 susceptibility and c-axes.

6. Grain scale evidence

The debris bands studied here are dominated by debris-laden ice, but with some layering parallel to the debris faces and a few regions having low concentrations. Careful study of our sections (e.g. Figure 27c and 27b), shows features that probably represent bulging grain boundaries and the nucleation of new grains. Evidence of boundary pinning was also observed in thin section (Figure 27d).

Ice crystal sizes in the dirtier ice were too small for c-axis analyses, so the results presented here are not fully representative of the ice present, being restricted to coarse-grained layers (Figure 28) or large crystals embedded in finer-grained matrix (Figure 29). These large crystals may have several origins, possibly including frazil crystals entrained in the upwelling water that filled the veins, or crystals form by "recovery" grain-growth following deformation.

Our sections bear some resemblance to ice from the cold (-17° C) dirty ice of Taylor Glacier, Antarctica (Samyn et al., 2008). Similar to our situation, they reported crystal ribbons in debris-bearing ice, which they attributed to discontinuous grain growth, and which tended to show c-axis orientations not unlike ours and which may arise from migration recrystallization (Kamb, 1959; Anderton, 1974; Gow and Williamson, 1976; Duval and Castelnau, 1995; Cuffey and Paterson, 2010).

Slip bands and a possible tilt boundary were also observed (Figure 30). Gold (1966) found similar observations in deforming ice in the laboratory where the ice was deformed in compression by 5% at -9° C. Others have also reported deformation features in the form of slip bands and tilt boundaries on the surfaces of ice grains (Kipfstuhl and others, 2006). Taken together with c-axis fabrics, these data suggest that some deformation has occurred in the vein ice after emplacement.

7. Paleoclimatic implications

The magnetic fabric approach is still in its infancy and may prove to be fruitful. This technique can be applied to the folded dirty ice from the base of the Greenland Ice Sheet (e.g. GISP2, GRIP, Dye 3 and Camp Century). Previous workers (Alley et al., 1997; Gow et al., 1997; Jacobson and Waddington, 2004; Bender et al., 2010) have verified disturbances in ice

layering (e.g. crystal striping and overturning) and have semiquantitatively assessed the mixing rate between the clean ice and the dirty ice. Furthermore, the dirt in these layers may provide a magnetic proxy for evaluating small deviations in shear strain directions, which may be vital for understanding the disrupted stratigraphy and its impact on the climatic record. Also merging of AMS data with the microstructural features and c-axis orientations would provide insight into the connections between these deformation elements.

Another consideration to address is that ice fabrics have a limited value for reconstructing strain because of recrystallization. Given this tenet, the insoluble mineral particles will be a better indicator of the bulk strain history.

Ensminger et al. (2001) of the Matanuska Glacier found that the dirty ice bands resulted from injection of turbid waters into basal crevasses; however, the Flàajökull veins clearly suffered more shear deformation after refreezing. In some circumstances debris will affect the deformability of ice, often softening it (Alley et al., 1986b; Paterson, 1991; Song et al., 2008). Thus, it is not surprising that the injected debris-rich layers served as shear zones. Furthermore, there is a high probability that shearing caused the fineness of the ice crystals; however, the effect of micro-inclusions on grain boundary sliding and grain growth cannot be ruled out (Herron and Langway, Jr., 1979). Further support for this was demonstrated by Baker and Gerberich (1979) who found that dispersed-solid inclusions (0.1mm) decrease the average ice-crystal size by inhibiting growth during recrystallization (see Figure 3). Cahn (1965) has also observed this phenomenon during recrystallization experiments from metals.

7. Conclusions

Both fabric techniques described in this work, optical and magnetic, have been successfully applied to two dirty ice veins located on the ice-margin of the Flàajökull Glacier, Iceland. The following preliminary results can be drawn from this study:

- HTS and hysteresis measurements indicate a magnetic mineralogy that is silt-sized or smaller. Magnetite is the dominant signal given the resultant magnetic properties.
- Insoluble inclusions from veins FL-1 and FL-2 indicate a cumulative strain signature of simple shear, which is reflected in the subvertical AMS ellipsoid orientation. However in FL-2, the lack of clustering of the K_1 susceptibilities suggests that the strain was insufficient to develop a fabric.
- Particle inclusions behaved as passive markers and are reliable indicators of strain. Most of the particles appeared along grain boundaries implying that the fabric formed primarily from slip along the grain boundaries during shear deformation.
- Recrystallized ice grains from the textural analysis (e.g. ribbons and elongated grains) suggest two shearing directions, which probably developed during intracrystalline deformation; subvertical and lateral slip (in the plane of foliation XZ).
- The mean K_1 plunge of 77° in samples FL-1 shows a strong correlation with the orientation of long axes of the recrystallized ice grains observed in thin section.
- Evidence of grain scale processes (e.g. nucleated grains, bulging of grain boundaries, boundary pinning by particles, slip bands and a tilt boundary) implies that intracrystalline deformation was inhomogeneous and resulted from migration recrystallization.

- The distribution of c-axes also suggests a deformation pattern characteristic of migration recrystallization, which requires high stresses and temperatures. This fabric likely developed from a combination of pure shear and simple shear resulting in a composite fabric.
- Foremost, this is the first study in which c-axis fabrics have been coupled with the magnetic fabric method.

Acknowledgements

I dedicate this paper to my mentor Thomas S. Hooyer who is battling a serious illness. I thank James Amato and Emily Joynt for their help and support in the field. Use of facilities at the University of Wisconsin-Milwaukee and Institute of Rock Magnetism (IRM) at the University of Minnesota is gratefully acknowledged. Special thanks to Kjartan Masson for logistical operations and transport of the dry ice. I wish to express my appreciation to the Foss Hotel Vatnajökull in Iceland for use of their commercial freezer.

Tables

Table 5. Debris Concentrations of the Fláajökull Ice Veins[a]

	Water (mL)	Debris weight (g)	Weight %	Mean weight %
Fl-1a	1759	81.0	4.6	9.7
Fl-1b	1847	264.6	14.3	
Fl-1c	1682	175.4	10.4	
Fl-2a	1134	70.0	6.1	5.3
Fl-2b	1883	86.8	4.6	
Fl-2c	1389	74.9	5.3	

[a]Debris concentration is measured in weight percent and averaged over three samples. Weight percent is calculated as : $\frac{weight\ of\ debris}{weight\ of\ water} * 100$

Table 6. AMS Data from the Debris-laden Veins

Site	n	K_v^a (μ SI)	K_1^a (μ SI)	K_2^a (μ SI)	K_3^a (μ SI)	P_j^a	T_j^a	P%[a](%)
FL-1	48	552±116	552±122	563±117	542±109	1.043±.152	1.69±0.24	1.7±1.8
FL-2	36	437±113	446±118	438±114	427±108	1.033±.152	0.31±0.19	3.2±1.6

[a]Values represent the mean and ± 1 standard deviation

Table 7. Hysteresis Loop Parameters for the Bulk Clay and Silt (<63μm) to sand (>63μm) Fractions of the Melted Debris

	M_{RS} (Am^2/kg)	M_S (Am^2/kg)	B_c (mT)	B_{CR} (mT)	M_{RS}/M_S	B_{CR}/B_C
FL-1	.2827	1.58	12.8	36.3	.178	2.82
FL-2	.3537	2.03	11.2	32.1	.174	2.85

Table 8. AMS Fabric Data

					Eigenvector V_1(°)				Eigenvector V_3(°)			
							95% Confidence Ellipse				95% Confidence Ellipse	
Site	*n*	S_1	S_2	S_3	Trend	Plunge	Maximum Angle	Minimum Angle	Trend	Plunge	Maximum Angle	Minimum Angle
FL-1	48	0.67	0.24	0.09	155	77	12.8	5.3	277	9	8.6	8.2
FL-2	36	0.60	0.21	0.19	156	65	16.7	14.5	25	16	14.7	9.9

Table 9. Statistical Ice Fabric Parameters[a] from the Fláajökull Glacier

	R (%)	S_3	S_2	S_1	I
FL-1a	38.45	0.53	0.25	0.22	0.41
FL-1b	40.37	0.51	0.28	0.21	0.41

[a]These parameters were calculated from 180 crystals randomly selected from 11 sections from FL-1a (parallel to foliation) and from 79 crystals from 5 sections from FL-1b (perpendicular to foliation).

Figures

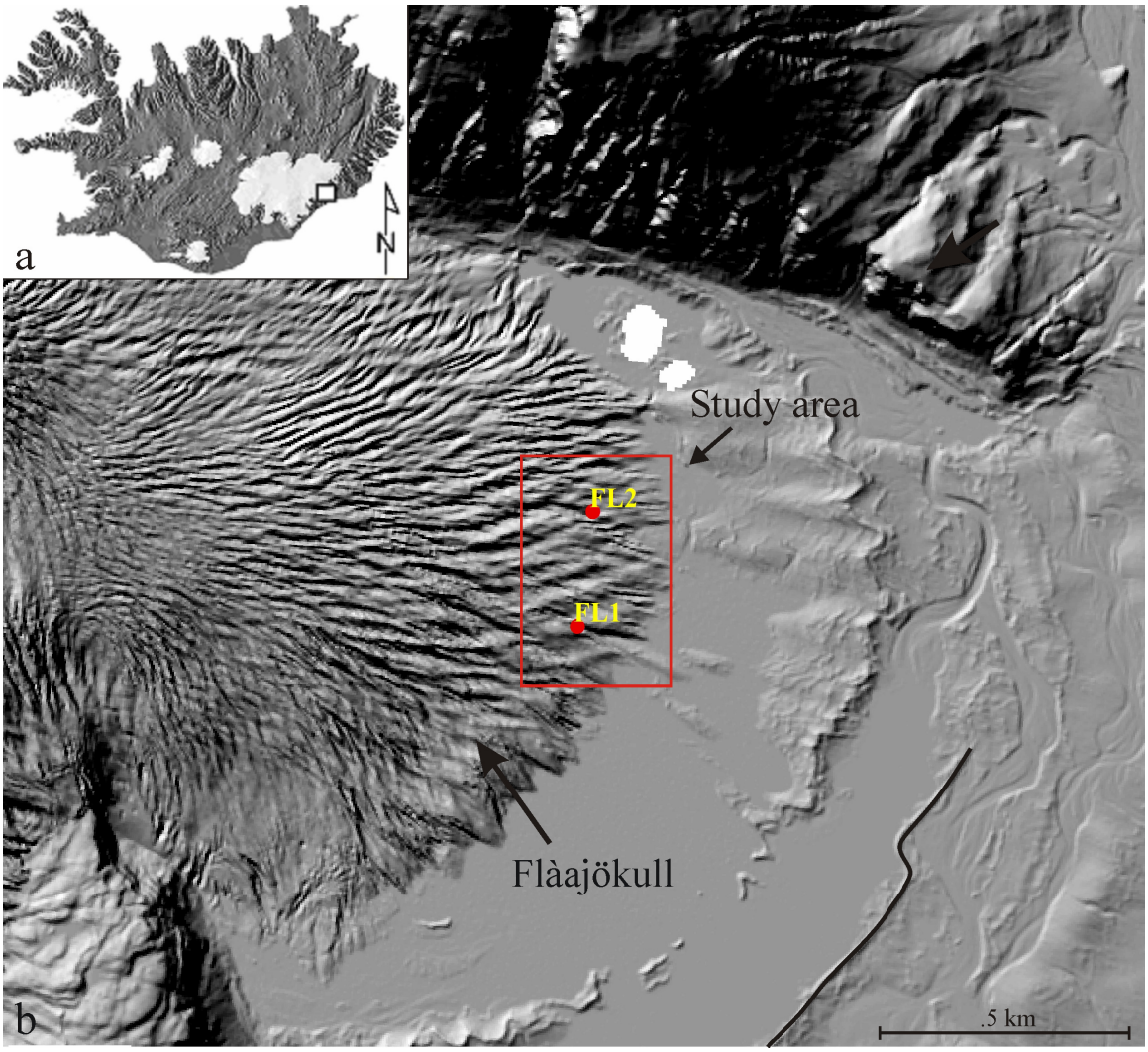

Figure 19. (a) Location of Vatnajökull ice cap (black square) at the south-eastern margin of the Flàajökull glacier (b) A LiDAR hillshade model from 2010 showing the ice margin and location sites (courtesy of the Icelandic Meteorological Office). Extensive glacier retreat has occurred since 2010. Ice flow is from the NNW to SSE. Icelandic man made rock levees are marked with black lines.

Figure 20a. An oblique view of the FL-1 ice vein looking north, note the drill holes in the vein and the well-defined boundary between the dirty ice and the annealed ice can be observed.

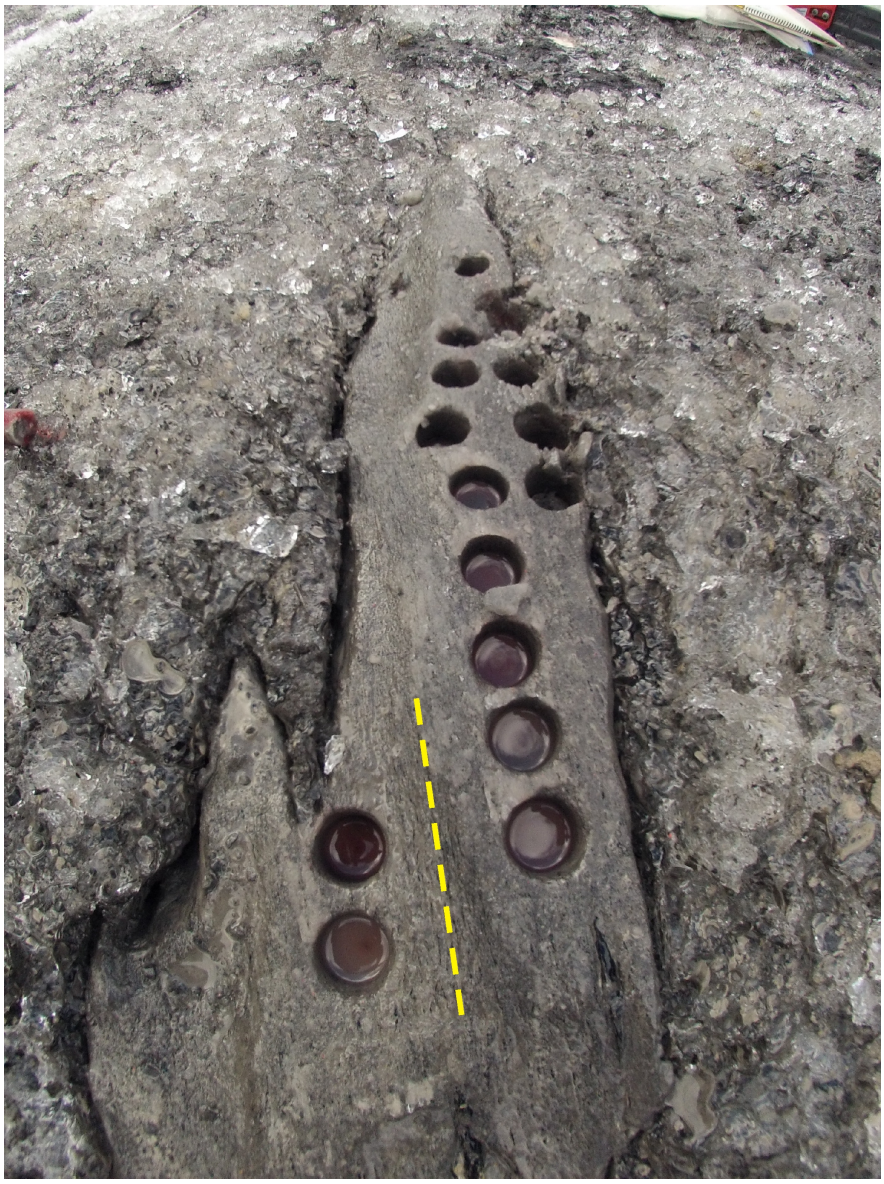

Figure 20b. Close-up view of the vein. Shearing was observed along the vein boundary where the dirty ice is interleaved with the clean ice, forming irregular folds. A well-defined foliation (subvertical) was also observed as indicated from the dashed line in vein.

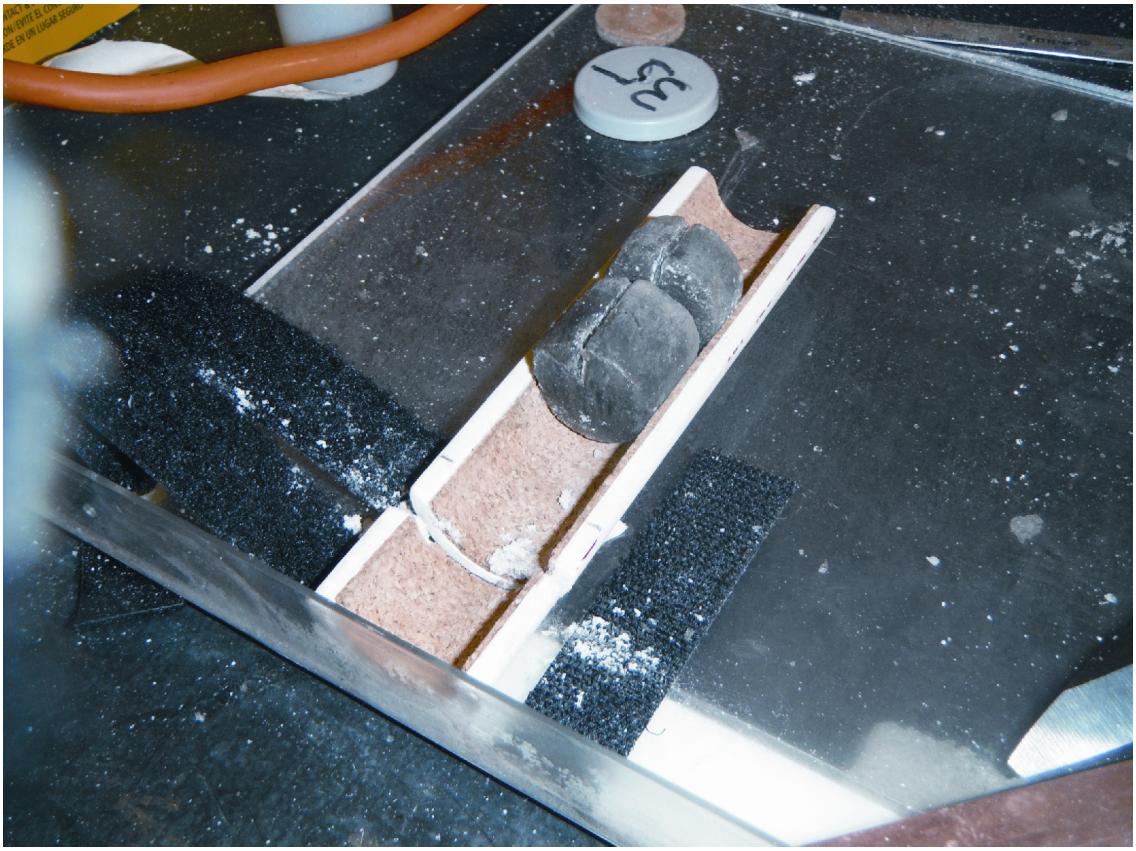

Figure 21. An oriented ice core sample shown after cutting. Both sections of the sample were used in the AMS analysis.

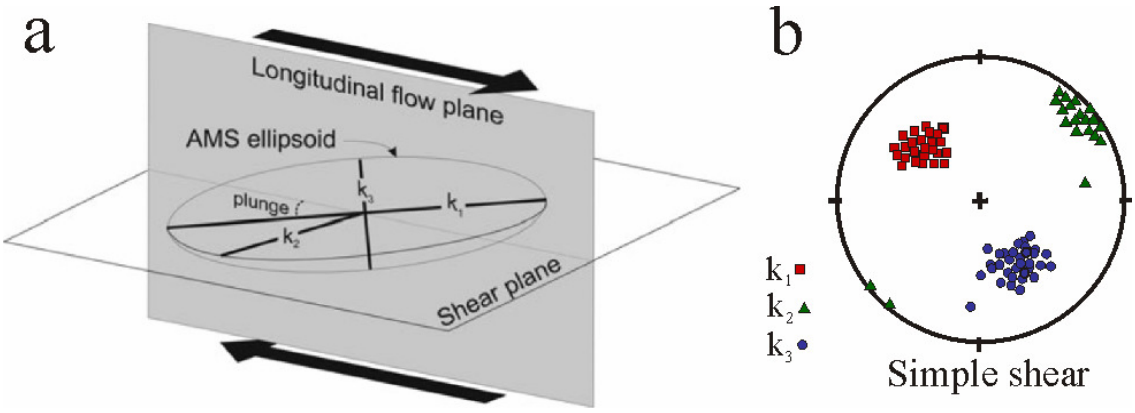

Figure 22. (a) Anisotropy ellipsoid illustrating the three principal axes: maximum: K_1, intermediate: K_2 and minimum: K_3 (from Shumway and Iverson, 2009). (b) Stereoplot with clustering of principal susceptibilities in simple shear.

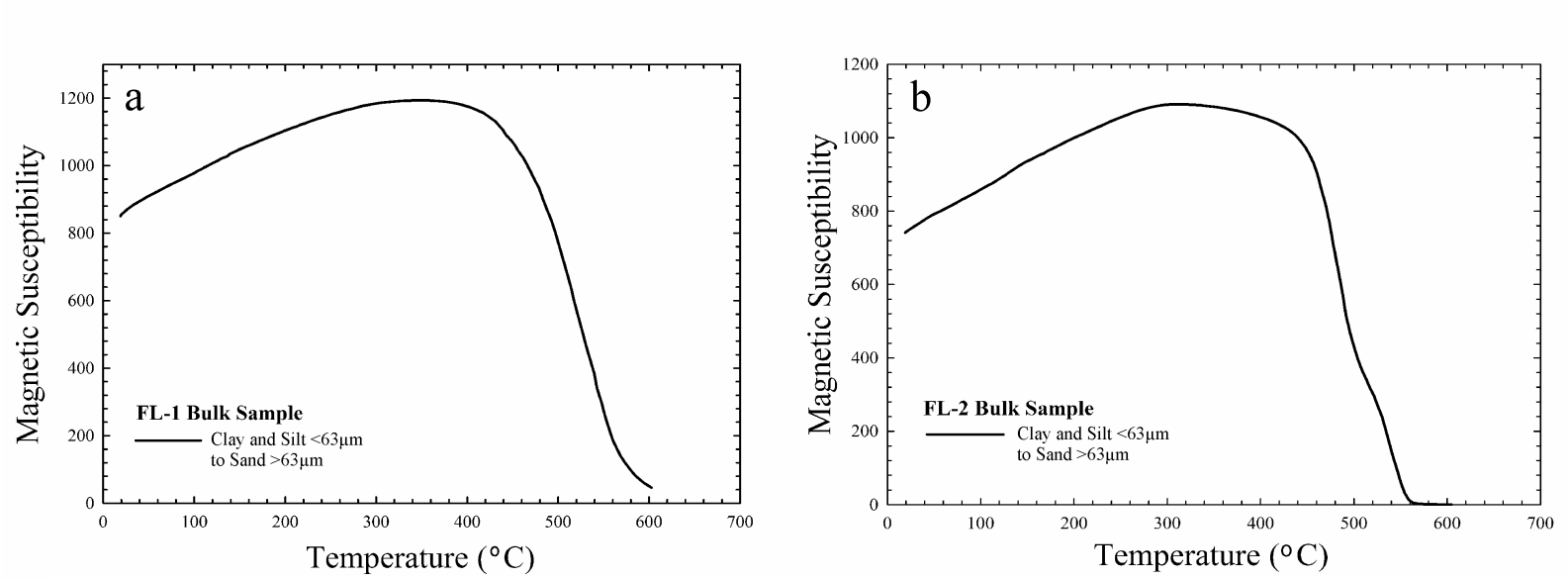

Figure 23. High temperature susceptibility experiments (a) FL-1 and (b) FL-2. Both show an abrupt decrease in susceptibility with temperature. The unblocking temperature or Curie temperature (~590-600° C) shown is indicative of the mineral magnetite.

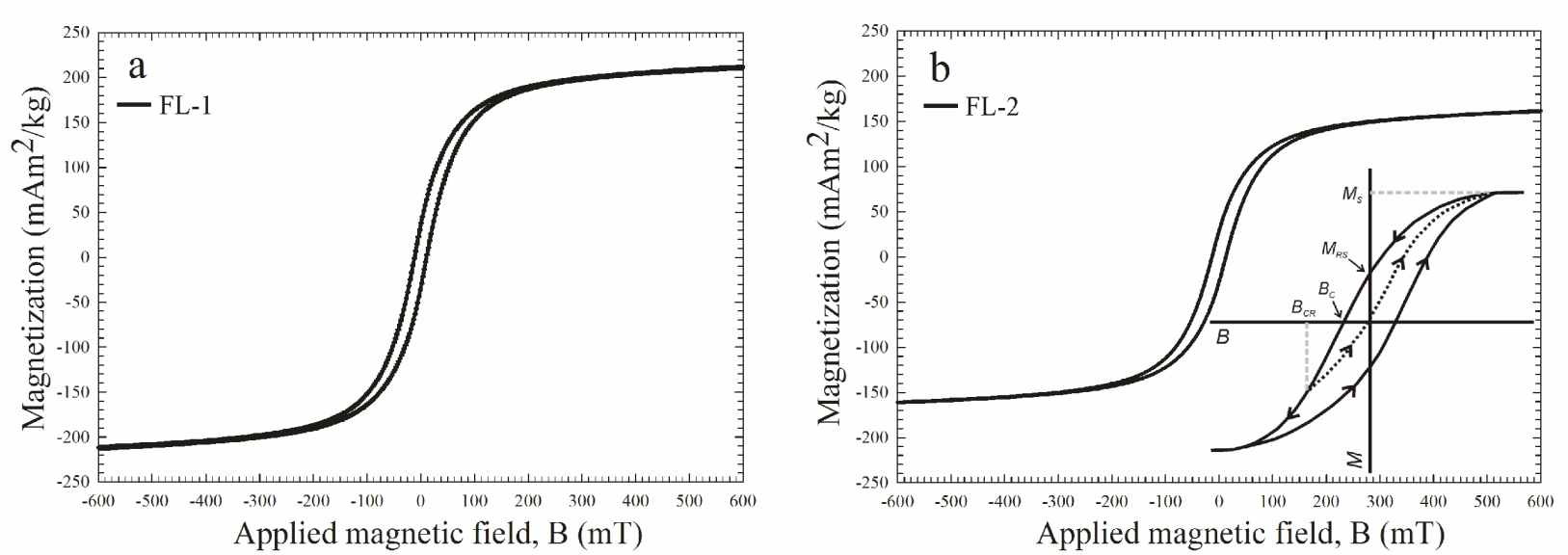

Figure 24. Magnetic hysteresis loops from (a) FL-1 and (b) FL-2. The inset in b shows an idealized loop with the associated parameters. B and M are the applied and induced magnetic fields, M_S is the saturation magnetization, M_{RS} is the remanent saturation magnetization, B_{CR} is the coercivity of remanence, and B_C is the coercivity. Hysteresis values (loop ratios see text) fall within the pseudo-single domain range, indicating a grain size of ~15 μm or smaller grains. M_S also revealed a saturation level consistent with a mineralogy of magnetite (saturation range typically for magnetite ~150-200 mT).

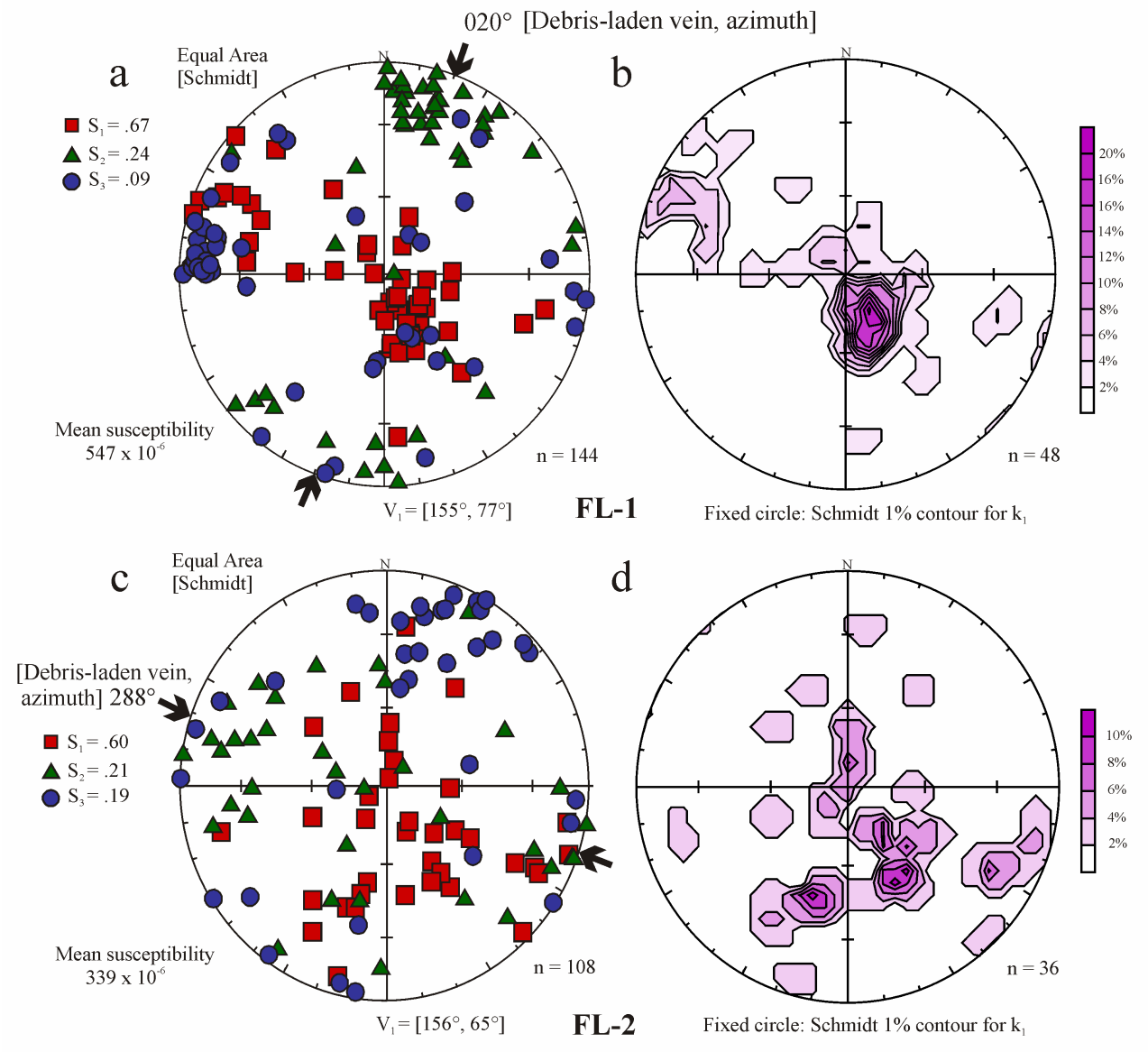

Figure 25. AMS fabrics depicted on equal area lower hemisphere stereoplots from veins FL-1 and FL-2. Each data point on the stereonets (a) and (c) represents the maximum (squares), intermediate (triangles), and minimum (circles) principal susceptibilities, n denotes the number of measurements. The eigenvalues and eigenvectors, magnetic susceptibility, and vein azimuths are shown beside the stereoplots. Stereonets (b) and (d) are based on the maximum K_1 orientation distributions, 1% contour.

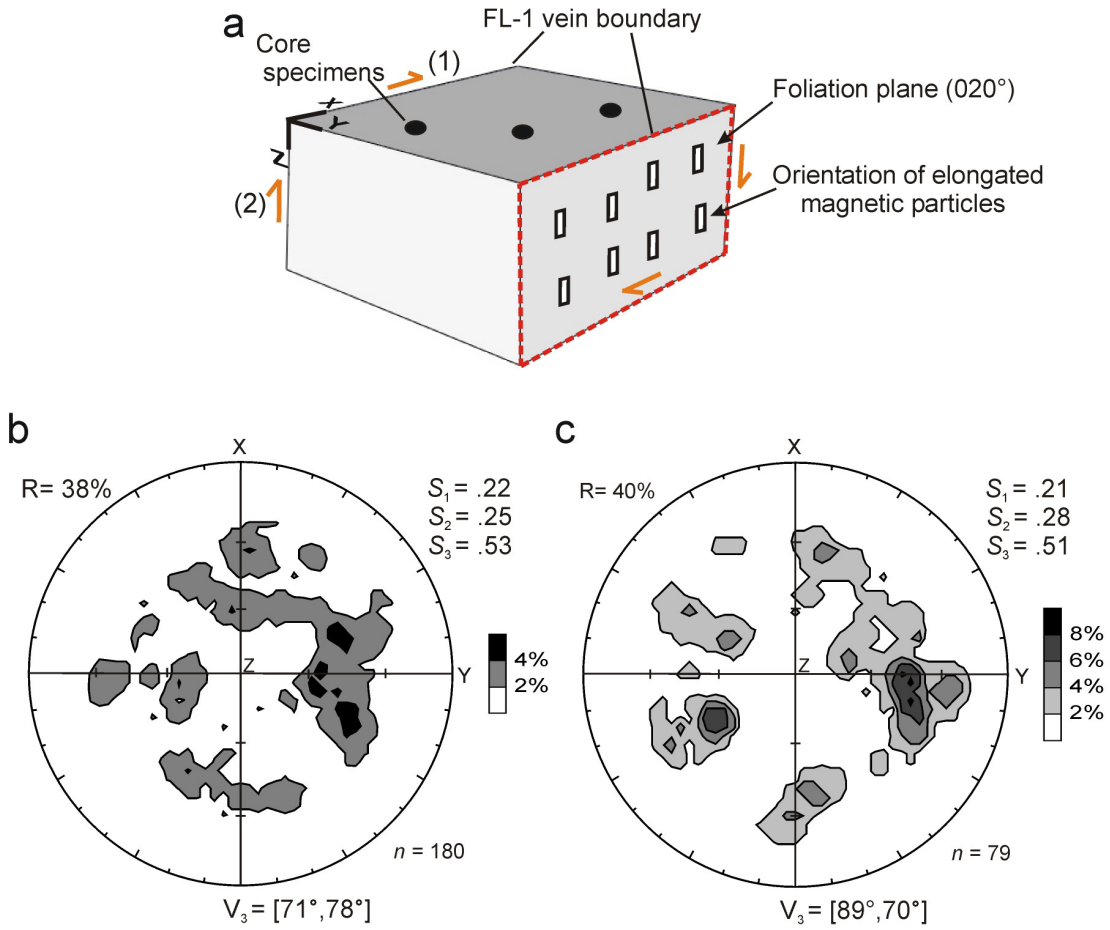

Figure 26. (a) Schematic block model illustrating the c-axes with reference to the magnetic particles, foliation and local strain axes. For clarity the foliation plane is displayed on the outer vein boundary (red dashed line) in the XZ plane (SSW-NNE). The orange arrows on the vein represent a complex system of (1) lateral shear and (2) subvertical shear. The direction of the magnetic ellipsoids within the foliation plane was probably caused by subvertical shear. The direction of glacier flow is NNW to the SSE. (b) and (c) actual data from c-axis distributions parallel to and normal to foliation with 1% contour. All stereonets are equal area lower-hemisphere projections; n, of measured c-axes and eigenvectors (V_3) are shown at the bottom of the stereonets. The orientation strengths (R) and eigenvalues (S_1-S_3) are shown beside the stereoplots.

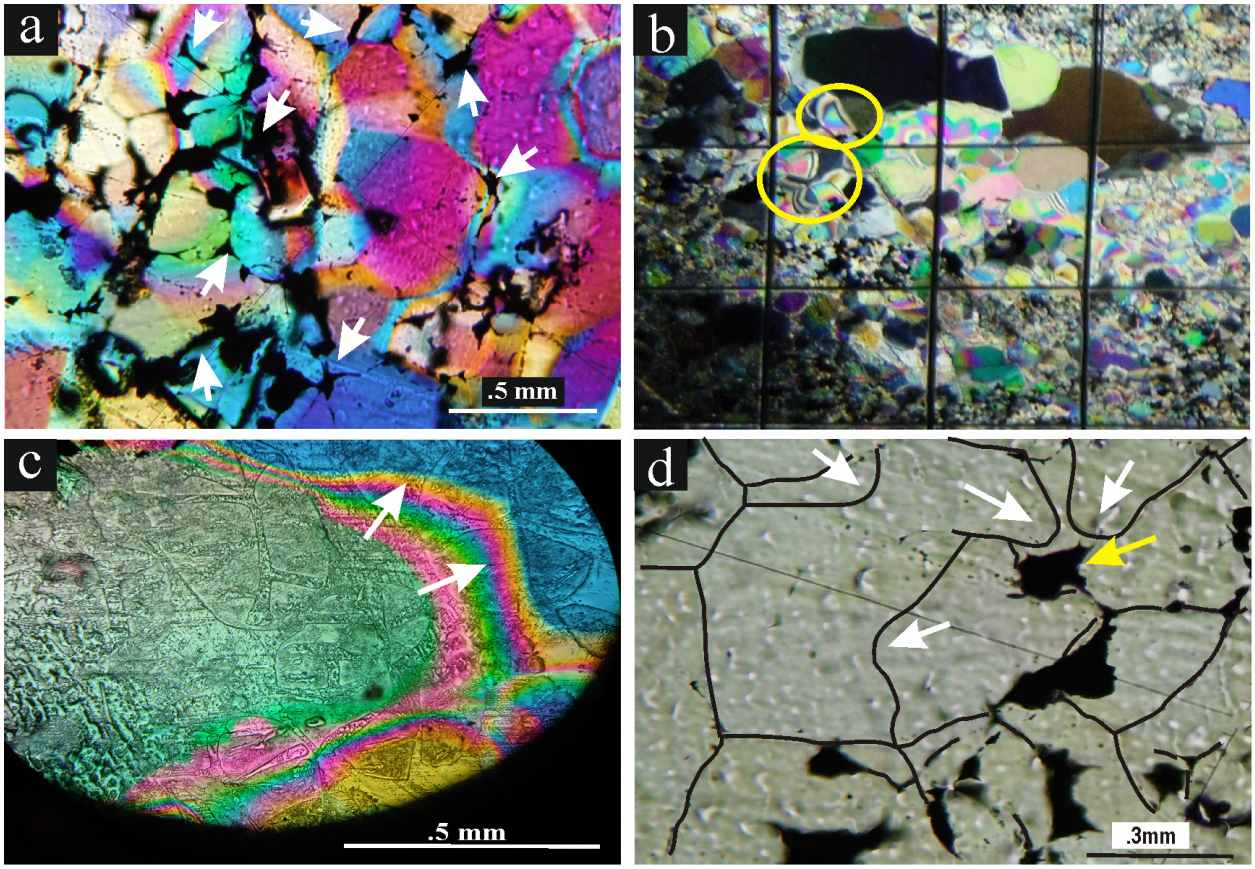

Figure 27. (a) Ice photographed under crossed polarizers note the location of particles along grain boundaries (opaque areas shown with arrows). Thin section from the XZ plane (SSW-NNE). (b) Possible evidence of nucleation (examples are circled). Grains usually form near triple junctions. The grain usually grows in the direction of the convex edge. Overlying grid is 1-cm. Thin section from the XZ plane (SSW-NNE). (c) Bulging part of a grain boundary (arrows) has penetrated its neighboring grain. Thin section from the YZ plane (WNW-ESE). (d) Bulging (white arrows) and pinning (yellow arrow) of grain boundaries by hard inclusions, shown in visible light. Thin section from the YZ plane (WNW-ESE).

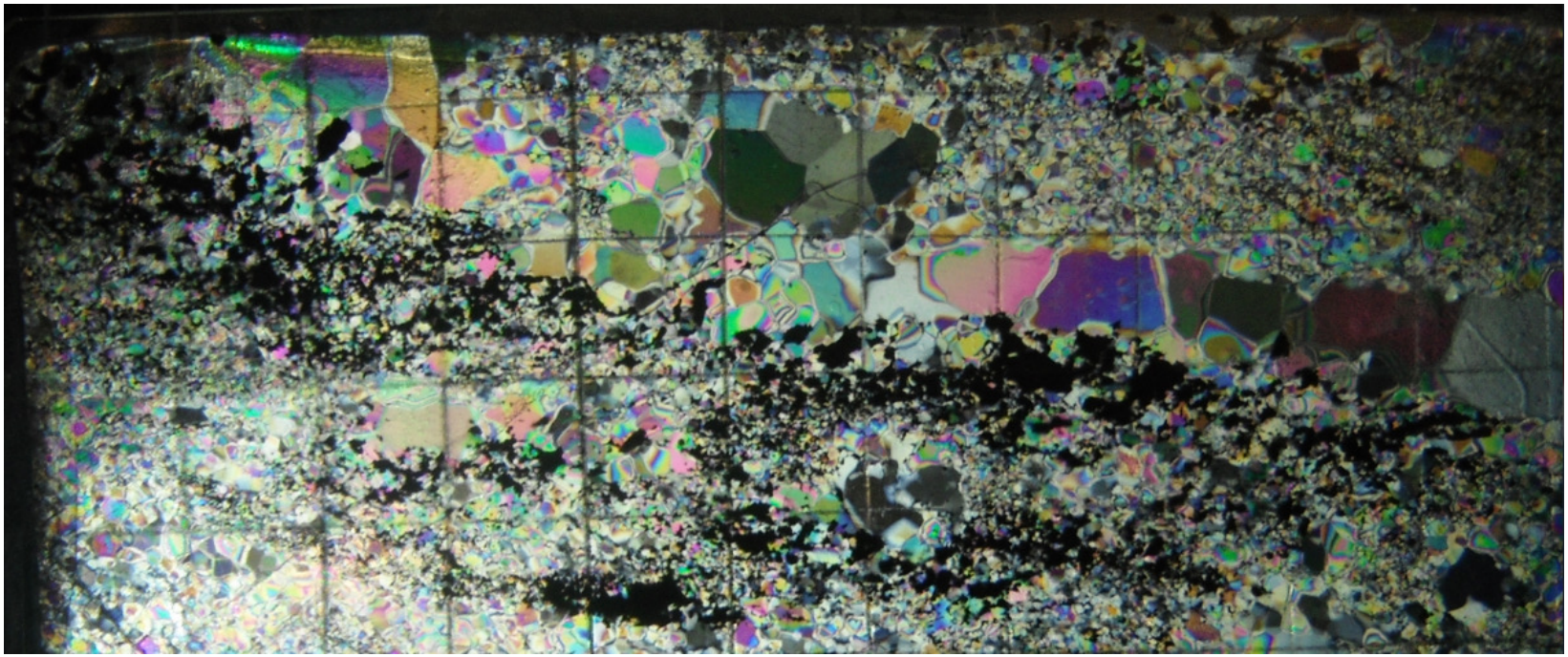

Figure 28. An example of an ice ribbon under crossed polarizers. Overlying grid is 1 cm. This sample was cut parallel to the foliation (XZ plane-SSW-NNE); note the opaque areas below the ribbon (scattered debris) and orientation of the ribbon.

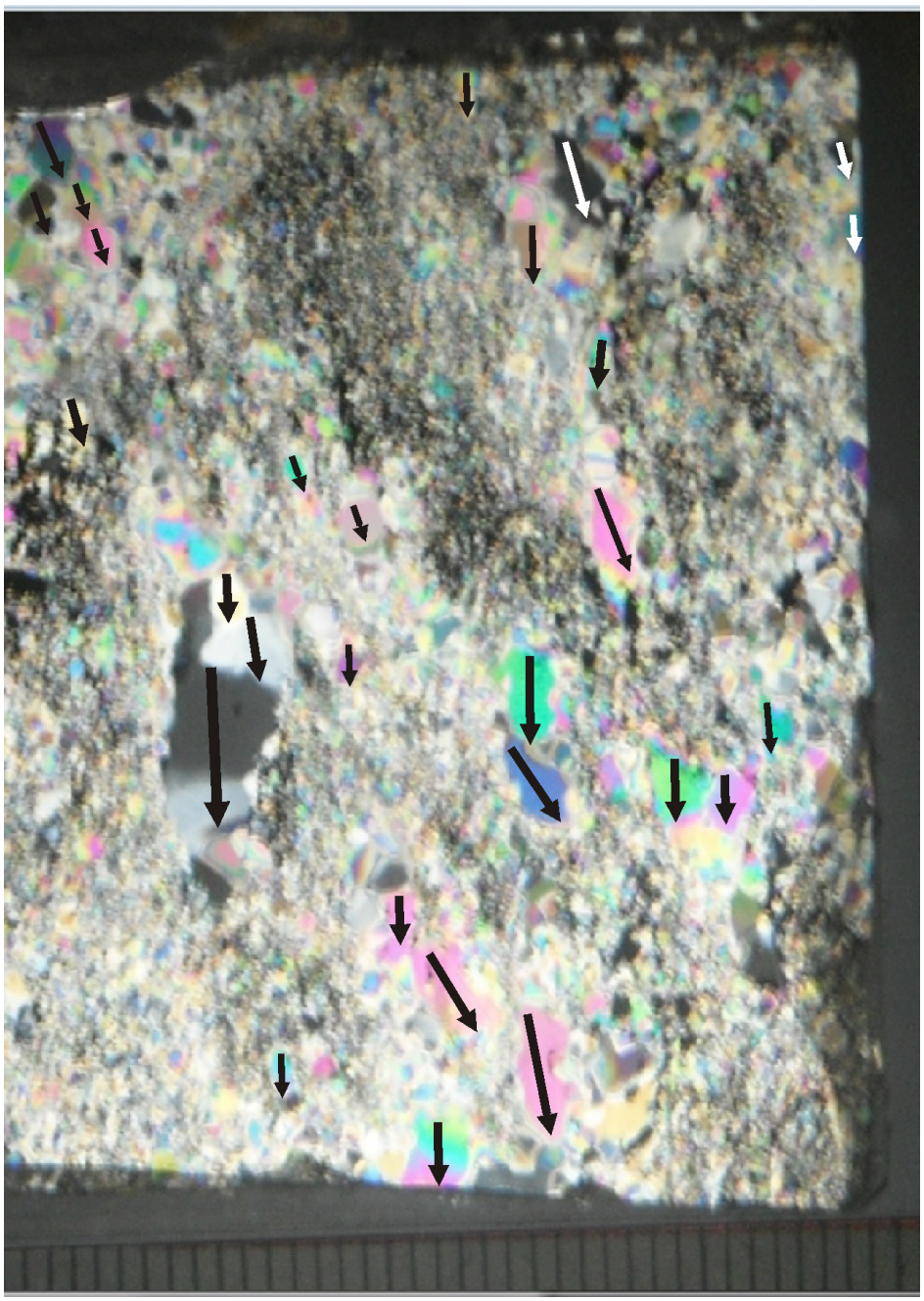

Figure 29. An example of a dirty ice thin section under crossed polarizers, showing grain elongations (black and white arrows), notice the subvertical alignment (top of image is "up" and bottom of image is "down". This sample was cut parallel to the foliation (XZ plane-SSW-NNE). Centimeter scale shown at bottom of thin section.

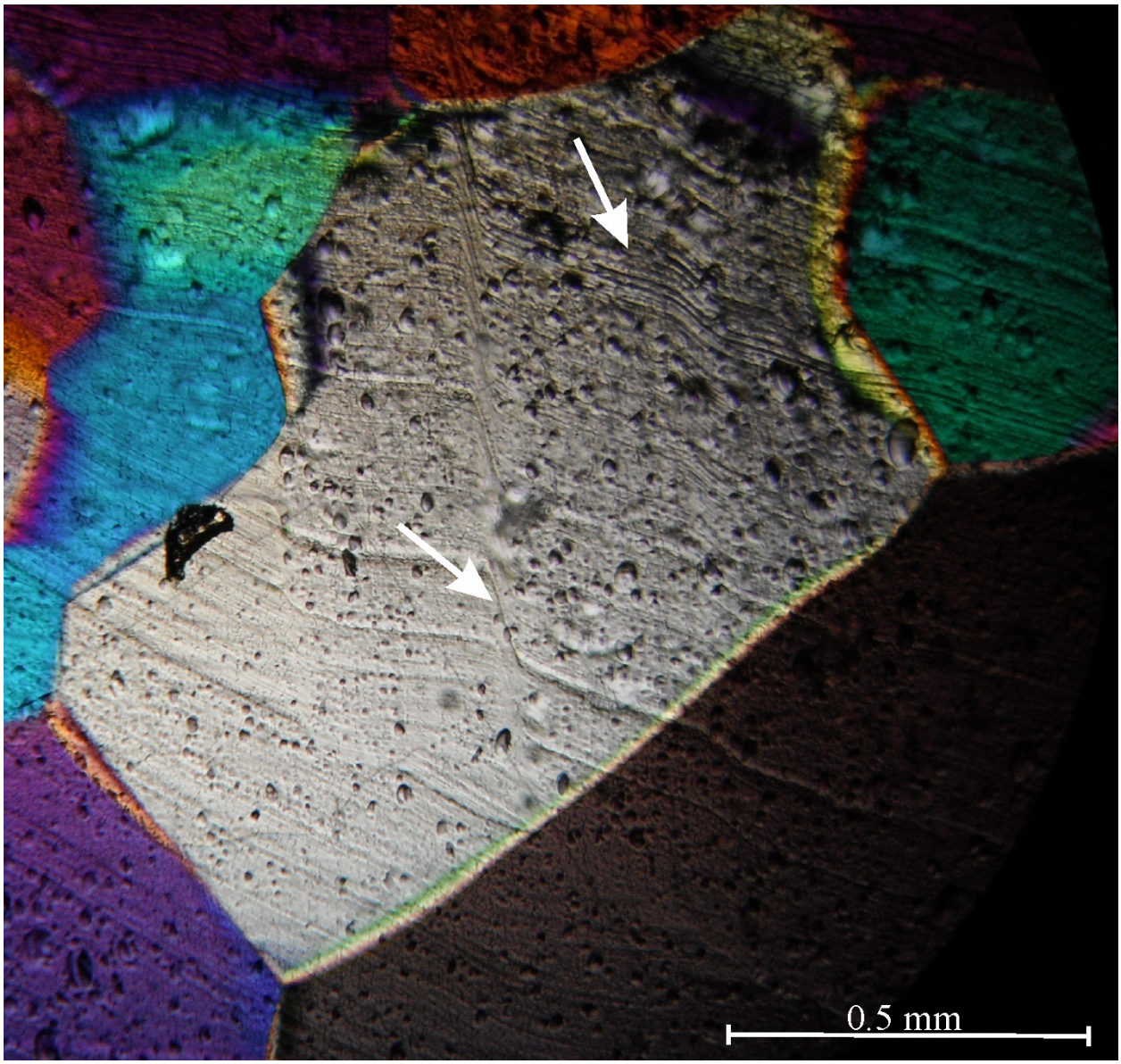

Figure 30. Microphotograph of possible slip bands in central grain (white arrows). Note the wavy and bent appearance of the slip bands. These bands result from strain localization and may be produced by shearing, bending and or twisting.

References

Adam, J.F., 1989. Methoden und Algorithmen zur Verwaltung und Analyse Axialer 3-D-Richtungsdaten und ihrer Belegungsdichten. Göttinger Arbeiten zur Geologie und Paläontologie, v. 40, 1317-1340.

Alley, R.B., 1992. Flow-law hypotheses for ice-sheet modeling. Journal of Glaciology, v. 38, 245-256.

Alley, R.B., Gow, A.J., Meese, D.A., 1995. Mapping c-axis fabrics to study physical processes in ice. Journal of Glaciology, v. 41, 197-203.

Alley, R.B., Gow, A.J., Meese, D.A., Fitzpatrick, J.J., Waddington, E.D., Bolzan, J.F., 1997. Grain-scale processes, folding, and stratigraphic disturbance in the GISP2 ice core. Journal of Geophysical Research, v. 102, 26819-26830, (doi: 10.1029/96JC03836).

Alley, R.B., Perepezko, J.H., Bentley, C.R., 1986b. Grain growth in polar ice: II. Application. Journal of Glaciology, v. 32, 425-433.

Anderton, P.W., 1974. Ice fabrics and petrography, Meserve Glacier, Antarctica. Journal of Glaciology, v. 13, 285-306.

Baker, R.W., Gerberich, W.W., 1979. The effect of crystal size and dispersed-solid inclusions on the activation energy for creep of ice. Journal of Glaciology, v. 24, 179-194.

Bender, M.L., Burgess, E., Alley, R.B., Barnett, B., Clow, G.D., 2010. On the nature of the dirty ice at the bottom of the GISP2 ice core. Earth Planetary Science Letters, v. 299, 466-473, (doi:10.1016/j.epsl.2010.09.033).

Bertotti, G., 1998. Hysteresis in Magnetism: For Physicists, Materials Scientists, and Engineers. Academic Press, Inc. 558 pp.

Borradaile, G.J., Henry, B., 1997. Tectonic applications of magnetic susceptibility and its anisotropy. Earth Science Reviews, v. 42, 49-93.

Borradaile, G.J., Jackson, M., 2004. Anisotropy of magnetic susceptibility (AMS): Magnetic petrofabrics of deformed rocks, in Magnetic Fabric: Methods and Applications. Geological Society Publications, v. 238, 299-360.

Cahn, R.W., 1965. Recovery and Recrystallization. In Cahn, R.W., ed. Physical metallurgy. New York, John Wiley and Sons, Inc., p. 925-987.

Cuffey, K.M., Paterson, W.S.B., 2010. The physics of glaciers, 4th edn. Butterworth-Heinemann, Oxford. pp. 33-48.

Daley, M.A., Kirby, S.H., 1984. Thin sectioning and surface replication of ice at low temperature. Journal of Glaciology, v. 30, 248-250.

Diprinzio, C.L., Wilen, L.A., Alley, R.B., Fitzpatrick J.J., Spencer, M.K., Gow, A.J., 2005. Fabric and texture at Siple Dome, Antarctica. Journal of Glaciology, v. 51, 281-290.

Dunlop, D.J., 2002. Theory and application of the Day plot (M_{rs}/M_s versus H_{cr}/H_c) 1. Theoretical curves and tests using titanomagnetite data. Journal of Geophysical Research, v. 107, 1-22, (doi: 10.1029/2001JB000486).

Duval, P., Castelnau, O., 1995. Dynamic recrystallization of ice in polar ice sheets. Journal de Physique (Paris), v. IV, 197-205.

Ensminger, S.L., Alley, R.B., Evenson, E.B., Lawson, D.E., Larson, G.J., 2001. Basal-crevasse-fill origin of laminated debris bands at Matanuska Glacier, Alaska, U.S.A. Journal of Glaciology, v. 47, 412-422.

Evans, M.E., Heller, F., 2003. Environmental Magnetism: Principles and Applications of Enviromagnetics. Elsevier, San Diego 295 pp.

Fitzpatrick, J.J., Voigt, D.E., Fegyveresi, J.M., Stevens, N.T., Spencer, M.K., Cole-Dai, J., Alley, R.B., Jardine, G.E., Cravens, E.D., Wilen, L.A., Fudge, T.J., McConnell, J.R., 2014. Physical properties of the WAIS Divide ice core.
Journal of Glaciology, v. 60, 1181-1198, (doi: 10.3189/2014JoG14J100).

Fleming, E.J., Lovell, H., Stevenson, C.T.E., Petronis, M.S., Benn, D.I., Hambrey, M.J., Fairchild, I.J., (2013) Magnetic fabrics in the basal ice of a surge-type glacier. *J. Geophys. Res*., v. 118, 2263-2278, (doi: 10.1002/jgrf.20144).

Gold, L.W., 1966. Dependence of crack formation on crystallographic orientation for ice. Canadian Journal of Physics, v. 44, 2757-2764.

Gow, A.J., Meese, D.A., Alley, R.B., Fitzpatrick, J.J., Anandakrishnan, S., Woods, G.A., Elder, B.C., 1997 Physical and structural properties of the Greenland Ice Sheet Project 2 ice core: A review. Journal of Geophysical Research, v. 102, 26559–26575, (doi: 10.1029/97JC00165).

Gow, A.J., Williamson, T., 1976. Rheological implications of the internal structure and crystal fabrics of the West Antarctic ice sheet as revealed by deep core drilling at Byrd Station. Cold Regions Research Engineering Laboratory Report, v. 76, 1665-1677.

Herron, S., Langway, Jr. C.C., 1979. The debris-laden ice at the bottom of the Greenland Ice Sheet. Journal of Glaciology, v. 23, 193-206.

Hockey, B., 1970. An improved coordinate system for particle shape representation, Journal of Sedimentary Petrology, v. 40, 1054-1056.

Hooke, Leb., R., 2005. Principles of Glacier Mechanics. 2th edn. Cambridge University Press. p. 40.

Hooyer, T.S., Iverson, N.R., Lagroix, F.,Thomason, J.R., 2008. Magnetic fabric of sheared till: A strain indicator for evaluating the bed deformation model of glacier flow. Journal of Geophysical Research, v.113, 1-15, (doi:10.1029/2007JF00075).

Hrouda, F., 1982. Magnetic anisotropy of rocks and its application in geology and geophysics. Survey of Geophysics, v. 5, 37-82, (doi: 10.1007/BF01450244).

Kennedy, J.H., Pettit, E.C., Di Prinzio, C.L., 2013. The evolution of crystal fabric in ice sheets and its link to climate history. Journal of Glaciology, v. 59, 357-373.

Kipfstuhl, S., Hamann, I., Lambrecht, A., Freitag, J., Faria, S.H., Grigoriev, D., Azuma, N., 2006. Microstructure mapping: a new method for imaging deformation-induced microstructural features of ice on the grain scale. Journal of Glaciology, v. 52, 398-406.

Jacobson, H.P., Waddington, E.D., 2004. Recumbent folding in ice sheets: a core-reference study. Journal of Glaciology, v. 50, 201-209.

Jelinek, V., 1978. Statistical processing of anisotropy of magnetic susceptibility measured on groups of specimens. Studia Geophysica Geodaetica, v. 22, 50-62.

Jelinek, V., 1981. Characterization of Magnetic fabric of rocks. Tectonophysics, v. 79, 563-567.

Kamb, W.B., 1959. Ice petrofabric observations from Blue Glacier, Washington, in relation to theory and experiment. Journal of Geophysical Research, v. 64, 1891-1909.

Lanci, L., Delmonte, B., Kent, D.V., Maggie, V., Biscaye, P.E., Petit, J.R., 2012. Magnetization of polar ice: a measurement of terrestrial dust and extraterrestrial fallout. Quaternary Science Reviews, v. 33, 1-12, (doi:10.1016/j.quascirev.2011.11.023).

Lanci, L., Kent, D.V., Biscaye, P.E., Steffensen, J.P., 2004. Magnetization of Greenland ice and its relationship with dust content. Journal of Geophysical Research, v. 109, 1-9, (doi:10.1029/2003JD004433).

Lanci L, Delmonte B., Maggi, V., Petit, J.R., Kent, D.V., 2008. Ice magnetization in the EPICA-Dome C ice core: Implications for dust sources during glacial and interglacial periods. Journal of Geophysical Research, v. 113, 1-7.

Langway, Jr. C.C., 1958. Ice fabrics and the universal stage. U.S. Snow, Ice and Permafrost Research Establishment. Technical Report v. 62, 1-16.

Lipenkov, V.Ya., Barkov, N.I., Duval, P., Pimienta, P., 1989. Crystalline texture of the 2083 m ice at Vostok station, Antarctica. Journal of Glaciology, v. 35, 392-398.

Lovell, H., Fleming, E.J., Benn, D.I., Hubbard, B., Lukas, S., Rea, B.R., Noormets, R., Flink, A.E., 2015. Debris entrainment and landform genesis during tidewater glacier surges. *Accepted*. Journal of Geophysical Research.

Mark, D.M., 1973. Analysis of axial orientation data, including till fabrics. Geological. Society of America Bulletin, v. 84, 1369-1374.

Montagnat, M., Azuma, N., Dahl-Jensen, D., Eichler, J., Fujita, S., Gillet-Chaulet, F., Kipfstuhl, S., Samyn, D., Svensson, A., Weikusat, I., 2014. Fabric along the NEEM ice core, Greenland, and its comparison with GRIP and NGRIP ice cores. The Cryosphere, v. 8, 1129-1138, (doi:10.5194/tc-8-1129-2014).

Paterson, W.S.B., 1991. Why ice-age ice is sometimes "soft". Cold Regions Science Technology, v. 20, 75-98.

Rigsby, G.P., 1960. Crystal orientation in glacier and experimentally deformed ice. Journal of Glaciology, v. 3, 589-606.

Rochette, P.,Vialon, P.,1984. Development of planar and linear fabrics in Dauphinois shales and slates (French Alps) studied by magnetic anisotropy and its mineralogical control. Journal of Structural Geology, v. 6, 33-38.

Samyn, D., Svensson, A., Fitzsimons, S.J., 2008. Dynamic implications of discontinuous recrystallization in cold basal ice: Taylor Glacier, Antarctica. Journal of Geophysical Research, v. 113, 1-13, (doi: 10.1029/2006JF000600).

Shumway, J.R., Iverson, N.R., 2009. Magnetic fabrics of the Douglas till of the Superior lobe: Exploring bed-deformation kinematics. Quaternary Science Reviews, v. 28, 107-119.

Song, M., Baker, I., Cole, D.M., 2008. The effect of particles on creep rate and microstructures of granular ice. Journal of Glaciology, v. 54, 533-537.

Song, M., Cole, D.M., Baker, I., 2006. An investigation of the effects of particles on creep of polycrystalline ice. Scripta Materialia, v. 55, 91-94.

Steffensen, J.P., 1997. The size distribution of microparticles from selected segments of the Greenland ice core project representing different climatic periods. Journal of Geophysical Research, v. 102, 26755-26763, (doi: 10.1029/97JC01490).

Tarling, D.H., Hrouda, F., 1993. The Magnetic Anisotropy of Rocks. Chapman and Hall, London. 218 pp.

Tison, J.L., 1994b. Diamond wire-saw cutting technique for investigating textures and fabrics of debris-laden ice and brittle ice. Journal of Glaciology, v. 40, 410-414.

Tison, J.L., Thorsteinsson, T., Lorrain, R.D., Kipfstuhl, J., 1994a. Origin and development of textures and fabrics in basal ice at Summit. Central Greenland. Earth and Planetary Science Letters, v. 125, 421-437.

Wilson, C.J.L., Peternell, M., 2011. Evaluating ice fabrics using fabric analyzer techniques in Sørsdal Glacier, East Antarctica. Journal of Glaciology, v. 57, 881-894.

ZongQi, D., Xing G., QingSong, L., BaiQing, X., Youliang, S., 2011. Magnetic characteristics of insoluble microparticles in ice core (Nojingkangsang) from the southern Tibetan Plateau and its environmental significance. Science China Earth Science, v. 54, 1635-1642.

Chapter 4. Drumlin formation at the Fláajökull Glacier, Iceland

William R. Jacobson, Jr.*

University of Wisconsin-Milwaukee, Geosciences Department P.O. Box 413, Lapham Hall 366, Milwaukee, WI 53201 USA

Abstract

Recent drumlin exposures near the margin of Fláajökull, a non-surge type outlet glacier of Vatnajökull, Iceland exhibits anisotropy of magnetic susceptibility (AMS) fabrics indicating a consistent long axis trend generally parallel (maximum principal susceptibility, K_1) to the drumlin long axis. The longitudinal flow plane, defined by the K_1 and K_3 magnetic susceptibilities plunge mildly up-glacier. These fabrics were observed in the drumlin cores (sand and gravels) and in the overlying basal till carapace. Moreover, on one of the drumlins the fabrics suggested only consolidation, inferring that the ice was static at that time. Rotary ring-shear tests provide a reference for strain and suggest shear strains of <10 during drumlinization.

It is concluded that the cores of the drumlins consisted of pre-existing deposits which have been likely eroded by proglacial meltwater prior to drumlinization. Subsequent ice overriding resulted in heterogeneous deformation of the drumlin cores following the deposition the upper basal till carapace. These composite bedforms, however, support a depositional model given the fact that they formed primarily from subglacial deposition. Additionally, the basal till carapace at site A might have formed in a crevasse beneath the ice instead of at the glacier margin which has been previously suggested.

---

*Author
Email address: wrjjr@uwm.edu (W.R. Jacobson, Jr.)

1. Introduction

Numerous theories for drumlin formation have been proposed; however, no consensus has been reached on their genesis (Knight, 2010), and it is likely that they are polygenetic. Despite this lack of consensus, Patterson and Hooke (1995) identified three factors that are common to drumlin growth; these include compressive flow, formation near the ice margin and high subglacial water pressures. These conditions have been observed in modern drumlin fields formed by active glaciers (Johnston et al., 2010; Jónsson et al., 2015). In any case, drumlins may represent erosional products of pre-existing deposits (Whittecar and Mickelson, 1979), depositional or both, and their formation is favored by the large sediment fluxes associated with warm-based glaciers (Boulton, 1987; Menzies, 1979; Krüger and Thomsen, 1984; Hart, 1995). Additionally, frozen sediment cores have been suggested and may provide the contrast favoring drumlinization (Hooke and Medford, 2013; Winguth et al., 2004).

Drumlins emerging from beneath retreating ice margins in Iceland provide particularly good targets for study of drumlin formation. As emphasized by Johnston et al. (2010) the active Múlajökull drumlin field in Iceland may be unique in being shaped by the current glacial regime. Moreover, Smith et al. (2007) documented the possible formation of a drumlin beneath an Antarctic ice stream.

In this paper, magnetic fabric measurements are presented from two drumlins which have been recently exposed along the margin of Fláajökull, a non-surging outlet glacier of the Vatnajökull ice cap, SE-Iceland. The kinematics of deformation is explored in these drumlins and interpreted from the fabrics using a customized ring-shear apparatus which allowed fabric to be calibrated to till strain (Shumway and Iverson, 2009; Thomason and Iverson, 2006). Jónsson et al. (2015) indicated that the Fláajökull drumlins were formed from sticky spots in the bed (e.g.

resistant glaciofluvial cores) which were later streamlined with a subglacial traction till. Furthermore it has been suggested that the drumlin cores may be erosional features of pre-existing deposits, on the other hand, our data suggests that one of the cores was deformed as a result of overriding ice.

2. Fláajökull Glacier

Fláajökull is a temperate glacier that drains the south-eastern part of the Vatnajökull ice cap (Fig. 31a). Fláajökull is approximately 25 km long with an area of 170 km^2 and an average thickness range of 313-317 m (Hannesdóttir et al., 2015). It descends from approximately 1480 to 40 m a.s.l. and terminates on a flat sandur plain called Mýrar. The climate at the terminus is characterized by an annual precipitation rate that may total up to 1,500 mm or more (Björnsson and Pálsson, 2008). The glacier flows to the south-east between Mt. Fláfjall and Mt. Heinbergsfjöll (Fig. 31b) and the ice margin is split into two lobes by flow around Mt. Jökulfell (Jónsson et al., 2015).

The fully exposed drumlins are located in the north-eastern part of the forefield in front of the glacier (Fig. 32). The drumlin are oriented SSE-NNW in accordance with the ice-flow direction. The drumlins are draped by a number of flutes and recessional push moraines. The drumlins have been formed proximal to a large end moraine complex described by Jónsson et al. (2015) as the 1995 end moraine. Drumlin dimensions range from 430-580 m in length, 115-130 m in width, and 8-13 m in height. The highest points on these drumlins are situated at the downglacier end near the moraine complex. The surface of these drumlins consisted of numerous streamlined boulders lodged in the substrate with striations trending in the direction of glacier flow.

3. Methods

Two drumlins within the forefield were selected for detailed investigations. The stratigraphy and sedimentology from Jónsson et al. (2015) is adopted in this preliminary report.

Till fabric samples were collected in the years 2012 and 2013 for anisotropy of magnetic susceptibility (AMS) measurements. A minimum of 25 plastic boxes (8 cm^3) were used in the sampling process and a total of 457 till samples were collected in four stream-cut sections (A-D Figure 2 for locations). The samples were collected vertically through the drumlins near their centerline. All of the till samples were collected within a depth range of 13 to 90 cm. Magnetic fabrics are presented in the form of equal area nets, lower hemisphere projections.

In the laboratory at the University of Wisconsin-Milwaukee each box was measured for the anisotropy of magnetic susceptibility (AMS) with an MF*K1*-FA Multi-Function Kappabridge system. This system measures magnetic susceptibility numerous times while rotating it through three orientations. The strength of the induced magnetization of a given till sample, *M*, is given by kH, where the constant of proportionality *k* is called the susceptibility and H is the magnetic field strength (Jelinek and Kropáček, 1978). In materials in which the shapes or crystallographic orientations of mineral grains have become aligned, *k* varies with direction, such that a second-rank tensor is required to characterize it (Tarling and Hrouda, 1993). This tensor is visualized with a susceptibility ellipsoid that has lengths of its long, intermediate, and short axes equal to the principal susceptibilities K_1, K_2, and K_3, (Figure 33). Estimations of three-dimensional strain, fabric strength and direction may be ascertained from these ellipsoids. In addition, the technique provides an excellent spatial resolution because of its averaging effect of many magnetic grains compared to traditional fabric techniques where only the long axis of pebbles are measured in outcrop with a compass. The fabric strength and direction were determined using

eigenvectors (V_1, V_2, and V_3) and corresponding eigenvalues (S_1, S_2, and S_3), respectively (Mark, 1973). The S_1 eigenvalue represents the degree of clustering of K_1 orientations around the V_1 eigenvector. An S_1 eigenvalue of 0.33 indicates random alignment of K_1 orientations; whereas an S_1 eigenvalue of 1.0 indicates K_1 orientations that are perfectly aligned. The magnetic fabric was analyzed using the software package *SpheriStat3* from Pangaea Scientific. In addition to the AMS measurements, we conducted high temperature susceptibility (HTS) and hysteresis experiments. These experiments were evaluated on the fine-grained particles (clay and silt) that were less than 65 μm. The unblocking temperature was used to identify the mineralogy and hysteresis loop parameters helped target the particle size.

4. Description of localities

4.1 Site A

Figure 34 displays a transverse cut through drumlin 1 exposing an upper till carapace (Till 1) and a lower unit of glaciofluvial outwash. As indicated these drumlins were likely the result of sticky spots in the bed (Boulton, 1987). At this site a total of 181 AMS samples were collected in the till carapace (Till 1) from three vertical profiles. Previously, the till carapace has been interpreted as a recessional push moraine by Krüger, (1995). Using K_1, the maximum principle susceptibility, S_1 eigenvalues for sites A1-A3 were 0.51, 0.60, and 0.54, respectively. These weak fabrics indicate that the till has not been sheared to steady state conditions which require high shear strains (see Fig. 35a, b for steady state ~20). Magnetic fabrics from A1 and A2, however, show a pure shear strain signature with longitudinal shortening oriented along the drumlin long axis X'-X (SSE-NNW) and vertical extension. Such a fabric signature is not surprising considering that the drumlin is deposited on an adverse slope just down ice from an

overdeepening due to glacier erosion. Most glaciers are in compression in such a situation. In contrast, fabric A3 reflects simple shear directed roughly parallel to the drumlin long axis. Fabrics from ring-shear experiments of other tills demonstrate similar results and reinforce that fabric A3 has likely experienced a shear strain of ~7 (Hooyer et al., 2008). The K_1 girdle, however, suggests that there was insufficient strain to cluster K_1 orientations (see fabric transition from B-13 to B-7-*Batestown till,* Fig. 35b).

4.2 Site B

Site B is located within Drumlin 2 (see Figure 32). At this site 31 samples were collected from a platform bench within the outwash core sediments approximately 90 cm from the drumlin crest (Figure 36). The S_1 fabric strength was moderate reflecting an eigenvalue of 0.73. The AMS K_1 eigenvector was 360° with a plunge of 18° up-glacier. The longitudinal flow plane (K_1 – K_3) was approximately parallel to the SSE-NNW drumlin long axis. This up-glacier K_1 dip orientation has been reported in numerous field studies (Gentoso et al., 2011; Evenson, 1971; Larsen and Piotrowski, 2003; Piotrowski et al., 2006) and has been reproduced in the laboratory by ring-shear tests (Jacobson, Jr. and Hooyer, 2015; Hooyer and Iverson, 2002). This fabric indicates that the outwash core has been likely sheared to strains of ~7 according to ring-shear tests (Iverson et al., 2008).

4.3 Site C

Figure 37 shows a meltwater stream cut through Drumlin 2 exposing the same units from site B. At this site 31 AMS samples were collected from Till 1 and 34 samples within the drumlin core sediments. The microfabrics from the sampling areas show significant clustering of

K_1, K_2, and K_3 susceptibilities. The S_1 eigenvalue for the upper Till 1 layer was 0.68 and 0.66 for the outwash sediments. The AMS V_1 eigenvectors for these fabrics were 12° and 2 ° with a plunge of 13° and 1°, respectively. Interestingly, these fabrics are well clustered although the fabric strength is relatively moderate in the range of 0.65 to 0.75. Both fabrics revealed a horizontal shear plane (defined by K_2 susceptibilities) which was approximately parallel to the drumlin long axis.

4.4 Site D

Site D is located in the proximal end of Drumlin 2 and is incised by a transverse meltwater channel (Figure 38). This site also shows the same two units from sites B and C, Till 1 and a lower unit of coarse outwash materials. The upper till unit is up to 0.7 m thick and the lower boundary is sharp (Jónsson et al., 2015). At this site three trenches were dug (D1, D2, and D3) and 60 samples were collected from each trench. The upper unit has been previously interpreted as a subglacial till and the lower unit as glaciofluvial outwash (Evans et al., 2006). AMS microfabric results of S_1 eigenvalues were 0.52, 0.54 and 0.46, respectively. These fabrics are relatively weak (similar to fabrics B-9, B-12, B-13 from Hooyer et al., 2008) and do not indicate shearing but simply consolidation of the till.

5. Discussion

Given the fact that the underlying bed materials consists of coarse-grained outwash the drumlin cores probably nucleated from the high-strength bed patches (low porewater pressure). As emphasized by Jónsson et al. (2015) these drumlins are similar to the drumlins formed at Breiðamerkurjokökull (Evans and Twigg, 2002) and Skeiðarárjökull (Waller and other, 2008).

Based on the AMS fabrics from Drumlin 1 the upper till may have formed at the base of the ice in a crevasse. This is supported by fabrics A1 and A2 that indicate that till was shortened nearly parallel to flow leading to upward and lateral extension of till. These fabrics are located on the downglacier side of the ridge; this is not surprising because the till would be confined by the ice there. In contrast, on the up-glacier side of the ridge it was sheared subglacially as is indicated by fabric A3 however to an insufficient strain. At the margin of Fláajökull it is not uncommon to observe crevasse squeeze-ups (sediment squeezed into cracks beneath the ice) forming in situ over the drumlin surface. Moreover, similar fabrics have been documented in old moraines from the Des Moines Lobe (Ankerstjerne, in press). Crevasse squeeze-ups have also been identified at Eyjabakkajökull, Iceland (Sharp, 1985). Formerly, this upper till has been interpreted as a recessional push moraine (Krüger, 1995) superimposed over the drumlin.

The AMS fabrics from sites B and C (Drumlin 2) revealed that the core of the drumlin was sheared in the direction of glacier flow in accordance with upper till layer. It is apparent that shearing of the till occurred on the distal end of the drumlin suggesting converging flow on the down-glacier sides during its readvance from 1966-1995. However, at the proximal end (e.g. stoss-side) of the drumlin at site D the fabrics only indicate consolidation implying that the ice was likely static at that time. Moreover, divergent shear or longitudinal shortening on the up-glacier sides was not observed.

Boulton's bed deformation model is a good fit for these drumlins because of the following evidence: proglacial cores of sand and gravel, occurrence of bullet-shaped clasts with striated surfaces in till, fissility of the till, and bed deformation in the upper till and outwash sediments. Moreover, it has been suggested that the drumlin cores predate drumlin formation indicating that meltwater erosion may have influenced the drumlin morphology prior to ice

overriding. This has been discussed elsewhere by Krüger and Thomsen (1984) and Möller and Murray (2015).

The variability in fabric strength (0.46-0.73) at sites B, C, and D is likely attributed to heterogeneous bed deformation during drumlin growth. Heterogeneous bed deformation has been previously demonstrated beneath modern glacier beds (Alley et al., 1993; Fischer and Clarke, 2001; Hooke et al., 1997; Iverson et al., 2007). As emphasized by Fisher and Clarke (2001) the ice-bed couple is strongly modulated by the water pressure and the stresses at the bed are heterogeneous often mimicking the distribution of the basal water system leading to irregularities in bed deformation and sliding. Moreover, drumlin nucleation at Fláajökull was likely driven by hydrologic heterogeneity due to strength differences in the bed (e.g. high effective stresses result in a high-strength patch) causing the upper till to be plastered onto these more resistant spots.

6. Ring-shear experiments

Laboratory ring-shear experiments have contributed a great deal of information on understanding the rheology and physical properties of subglacial tills (Iverson, 1997; Hooke and Iverson, 1995). More recently, ring-shear studies have focused on estimating the amount of strain that a till has experienced by use of magnetic fabric (Vreeland and Iverson, 2015). Magnetic fabric results from ring-shear tests on multiple tills subjected to shear indicate that K_1 orientations tightly cluster and plunge 20-30° up-glacier (Iverson et al., 2008). The K_1 orientations thereby indicate the direction of shear whereas the degree of K_1 clustering is an indicator of the approximate strain magnitude (Hooyer et al., 2008). Steady state fabric strength indicated by the S_1 eigenvalue of K_1 susceptibilities, however, does not occur until shear strains

greater than ~10 (S_1 eigenvalue >0.8 see Fig. 35b). Using ring-shear tests as a reference, Fláajökull S_1 eigenvalue strengths were 0.54-Site A3, 0.73-Site B, C1-0.68 and C2-0.66 from Site C. Clearly, these fabrics indicate shear strains <10 according to the fabric strength curve. Obviously, the sheared fabrics did not attain the steady state values indicative of high strains (e.g. 100). Furthermore, the fabrics unequivocally demonstrate simple shear which is in accordance with ring-shear experiments on other tills (e.g. fabric from Site B is strikingly similar to the D-1 fabric from the Douglas till member, eigenvalue strength is also similar 0.76, see Fig. 35a). Foremost the fabrics are not representative of the high pervasive shear strains required by the bed deformation model. In contrast the weak fabrics observed at site D (e.g. 0.46-0.54) represent a consolidation fabric which is often observed prior to shearing (e.g. 0 shear strain).

7. Conclusions

From our multi-testing approach and study of the Fláajökull drumlins, it can be concluded that:

- Proglacial meltwater erosion reshaped the original morphology of the sand and gravel cores in front of Fláajökull prior to drumlinization. Subsequent advancement of the ice over Drumlin 2 (formed sub-marginally during 1966-1995) led to deformation of the core materials and deposition of the overlying basal till. AMS fabrics are in accordance at Sites B and C and indicate shearing in the direct of glacier flow approximately parallel to the drumlin long axis. Although this landform composite resulted from a complex interaction of subglacial erosion, bed deformation, and lodgement, a depositional model is best suited for these drumlins.

- Based on the AMS fabrics from the upper till carapace from Drumlin 1 (Site A) it may be re-interpreted as a crevasse-squeeze-up instead of a recessional push moraine which has been previously hypothesized.
- Site D located on the stoss end of the drumlin demonstrates no evidence of subglacial shearing suggesting a static environment.
- According to ring-shear experiments the Fláajökull tills reflect shear strains of <10.
- These drumlins are polygenetic in origin which is not a surprise; however, hydrologic heterogeneity was likely the main cause for drumlinization.

Acknowledgements

I thank James Amato and Emily Joynt for their assistance in till sampling. I would like to thank Julie Bowles (Institute for Rock Magnetism, University of Minnesota) for generously allowing us to use their analytical facilities for measuring AMS. This work was supported by a grant from the Geological Society of America.

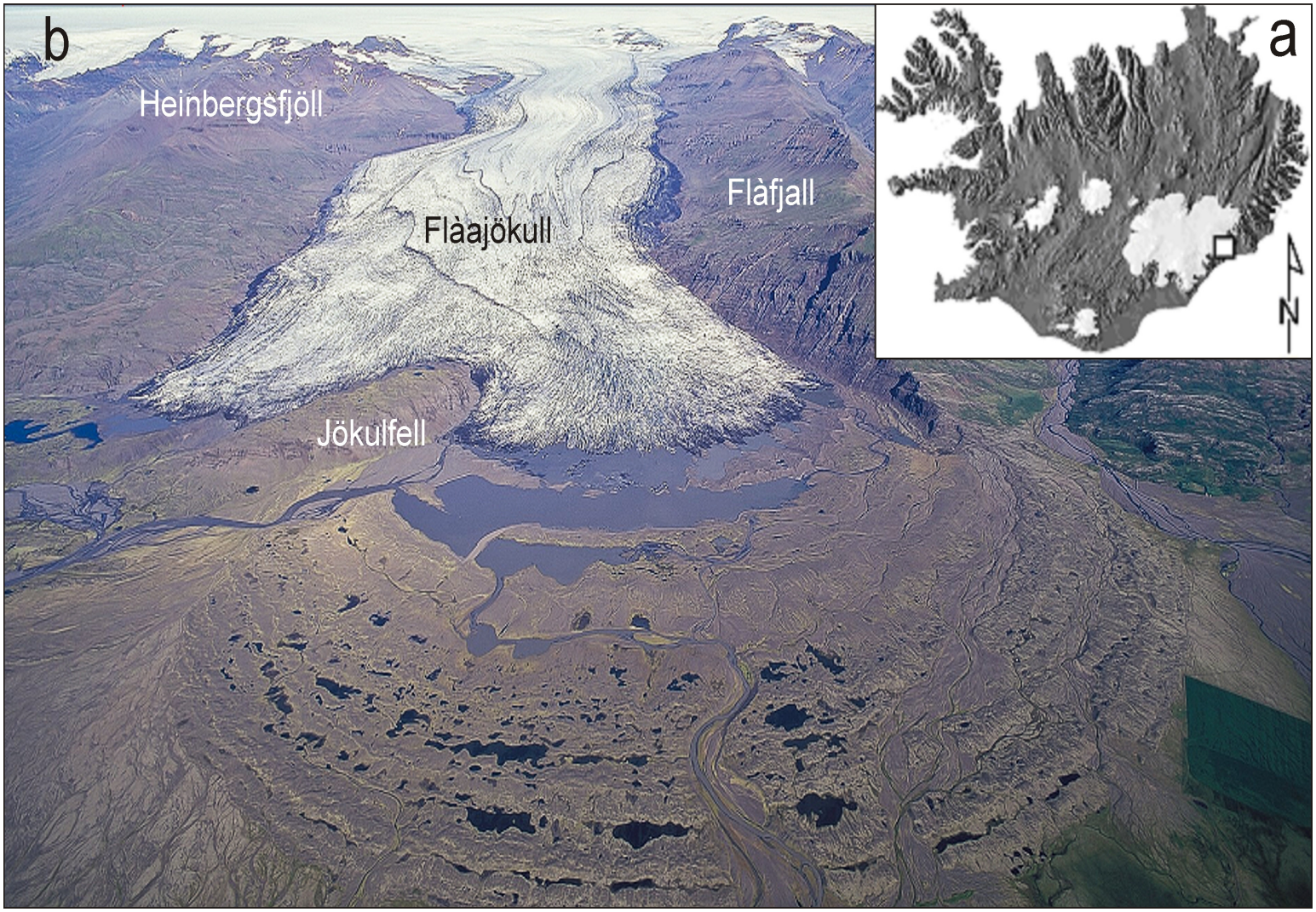

Figure 31. (a) Location of Fláajökull (square) at the southeastern margin of the Vatnajökull ice cap. (b) A panoramic view of Fláajökull and its forefield from the southeast in 2007. Photo acquired from Snaevarr Guðmundsson.

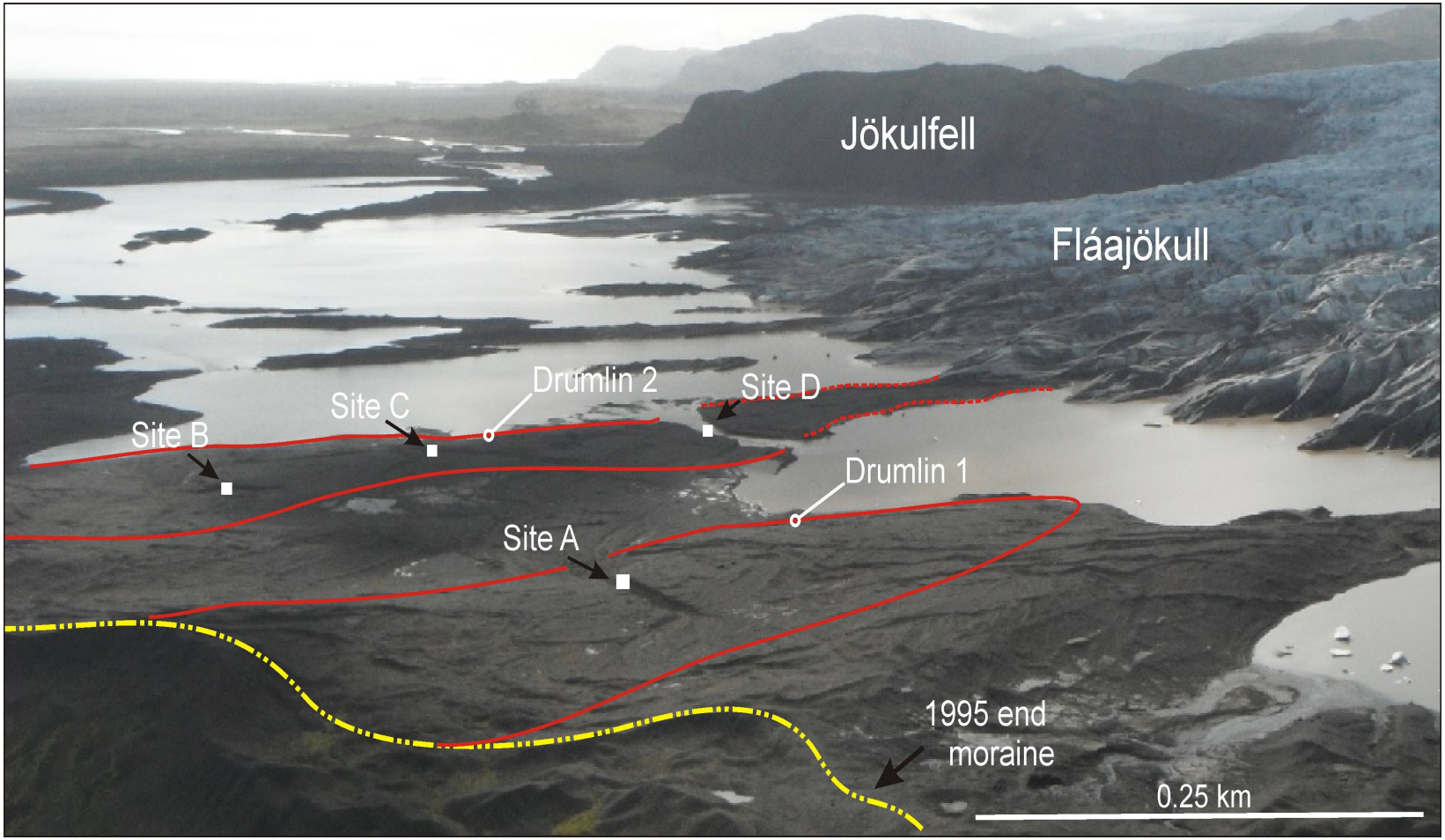

Figure 32. Close-up view from the northeast toward the south-southwest showing the location of Drumlin 1 and Drumlin 2 (outlined by red lines) and site locations. Note the yellow dashed line represents the 1995 end moraine. The ice lobe of Fláajokull is split by Jökulfell as seen in the distant horizon. Glacier flow is from right to left.

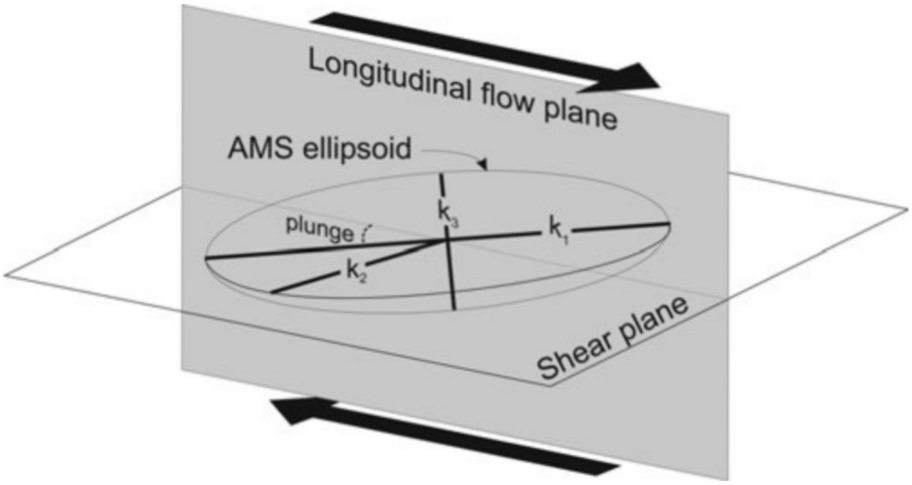

Figure 33. Anisotropy ellipsoid illustrating the three principal axes: maximum: K_1 , intermediate: K_2, and minimum: K_3. In this case, the maximum axis of the ellipsoid is aligned parallel to the shear direction (from Shumway and Iverson, 2009).

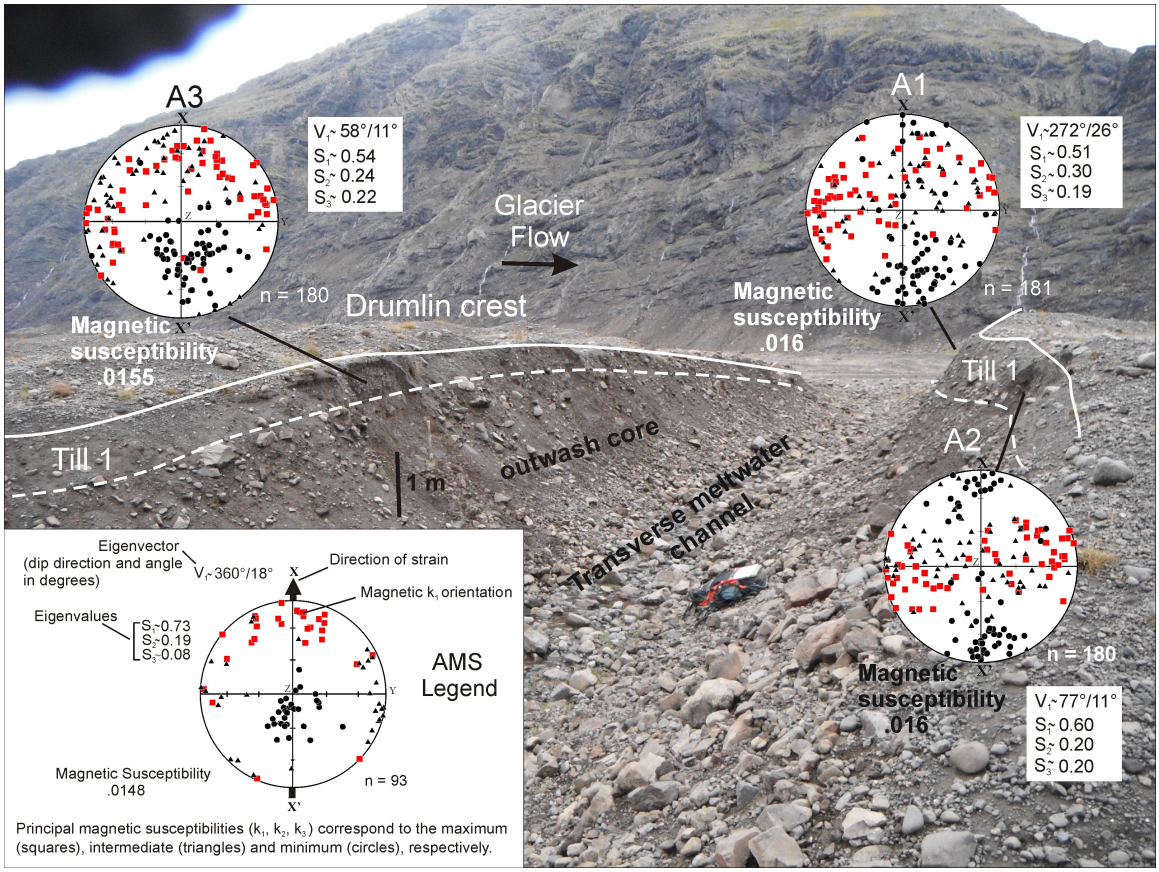

Figure 34. Drumlin 1 Site A looking north-northwest showing the upper Till 1 layer and the core of glaciofluvial sediments. Magnetic fabrics are shown in profiles A1, A2, and A3. Note the different fabric pattern (e.g. K_1 and K_2 susceptibilities arranged in a band) shown in A1 and A2 in contrast to A3. Glacier flow is from left to right.

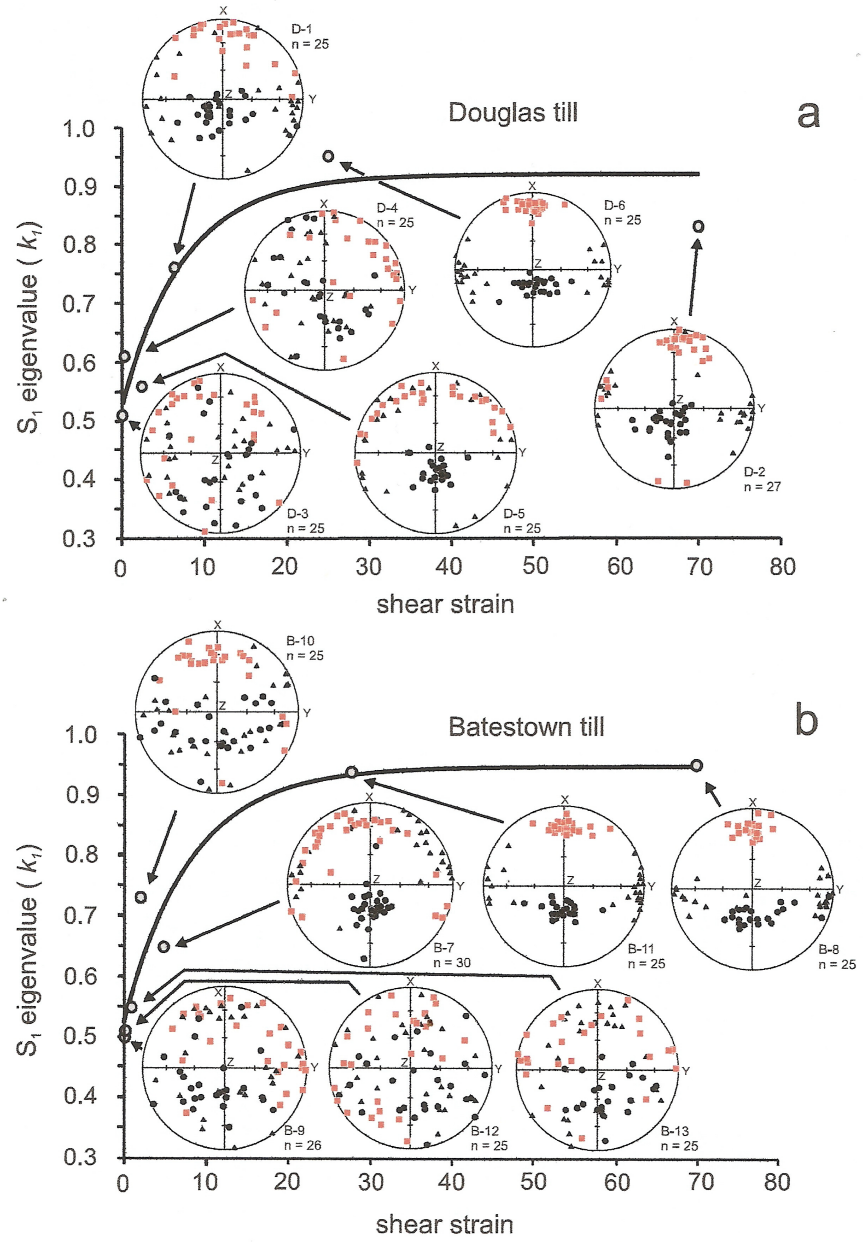

Figure 35. AMS fabrics from laboratory experiments using a mechanical ring shear apparatus, showing the eigenvalue strength as a function of shear strain from the Douglas till (a) and Batestown till (b). The eigenvalue strength is a measure of clustering of the K_1 susceptibility. Principal susceptibilities are plotted on lower-hemisphere stereoplots from a minimum of 25 or more till samples. Estimated shear strain magnitude for the Fláajökull fabrics may be less than 10 as indicated from laboratory shear strain values (from Hooyer et al., 2008).

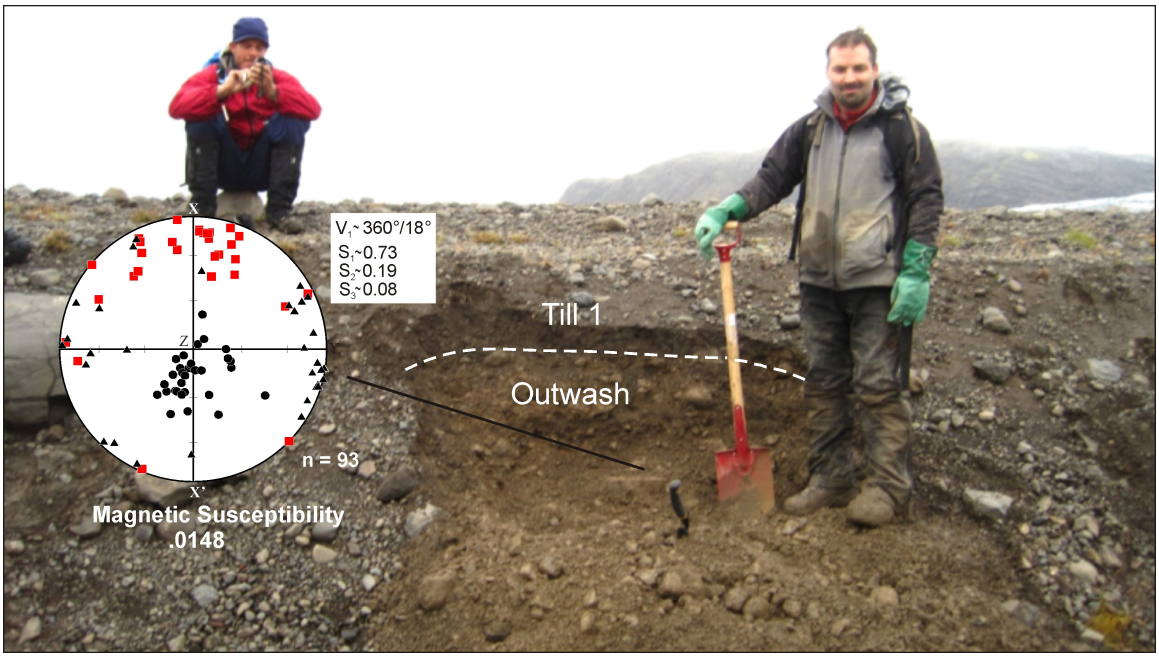

Figure 36. Drumlin 2 Site B looking westward showing the upper Till 1 layer and the underlying outwash core in a lateral meltwater channel. Note the moderate eigenvalue strength S_1 and its similar fabric pattern from ring-shear experiments (see Figure 35a Douglas till D-1).

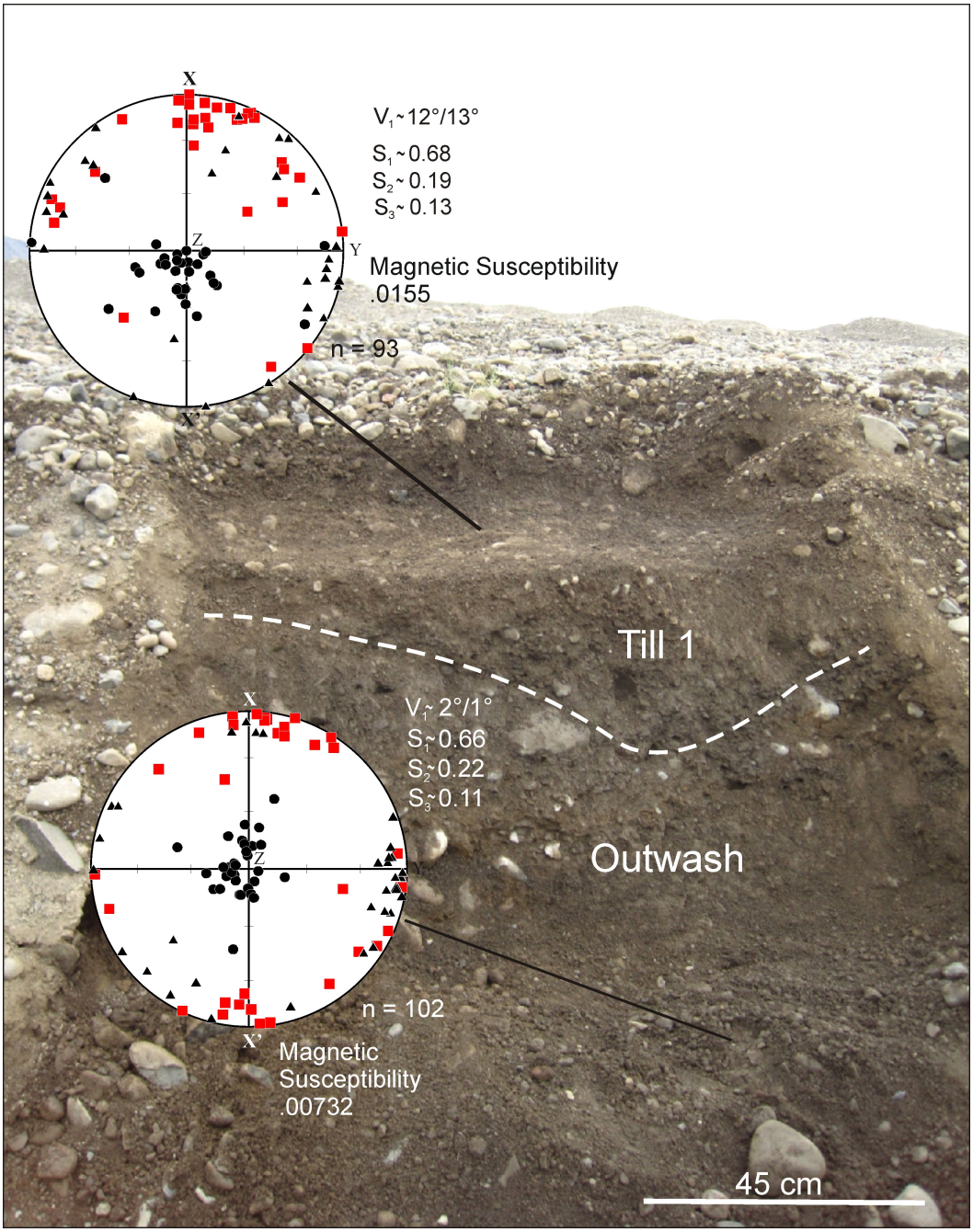

Figure 37. Drumlin 2 Site C showing the upper Till 1 layer and the lower outwash core materials. Note the well developed clustering of the magnetic susceptibilities and the upglacier plunge of the maximum K_1 in the upper till 1. Dashed-line represents approximate contact between Till 1 and outwash materials.

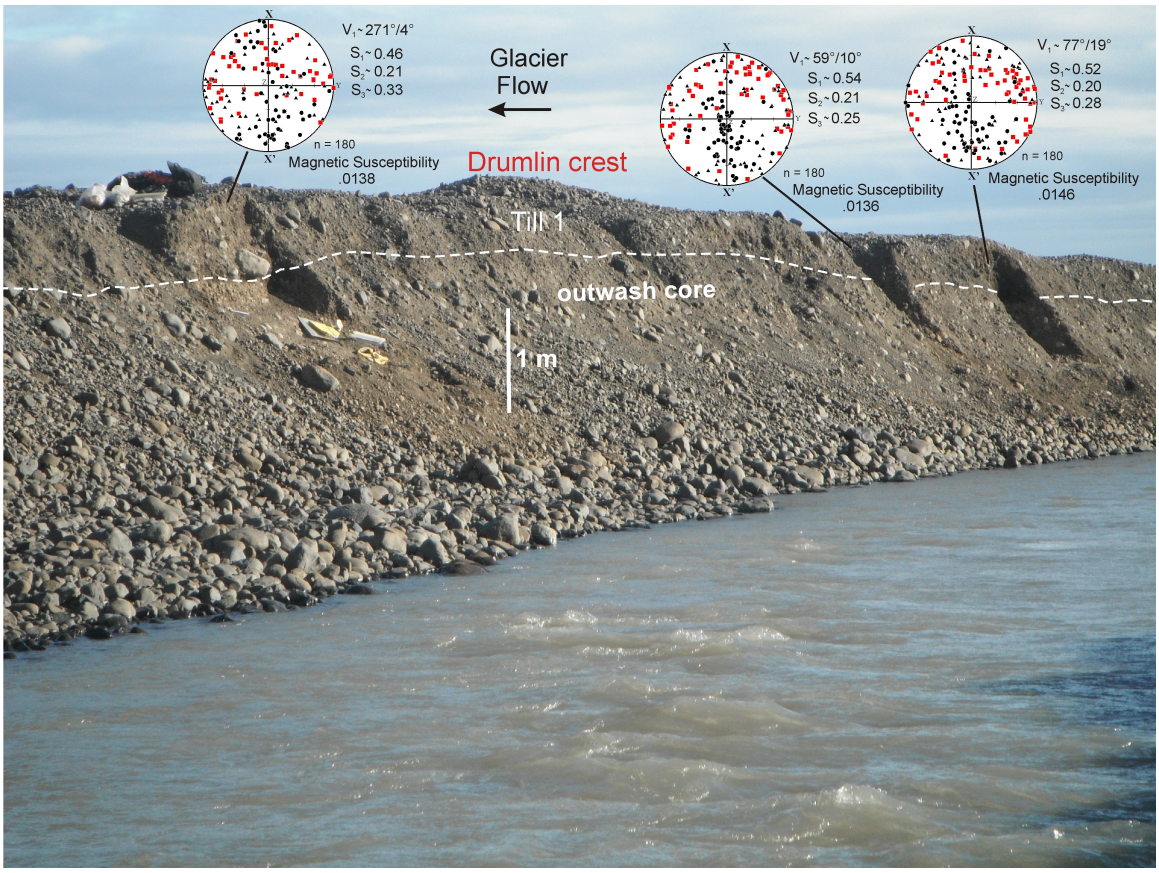

Figure 38. Site D looking south-southeast showing the exposed upper till 1 and outwash core of Drumlin 2 in a transverse meltwater channel. Dashed-line represents approximate contact between Till 1 and outwash materials. Note the weak fabric clustering of magnetic susceptibilities.

References

Alley, R.B., 1993. In search of ice-stream sticky spots. Journal of Glaciology v. 39, 447-454.

Ankerstjerne, S., Iverson, N.R., Lagroix, F., in press. Origin of a washboard moraine of the Des Moines Lobe inferred from sediment properties. Geomorphology

Björnsson, H., Pálsson, F., 2008. Icelandic glaciers. Jökull v. 58, 365-382.

Boulton, G.S., 1987. A theory of drumlin formation by subglacial sediment deformation, in Menzies, J., and Rose, J., eds., Drumlin symposium: Rotterdam, Balkema, 25-80.

Evans, D.J.A., Twigg, D.R., 2002. The active temperate glacial landsystem: a model based on Breiðamerkurjökull and Fjallsökull, Iceland, Quaternary Science Reviews, v. 21, 2143-2177.

Evans, D.J.A., Phillips, E.R., Hiemstra, J.F., Auton, C.A., 2006. Subglacial till: Formation, sedimentary characteristics and classification, Earth-Science Reviews, v. 78, 115-176.

Evenson, E.B., 1971. The relationship of macro-and microfabric of till and the genesis of glacial landforms in Jefferson County, Wisconsin. In Goldthwaite, R.P. (ed.): Till: A Symposium, 345-364. The Ohio State University Press, Columbus.

Fischer, U. H., Clarke, G.K.C., 2000. Review of subglacial hydro-mechanical coupling: Trapridge Glacier, Yukon Territory, Canada, Quaternary International, v. 86, 29-43.

Gentoso, M.J., Evenson, E.B., Kodama, K.P., Iverson, N.R., Alley, R.B., Berti, C., Kozlowski, A., 2011. Exploring till bed kinematics using AMS magnetic fabrics and pebble fabrics: the Weedsport drumlin field, New York State, USA, Boreas, v. 41, 31-41, (doi: 10.1111/j.1502-3885.2011.00221.x.).

Hannesdóttir, H., Björnsson, H., Pálsson, Aðalgeirsdóttir, G., Guðmundsson, Sv., 2015. Changes in the southeast Vatnajökull ice cap, Iceland, between ~1890 and 2010, The Cryosphere, v. 9, 565-585.

Hart, J.K., 1995. Recent drumlins, flutes and lineations at Vestari-Hagafellsjökull, Iceland, Journal of Glaciology, v. 41, 596-606.

Hooke, R. LeB., Hanson, B., Iverson, N.R., Jansson, P., Fischer, U.H., 1997. Rheology of till beneath Storglaciären, Sweden, Journal of Glaciology, v. 43, 172-179.

Hooke, R.LeB., Medford, A., 2013. Are drumlins a product of a thermo-mechanical instability, Quaternary Research, v. 79, 458-464.

Hooke, R. LeB., Iverson, N.R., 1995. Grain-size distribution in deforming subglacial tills: Role of grain fracture, Geology, 23, 57-60.

Hooyer, T.S., Iverson, N.R., 2000. Clast-fabric development in a shearing granular material: Implications for subglacial till and fault gouge, Geological Society of America Bulletin, v. 112, 683-692.

Hooyer, T.S., Iverson, N.R., Lagroix, F., Thomason, J.F., 2008. Magnetic fabric of sheared till: A strain indicator for evaluating the bed deformation model of glacier flow, Journal of Geophysical Research, v. 113, 1-15, (doi: 10.1029/2007JF000757).

Iverson, N.R., Hooyer, T.S., Fischer, U.H., Cohen, D. Moore, P.L., Jackson, M., Lappegard, G., Kohler, J., 2007. Soft-bed experiments beneath Engabreen, Norway: regelation infiltration, basal slip and bed deformation. Journal of Glaciology, v. 53, 323-340.

Iverson, N.R., Hooyer, T.S., Thomason, J.F., Graesch, M., Shumway, J.R., 2008. The experimental basis for interpreting particle and magnetic fabrics of sheared till, Earth Surface Processes and Landforms, v. 33, 627-645.

Iverson, N.R., Baker, R.W., Hooyer, T.S., 1997. A ring-shear device for the study of sediment deformation: Tests on tills with contrasting clay contents. Quaternary Science Reviews, v. 16, 1057-1066.

Jelínek, V., Kropáček, R.V., 1978. Statistical processing of anisotropy of magnetic susceptibility measured on groups of specimens, Studia geophysica et geodaetica, v. 22, 50-62.

Jacobson Jr. W.R., Hooyer, T.S., 2015. Laboratory study of fabric development in shearing till: The importance of effective pressure and shearing rate, Geomorphology, v. 250, 249-257.

Jónsson, S.A., Benediktsson, Í. Ö., Ingólfsson, Ó., Schomacker, A., Bergsdóttir, H.L., Jacobson Jr. W.R., Linderson, H., 2015. *in press.* Submarginal drumlin formation and late Holocene history of Fláajökull, southeast Iceland, Annuals of Glaciology.

Johnson, M.D., Schomacker, A., Benediktsson, Í. Ö., Geiger, A.J., Ferguson, A., and Ingólfsson, Ó., 2010. Active drumlin field revealed at the margin of Múlajökull, Iceland: A surge-type glacier, Geology, v. 38, 943-946, (doi: 10.1130/G31371.1.).

Knight, J., 2010. Drumlins and the dynamics of the subglacial environment, Sedimentary Geology, v. 232, 91-97, (doi: 10.1016/j.sedgeo.2010.10.001.).

Krüger, J., 1995. Origin, chronology and climatological significance of annual-moraine ridges at Mýrdalsjökull, Iceland, The Holocence, v. 5, 420-427.

Krüger, J., Thomsen, H.H., 1984. Morphology, stratigraphy, and genesis of small drumlins in front of the glacier Mýrdalsjökull, South Iceland, Journal of Glaciology, v. 30, 94-105.

Larsen, N.K., Piotrowski, J.A., 2003. Fabric pattern in a basal till succession and its significance for reconstructing subglacial processes, Journal of Sedimentary Research v. 73, 725-734.

Mark, D.M., 1973, Analysis of axial orientation data, including till fabrics, Geological Society of America Bulletin, v. 84, 1369-1374.

Menzies, J., 1979. A review of the literature on the formation and location of drumlins, Earth-Science Reviews, v. 14, 315-359.

Möller, P., Murray, A.S., 2015. Drumlinised glaciofluvial and glaciolacustrine sediments on the Småland peneplain, South Sweden e new information on the growth and decay history of the Fennoscandian Ice Sheets during MIS 3, Quaternary Science Reviews, v. 122, 1-29.

Patterson, C.J., and Hooke, R. LeB., 1995. Physical environment of drumlin formation. Journal of Glaciology, v. 41, 30-38.

Piotrowski, J.A., Larsen, N.K., Menzies, J., Wysota, W., 2006. Formation of subglacial till under transient bed conditions: deposition, deformation, and basal decoupling under a Weichselian ice sheet lobe, central Poland. Sedimentology, v. 53, 83-106.

Smith, A.M., Murray, T., Nicholls, K.W., Makinson, K., Aðalgeirsdóttir, G., Behar, A.E., Vaughn, D.G., 2007. Rapid erosion, drumlin formation, and changing hydrology beneath an Antarctic ice stream, Geology v. 35, 127-130.

Sharp, M., 1985. "Crevasse-fill" ridges-A landform type characteristic of surging glaciers? Geografiska Annaler, v. 67A, 213-220.

Shumway, J.R., Iverson, N.R., 2009. Magnetic fabrics of the Douglas Till of the Superior lobe: exploring bed-deformation kinematics, Quaternary Science Reviews, v. 28, 107-119.

Tarling, D.H., Hrouda, F., 1993. The Magnetic Anisotropy of Rocks. Chapman and Hall, London. 218 pp.

Thomason, J.F., Iverson, N.R., 2006. Microfabric and microshear evolution in deformed till. Quaternary Science Reviews, v. 25, 1027-1038.

Vreeland, N.P., Iverson, N.R., Graesch, M., Hooyer, T.S., 2015. Magnetic fabrics of drumlins of the Green Bay Lobe. Quaternary Science Reviews, v. 112, 33-44.

Waller, R.I., van Dijk, T.A.G.P., Knudsen, Ó., 2008. Subglacial bedforms and conditions associated with the 1991 surge of Skeiðarárjökull, Iceland, Boreas, v. 37, 179-194.

Whittecar, G.R., Mickelson, D.M., 1979. Composition, internal structures, and an hypothesis of formation for drumlins, Waukesha County, Wisconsin, U.S.A., Journal of Glaciology, v. 22, 357-371.

Winguth, C., Mickelson, D. M., Colgan, P. M., Laabs, B. J. C., 2004. Modeling the deglaciation of the Green Bay Lobe of the southern Laurentide Ice Sheet. Boreas v. 33 34–47, (doi: 10.1080/03009480310008662.).

Chapter 5: Conclusions

Our understanding of the ice dynamics and depositional and deformational landform systems remains limited because soft-bedded glaciers are difficult to access. To resolve this issue experimental research with a ring-shear laboratory device was implemented to investigate the shear rate and effective pressure upon fabric strength. Magnetic till fabrics were collected recently from several drumlins which have been discovered along the rapidly receding ice margin of Fláajökull. Previous ring-shear experiments (Hooyer et al., 2008) provided a benchmark for shear strain estimations on till samples which have formed under current glacial conditions.

In the second chapter the laboratory ring-shear device revealed that the fabric strength is independent of effective pressure (30 kPa to 150 kPa) and shearing rate (110 to 860 m $year^{-1}$). Regardless of varying the shearing rate and effective pressure, S_1 eigenvalues remained strong (0.91-0.98). Clustering of the maximum K_1 susceptibilities in the direction of shear is controlled by magnetite particles that are silt sized or smaller.

The observed strengthening effect over the pressure range may be a result of a small decrease in critical state porosity with fabric strength; however, this could not be confirmed in these experiments because it was not directly measured. In addition, our data suggests that the sheared sediments behaved like a Coulomb plastic material and that the magnetic fabric developed according to the "March model." Furthermore, this ring-shear data cannot be used as proxy for interpreting fabric strength in basal tills.

From a soil mechanics perspective, these results are consistent with the fact that once a steady state is achieved (constant void ratio and volume) there is a little variance in fabric strength.

In the third chapter the magnetic mineral particles within the ice were analyzed to test whether the dirty ice veins were sub-vertically sheared from the bed near the ice front, but then moderately deformed. The highlights from this chapter indicate that the magnetic particles in the temperate ice behaved as passive markers and are reliable indicators of strain. Most of the particles appeared along grain boundaries implying that the fabric formed primarily from slip along the grain boundaries during shear deformation. The magnetic proxy indicated a bulk three-dimensional strain (K_1, K_2, and K_3) signature of subvertical shear consistent with field relations.

The orientation of c-axes (e.g. derived from a block of dirty ice collected via chainsaw from the vein) revealed a multi-maximum girdle distribution characteristic of migration recrystallization. The eigenvector plunge of the c-axes was approximately normal to the shear plane which supports previous theory that c-axes rotate away from the shear plane toward the vertical.

Our sections also bear some resemblance to ice from the cold (-17° C) dirty ice of Taylor Glacier, Antarctica (Samyn et al., 2008). Similar to our situation, they reported crystal ribbons in debris-bearing ice, which they attributed to discontinuous grain growth, and a tendency to display c-axis orientations not unlike ours, which may have arisen from migration recrystallization (Kamb, 1959; Anderton, 1974; Gow and Williamson, 1976; Duval and Castelnau, 1995; Cuffey and Paterson, 2010). Slip bands and a possible tilt boundary were also observed. These fabrics likely developed from a combination of pure shear and simple shear resulting in a composite fabric.

In short, the three-dimensional state of strain recorded from the principal susceptibility axes (K_1, K_2, and K_3) in the ice may provide a better gauge than c-axis fabrics. The veins were

most likely formed from injection of an overpressured basal water system into crevasses followed by *in situ* freezing and deformation.

This technique may further serve as a tool for paleoclimatic investigation on the dirty ice cores retrieved from the Greenland Ice Sheet (Alley et al., 1997; Bender et al., 2010). As Bender et al. (2010) demonstrated in the GISP2, shearing in the ice core reduces layer inclination making deformation unrecognizable in the core width. Given this principle, magnetic anisotropy of the debris may provide a fingerprint for recognizing deformation and provide a directional window for tracing sheared layers in an ice sheet.

The fourth chapter introduces mechanisms of drumlin formation in the forefield of Fláajökull. It is suggested that the drumlins are nucleated from hydrological heterogeneity in bed hereafter called the Boulton hypothesis (Boulton, 1987). Some of the major highlights from this manuscript include the following: (1) Proglacial meltwater erosion reshaped the original morphology of the sand and gravel cores in front of Fláajökull prior to drumlinization. Subsequent advancement of the ice over Drumlin 2 (formed during 1966-199) led to deformation of the core materials and deposition of the overlying basal till. Fabrics are in accordance at Sites B and C and indicate shearing in the direction of glacier flow, which was approximately parallel to the drumlin long axis. (2) The drumlins likely resulted from a complex interaction of subglacial erosion, bed deformation, and lodgement, a depositional model is best suited for these drumlins. (3) The till carapace from Drumlin 1 (Site A) may be re-interpreted as a crevasse-squeeze-up instead of a recessional push moraine, which has been previously interpreted. These drumlins are also similar to the drumlins formed at Breiðamerkurjokökull (Evans and Twigg, 2002) and Skeiðarárjökull (Waller et al., 2008). Another important highlight is that the Fláajökull tills likely only experienced shear strains of <10 according to ring-shear tests.

The results of this work have contributed new evidence as well as confirmed existing hypotheses of drumlin genesis, demonstrated traditional methods with more sophisticated techniques, (e.g. optical c-axis measurements coupled with magnetic fabrics), and employed engineering mechanics of shearing sediment from an experimental standpoint. The results presented from this research will hopefully provide further insight into magnetic ice fabrics and their much anticipated use in paleoclimatic ice core analysis.

APPENDIX

Submarginal drumlin formation and late Holocene history of Fláajökull, southeast Iceland

Sverrir Aðalsteinn Jónsson[1], Ívar Örn Benediktsson[2], Ólafur Ingólfsson[1,3] Anders Schomacker[4,5], Helga Lucia Bergsdóttir[1], William R. Jacobson Jr.[6] & Hans Linderson[2]

[1]Institute of Earth Sciences, University of Iceland, Sturlugata 7, IS-101 Reykjavík, Iceland.

[2]Lund University, Department of Geology, Sölvegatan 12, S-223 62 Lund, Sweden.

[3]University Centre in Svalbard (UNIS), P.O. Box 156, N-9171 Longyearbyen, Norway.

[4]Norwegian University of Science and Technology (NTNU), Department of Geology, Sem Sælands veg 1, N-7491 Trondheim, Norway.

[5]Centre for GeoGenetics, Natural History Museum of Denmark, University of Copenhagen, Øster Voldgade 5-7, DK-1350 Copenhagen K., Denmark.

[6]University of Wisconsin-Milwaukee, Geosciences Department P.O. Box 413, Lapham Hall 366, Milwaukee, WI 53201 USA.

Abstract

Fláajökull is a non-surging outlet glacier draining the south-eastern part of the Vatnajökull, SE-Iceland. Fláajökull was stationary or advanced slightly between 1966 and 1995 and formed a prominent end moraine. Glacial retreat since then has revealed a cluster of 15 drumlins. This study focuses on the morphology and sedimentology of the drumlins. They are 100-600 m long, 40-130 m wide, and have cores of glaciofluvial sediment or till. The drumlins are draped by about 1 m thick, massive subglacial traction till. The glacier forefield is characterized by a number of arcuate and saw-tooth, terminal and recessional moraine ridges, overridden moraines with fluted surfaces, and glaciofluvial outwash. Some of the drumlins extend towards the 1995 end moraine but terminate abruptly at the moraine and are not observed in front of it. This suggests that they were formed sub-marginally during the 1966-1995 terminal

position. The sedimentary structure of the drumlins is best explained by the *sticky spot* model. Dating and dendrochronological analyses of birch logs found on the surface of one of the drumlins indicate that the valley was forested around 2100 cal. yr BP, after which the glacier started to reform, possibly due to an abrupt change in climate.

1. Introduction

Drumlins are important landforms of many Pleistocene landscapes and, although they have been extensively studied, the exact nature of their formation is still enigmatic (Menzies, 1979; Patterson and Hooke, 1995; Clark and others, 2009). It is widely accepted that drumlins form beneath glaciers through ice-substrate interaction (Benn and Evans, 2006); i.e. through deposition, erosion, deformation or a combination of these processes. Drumlins are usually thought to have formed some distance behind the ice front. This is reflected in ice stream models (Stokes and Clark, 2001), in the active temperate glacial landsystem model by Evans (2003), and has been suggested for well-studied drumlin fields, such as the Great Lakes region drumlin fields of North America (Kerr and Eyles, 2007; Maclachlan and Eyles, 2013).

Drumlins are not as common in the forefields of modern glaciers as in Pleistocene landscapes. Single drumlins or drumlins in small groups have been observed in modern glacial environments in Iceland (Krüger and Thomsen, 1984; Boulton, 1987; Kjær and others, 2003; Schomacker and others, 2006; Waller and others, 2008; Schomacker and others, 2012) , Antarctica (Rabassa, 1987), Switzerland (van der Meer, 1983) and Alaska (Haselton, 1966). To date, however, the only modern drumlin field that has been described is at Múlajökull, Central Iceland (Johnson and others, 2010; Jónsson and others, 2014).

The Little Ice Age (LIA) in Iceland started around AD 1250 (Geirsdóttir and others, 2009) and peaked at the end of the 19th century. After a more or less continuous retreat from their LIA terminal positions during the most of the 20th century, most Icelandic outlet glaciers experienced a minor re-advance during the last quarter of the 20th century that generally culminated around 1995 (Sigurdsson, 2003). During the following accelerated retreat (Sigurdsson, 2013), drumlins have been revealed at the margins of some Icelandic glaciers, including Múlajökull (Johnson and others, 2010; Jónsson and others, 2014), Sólheimajökull (Schomacker and others, 2012; Slomka and Eyles, 2015), Breiðamerkurjökull (Evans and Twigg, 2002), Sléttjökull (Kjær and others, 2003) and Skeiðarárjökull (Baltrūnas and others, 2014; Waller and others, 2008).

At Fláajökull (Fig. 1), an outlet glacier from Vatnajökull, south-east Iceland, a cluster of fifteen drumlins has become exposed following a retreat of the glacier from a large end moraine formed in 1995 (termed the 1995 end moraine in this paper). Fláajökull is a non-surging glacier, and like all Icelandic outlet glaciers considered to be a temperate glacier (Björnsson and Pálsson, 2008). We describe Fláajökull with reference to the active temperate glacier landsystem model of Evans and Twigg (2002) and Evans and others (1999), and in line with the approach of Evans and others (2015). According to this model, the forefield of temperate outlet glaciers is divided into three depositional domains: a) areas of extensive, low amplitude marginal dump, push and squeeze moraines derived largely from material on the glacier foreland and often recording annual recession of active ice, b) glaciofluvial landforms, and c) subglacial landforms such as flutes, drumlins and overridden end moraines.

We describe the morphology and sedimentology of the fifteen drumlins within the recently exposed forefield and present a detailed geomorphological map in order to understand

drumlin formation and the development of the active temperate landsystem at Fláajökull. In addition, a simplified Holocene glaciation history for Fláajökull is reconstructed based on previously published research and ^{14}C dates and dendrochronological analysis of birch logs sampled from the surface till of one of the drumlins.

2. Methods

2.1 Geomorphological mapping

Mapping of landforms was undertaken using a combination of remote sensing and ground surveys (2012-2014). An airborne 2.5-m LiDAR DEM covering the glacier and about 2 km into the forefield was visualized as a terrain shade-relief model and used along with panchromatic aerial photographs, with 0.5-m pixel size, taken in 1982 and 1989 by Landmælingar Íslands (National Land Survey) for mapping the forefield. The LiDAR data were recorded in 2010 by the Icelandic Meteorological Office and the Institute of Earth Sciences of the University of Iceland (Jóhannesson and others, 2013). All data were handled in ESRI ArcGIS 10 in the UTM/WGS84 reference system, and elevations are in meters above sea level. Sediments and landforms were mostly mapped on the basis of the LiDAR DEM data but the orthophotographs were used both with the LiDAR and exclusively in the south-east part of the forefield, where LiDAR data were unavailable. The length and width of the drumlins were measured in ArcGIS. The height of drumlins that are surrounded with water was measured from the water surface, which defines their basal plane height. Four drumlins were not fully exposed from under the ice margin and were not measured.

2.2 Sedimentological logging

Four stream-cut sections (A-D; see Fig. 6 for locations) in the drumlins were cleaned and logged following the data chart by Krüger and Kjær (1999). The lithology and principal sedimentological characteristics, i.e. grain size, sorting, clast content, matrix-clast relationship, and clast roundness of each unit were described in the field along with the nature of their basal contacts and their lateral extent. Interpretation of units was both done in the field and on basis of anisotropy of magnetic susceptibility measurements, see below (section 2.4).

2.3 ^{14}C dating of birch logs

Three birch logs were discovered embedded in sediments on top of the northernmost drumlin. The dendrochronology of the logs was analyzed at the Swedish National Laboratory for Wood Anatomy and Dendrochronology, Lund University, and two of them were dated using Accelerator Mass Spectrometry (AMS) at Lund University Radiocarbon Dating Laboratory. The dates were calibrated in OxCal 3.10 using the atmospheric data from Reimer and others, (2013).

2.4 Anisotropy of magnetic susceptibility (AMS)

We collected till specimens in the years 2012 and 2013 for anisotropy of magnetic susceptibility (AMS) measurements. These measurements were taken from three drumlin sections (A, B, C see Fig. 6). A minimum of 25 plastic boxes (8 cm^3) were used in the collection process for sampling. Principal directions of magnetic susceptibility (K_1, K_2, and K_3) were measured using the AGICO MF*K1*-FA Fully Automatic KappaBridge to determine the three-dimensional state of strain, which is visualized with a susceptibility ellipsoid (Jelínek and Kropáček, 1978). Furthermore, the ellipsoids are used to identify the three-dimensional strain

style, direction and magnitude of the microfabric (e.g. allows simple shear to be distinguished from pure shear) and therefore to infer patterns of till deformation. Perhaps more importantly, the magnetic fabric provides excellent spatial resolution because of its averaging effect of many magnetic grains rather than the orientation of a single grain.

In addition to the AMS measurements, we conducted high temperature susceptibility (HTS) and hysteresis experiments. These experiments were performed in order to determine the magnetic carrier and grain size. HTS experiments were evaluated on the fine-grained particles (clay and silt) that were less than 65 μm. The unblocking temperature was used to identify the mineralogy and hysteresis loop parameters helped target the particle size. The magnetic fabric data were analyzed using the procedure outlined by Mark (1973).

3. Regional setting and geomorphology

3.1 Fláajökull

Fláajökull is an approximately 13 km long, non-surging outlet glacier draining the south-eastern part of the Vatnajökull ice cap (Björnsson, 2009; Fig. 1). The glacier flows to the south-east between Mt. Fláfjall and Mt. Heinabergsfjöll, and terminates on a flat sandur called Mýrar. The present glacier snout is split into two lobes by Mt. Jökulfell. The small drumlin field is associated with the north-eastern lobe (Figs 1c and 2).

The ice front variations of Fláajökull have been recorded from 1894 and with some continuity from 1930 (Fig. 1b). There is, however, a gap in the records between 1972 and 1991 and again from 2000 to 2009. We added two ice front positions from aerial images taken in 1982 and 1989 to get a more complete record (Fig. 1b). The record shows a rapid retreat between ca. 1930 and 1942, and again after 1998, but a still-stand or even a minor re-advance between 1966

and 1995. After 1995 the Fláajökull ice margin has retreated rapidly and is now (2013) located 706 m inside the moraine.

According to radio echo soundings from year 2000, the glacier occupies a 60-m deep depression inside the present ice margin North of Mt. Jökulfell (Fig. 1c). This depression gets gradually shallower towards the 1995 end moraine (Pálsson and Björnsson, 2000).

Direct velocity measurements of Fláajökull do not exist. However, a velocity of a few meters to a few tens of meters per year is presumed based on both measured and modeled velocities at the adjacent Hoffellsjökull glacier, which rests in a similar topographic and climatic setting just 11 km east of Fláajökull (Aðalgeirsdóttir and others, 2011).

3.2 Geomorphology of the forefield

The landforms at Fláajökull are divided into four groups based on the glacial environment in which they are formed, i.e. subglacial, ice-marginal, supraglacial and glaciofluvial. Subglacial sediments and landforms are common in the forefield of Fláajökull. About half of the forefield is classified as a subglacial till plain (Fig. 2). The till plain is generally fluted with the most prominent flutes occurring on overridden, drumlinized end moraines, such as the one located about 1.3 km from the ice front (Figs 2 and 4), (Evans and others, 2015). The flutes range between 1 and 90 m in length and ~0.5 and 1.5 m in width. More flutes than indicated on Fig. 2 were observed in the field but were not mapped because of their small size or low resolution of the LiDAR image and/or aerial photographs. In addition to the flutes, we have mapped 15 drumlins, which are described in more detail in section 4. Evans and others (2015) described a number of crevasse fill ridges but most of these ridges are interpreted as recessional moraines in the present study.

Ice-marginal landforms are widespread at Fláajökull. Multiple arcuate (dark brown in Fig. 2) and saw-tooth (red in Fig. 2; Burki and others, 2009) moraine ridges can be found in the forefield (Figs 2 and 6). The outermost terminal moraine is from the Little Ice Age (LIA) maximum in 1894 (Hannesdóttir and others, 2014) and the innermost one from the re-advance that terminated in 1995. This moraine is about 30 m wide and 10-25 m high above the surroundings, and conspicuous in the proximal part of the forefield, which probably owes to the fact that the ice margin was stationary around this position for a long time, supplying large amounts of sediment for moraine build-up (Fig. 5c).

There are a number of smaller recessional moraines in the forefield, formed during minor late winter/early spring re-advances. These moraines are best preserved in the area inside the 1995 end moraine (Figs 2 and 5a). The recessional moraines are continuous for only short distances with individual segments ranging from a few meters to a few tens of meters in length and displaying a saw-tooth pattern. They are usually about 1.5 m wide and 0.5-1 m high and consist most commonly of till.

Supraglacial landforms are rare at Fláajökull. However, surface fractures were observed within the hummocky moraine on the proximal slope of the 1995 end moraine (Fig. 2), indicating melting of buried ice. Glaciofluvial sediments (sand and gravel) and landforms (drainage channels, sandur plains) from various meltwater outlets are conspicuous in the Fláajökull forefield (Fig. 2). The river Hólmsá drains Fláajökull and runs towards south, just east of Mt. Jökulfell, (Figs 1, 2, and 6), leaving behind a braided sandur. Fluvial plains and drainage channels are most extensive close to the present day Hólmsá outlet. In the northern part of the forefield, channels from former outlets close to Fláfell are inactive because of the retreat of the glacier and damming of river outlets.

4. Drumlin morphology and sedimentology

4.1 Size and morphology

We mapped 15 drumlins at Fláajökull, four of which are only partly exposed and their exact size is thus not known (Fig. 6). The size of the fully exposed drumlins varies greatly. In the northern part, four large drumlins occur (numbered 1-4 in Fig. 6), ranging from 430-580 m in length, 115-130 m in width, and 8-13 m in height above the surrounding water table (Figs 2, 3a, and 6), and with an elongation ratio of 2.4-4.8. All these drumlins extend towards the 1995 end moraine but not beyond it. This is most obvious at drumlin 3, which is parabolic in shape at the downglacier end (Fig. 6). Further south, there are four more drumlins (drumlins 5-8 in Fig. 6), extending to the 1995 end moraine. These drumlins are 120-210 m in length, 40 to 110 m in width and 3-8 m high, with an elongation ratio of 1.4-3.

Closer to the ice, three spindle shaped drumlins have completely emerged from the ice (drumlins 9-11 in Figs 3c and 6). These drumlins are located in a proglacial lake that is dammed by man-made dikes but also represents the downglacier end of the subglacial overdeepening. Because these drumlins are partly under water, their full size could not be determined. Even when this is taken into account it seems clear that they are considerably smaller than the drumlins further north, all being about 50 m wide and ranging in length from around 160 to 280 m, giving an elongation ratio between 3.2 and 4.7.

Four more drumlins are currently emerging from the ice margin and have not been completely exposed (drumlins 12-15 in Figs 2 and 6). Their size is therefore not known but three of them seem to be relatively small while the one furthest south appears to be larger according to Figs 2 and 6. The geometry and elongation ratio of the fully exposed drumlins, number 1-11, is summarized in Table 1.

4.2 Stratigraphy and sedimentology

The stratigraphy and sedimentology of the drumlins was investigated in four excavated sections (A, B, C and D; see Fig. 6). The sections are located in three large drumlins in the northern part of the forefield and oriented perpendicular to the long axis of the drumlins. Section A is located in the proximal end of drumlin 1 (Fig. 7a), section B (Fig. 9a) is in the centre of drumlin 2 (Fig. 9a), and sections C and D are located within drumlin 4, with section C in the proximal part and section D in the distal part (Figs 9c and 11).

Section A — Section A is located at the proximal end of drumlin 1 (Fig. 6). The section is 4.2 m high and consists of two stratigraphic units (Figs 7 and 9a). The lower unit, A-1, comprises massive, rounded gravel that is at least 4 m thick with its lower contact being unexposed (Fig. 8). The upper unit, A-2, is, at the macroscale, a massive, matrix-supported diamict that has silty-sandy matrix and is unconsolidated (easy to excavate). The unit is rich in sub-rounded to sub-angular clasts, typically ranging from 2-50 cm in diameter. The unit is about 0.6 m thick but the thickness varies laterally between 0.3 and 0.8 m. The contact with the underlying gravel is sharp. The surface is covered with a clast pavement. The AMS microfabric shows significant clustering of the K_1, K_2 and K_3 susceptibilities, with a shallow dip of K_1. This indicates a till shearing direction toward the southeast roughly parallel to the drumlins long axis (K_1 up glacier plunge of 11°) with an approximately horizontal shear plane (defined by K_2 susceptibilities). The gravel is interpreted as proglacial outwash and the surface diamict as subglacial traction till (Table 1, Fig. 8; Evans and Benn, 2004; Evans and others, 2006, 2015).

Section B — Section B is located in the centre of drumlin 2 (Fig. 6). The section is 3.2 m high and consists of two till units (Figs 10a and 10). The lower unit, B-1, is a diamict that is at least 2 m thick but its base is unexposed. At the macroscale, the diamict is massive, matrix-

supported with sandy-gravelly matrix. It is rich in clasts that are up to 40 cm in diameter and mainly sub-angular to sub-rounded. Unit B-1 is unconsolidated and easy to excavate. The upper unit, B-2, is generally about 1 m thick diamict but the thickness varies between 0.4 and 1.2 m with the lower boundary being gradational. At the macroscale, the diamict is massive, matrix-supported with silty-sandy matrix and moderately clast rich, with clasts being mainly sub-rounded to sub-angular and up to about 30 cm in diameter. The diamict is poorly consolidated and easy to excavate and the surface is covered with a clast pavement. The AMS microfabric illustrates a girdle distribution of K_1 and K_2 susceptibilities with an average K_3 plunge of 54° defining the pole to the shear plane (K_1-K_2 plane). The mean K_1 susceptibility orientation plunges 11° upglacier, which is approximately parallel to the shearing direction and drumlin long axis. The lower unit, B-1, is interpreted as a subglacial traction till (Evans and others, 2006; Evans and others, 2015). The upper unit, B-2, is expressed in a recessional push moraine at this site (Krüger, 1995). However, it has similar characteristics as unit B-1 below and was thus probably initially deposited as a subglacial traction till that subsequently got pushed by the ice margin during a recent late winter/early spring re-advance (Krüger, 1995).

Section C — Section C is located in the proximal end of drumlin 4 (Fig. 6). The section is 2.8 m high and shows two units (Fig. 11). The lower unit, C-1, comprises a massive, coarse gravel with an exposed thickness of over 2 m. The upper unit, C-2, is a diamict that is at the macroscale massive, matrix-supported with silty-sandy matrix, rich in 5-40 cm large, sub-angular to sub-rounded clasts and easy to excavate. The surface is covered with a clast pavement. The diamict is up to 0.7 m thick and the lower boundary is sharp. Section C, shows an AMS fabric broadly similar to section B; however, K_1 axes cluster at 77° and gently plunge at 19° upglacier. K_3 axes cluster at 190° and plunge moderately at 73°, perpendicular to the shear plane. Shearing

is subparallel to the glacier flow direction toward the southeast. The lower unit was interpreted as glaciofluvial outwash and the upper unit as subglacial traction till (Evans and Benn, 2004; Evans and others, 2006, 2015).

Section D — Section D is located in the distal end of the same drumlin as section C, i.e., drumlin 4 (Fig. 6). The section is 2.1 m high and consists of two units (Figs 12 and 13). The lower unit, D-1, is over 1 m thick diamict with its lower boundary unexposed. At the macroscale, the diamict is massive, matrix-supported with sandy-gravelly matrix and rich in <30 cm large clasts. The diamict is easy to excavate. The upper unit, D-2, is an easily excavated diamict, at the macroscale massive, matrix-supported with silty-sandy matrix and moderate content of up to 20 cm large clasts. The diamict is typically about 1 m thick but the thickness is variable, with a sharp conformable lower contact to D-1. The surface is covered with clast pavement and there is a sand lens in the top of the unit. This AMS fabric site displays significant clustering of K_1, K_2, and K_3 susceptibilities, as also revealed from section A. The mean K_1 susceptibility axes cluster at 002° and plunge 1° upglacier. K_2 susceptibilities cluster at 093° approximately normal to the K_1 clusters. K_3 clusters are oriented at 183° and steeply plunge at 85°. The longitudinal flow plane (K_1-K_3 plane) is approximately parallel to the drumlin long axis. Both units, D-1 and D-2, are interpreted as subglacial traction tills and the sand lens at the top as a small channel fill (Evans and others, 2006, 2015).

5. Chronology

About 70 m south-west of section A (Fig. 6), compact, greyish to bluish sediment was observed at the surface of drumlin 1 down to about 10-20 cm depth. We interpret this sediment to be peat/palaeosol originating in the valley now occupied by the glacier. The sediment has been

deformed and dislocated by the advancing glacier and finally deposited on top of the drumlin. The sediment contains birch logs that are 15-60 cm long and 10-20 cm in diameter (Fig. 14). Two of the birch logs were sampled for ^{14}C dating. The first sample, LuS 10801, gave ^{14}C age of 2165 ± 35 BP and calibrated age range with 95,4% probability of 2310-2055 BP. Analysis of the shape of this specimen and its tree-rings indicates that this tree was 20-30 cm in diameter and rather fast growing, suggesting relatively warm conditions (Fig. 14a). The second sample, LuS 10802, gave ^{14}C age of 2105 ± 35 BP and calibrated age range with 93,1% probability of 2155-1990 BP. Dendrochronological analysis indicates that the sample is from a 25-40 yr old tree with dense tree-rings, suggesting colder growing conditions (Fig. 14b). The third sample, IS000 (Fig. 14c), was not dated but allowed for a more accurate dendrochronological analysis showing 84 tree-rings (Fig. 14d). This tree was growing by 0.5 mm/yr on average during the first 60 years when an abrupt decrease in growth rate (tree-ring width) to 0.05 mm/yr occurred (Fig. 14d and e). The dense rings in the outer part of this tree could indicate that it is of a similar age as the second sample (LuS 10802). The dates and the dendrochronological analyses of the tree logs not only suggests that the valley was forested and that Fláajökull was considerably smaller or absent at that time, but also that the glacier started to expand sometime after c. 2100 BP, possibly due to an abrupt climate deterioration.

6. Discussion

6.1 Drumlin formation

In two sections located at the proximal end of drumlins, sections A and C, glaciofluvial sediments make up about four fifths of the section height and are overlain by subglacial traction till on top. Although our dataset lacks definitive indications of erosion in the form of erosional

unconformities, this could suggest that the drumlins at Fláajökull are formed by a combination of erosion of pre-existing outwash sediments and deposition and shearing of till.

The glaciofluvial sediment in the drumlin cores suggests that the drumlins were formed around sticky spots in the substrate where higher resistance to basal sliding, erosion and deformation caused the deposition of the subglacial traction till (Boulton 1987; Piotrowski and others, 2004; Stokes and others, 2007). Subsequently, the continuous flow of the glacier in this area between 1966 and 1995 shaped the till-draped sticky spots into drumlins. This corresponds to proposed mechanisms of drumlin formation at Breiðamerkurjökull (Evans and Twigg, 2002) and Skeiðarárjökull (Boulton 1987; Waller and others, 2008), both southern outlets of the Vatnajökull ice cap, and suggests that the location and distribution of the drumlins is mainly controlled by the hydrological and sedimentological properties of the substrate, rather than e.g. being related to crevasses (Alden, 1911; Johnson et al., 2010).

The drumlins at Fláajökull have a relatively low elongation ratio (1.4-4.8) and they all terminate abruptly at the 1995 moraine; however, there is no indication of erosion and truncation by meltwater at their distal end in front of the moraine. We suggest that the drumlins were formed sub-marginally during the 1966-1995 advance that terminated at this position; hence, they do not extend beyond it. It is worth stressing that this advance was not a surge but rather a response of the glacier to a continuously positive net mass balance over this period. It can thus also be concluded that the drumlins at Fláajökull were formed under 'normal' ice velocities like previously reported from e.g. Sléttjökull and Sólheimajökull in Iceland (see Krüger, 1987, 1994; Krüger and Thomsen, 1984; Schomacker and others, 2012) rather than under substantially enhanced velocities (ice streaming or surging), as has been suggested for highly elongate Pleistocene drumlins (e.g. Hart, 1999; Stokes and Clark, 1999, 2002; Briner, 2007; Hess and

Briner, 2009) and for drumlins formed by surge-type glaciers in Iceland (e.g. Boulton, 1987; Hart, 1995; Waller and others, 2008; Johnson and others, 2010).

6.2 Glaciation history

The dates of the tree logs in the drumlins at Fláajökull of around 2100 years BP indicate that the valley now occupied by the glacier had been ice-free and that the glacier started to reform at around that time. This correlates with the glacial history of Eyjabakkajökull, a surge-type outlet of the north-eastern part of the Vatnajökull ice cap, as reconstructed from sediment cores from Lake Lögurinn that receives meltwater from the glacial river draining Eyjabakkajökull. The results from Lögurinn indicate that Eyjabakkajökull did not exist from 9000-4400 years BP after which the glacier started to reform. The surges of Eyjabakkajökull started around 2200 years BP and the glacier continued to expand until about 1700 years BP when it reached a size it maintained until the onset of the Little Ice Age (Striberger and others, 2012). This is somewhat similar to the results of Geirsdóttir and others (2009), who suggest that the onset of the Neoglaciation in Iceland was sometime after 6000 years BP with increasing glacial activity between 4500 to 4000 years BP and even more between 3000 and 2500 BP, when temperatures were the lowest during the Holocene apart from the LIA. This is in line with chronological data from e.g. Sólheimajökull (a southern outlet of the Mýrdalsjökull ice cap) and Kvíárjökull (at southern outlet of the Vatnajökull ice cap) which suggest that these glaciers had their maximum Late Holocene extent around 1800 and 3000 BP, respectively (Thorarinsson, 1956; Schomacker and others, 2012). The results from Fláajökull, therefore, contribute to a growing set of evidence from different locations in Iceland that outlet glaciers reformed in the

late Holocene after having been absent or considerably smaller since the early Holocene, and that these fluctuations were driven by climate changes.

Conclusions

- The forefield of Fláajökull contains fifteen drumlins that have become exposed during ice marginal retreat since 1995. The drumlins are 100-600 m long, 40-130 m wide and 5-10 m high, with an elongation ratio of (1.4-4.8).
- The drumlins consist of glaciofluvial sediment in their cores and subglacial traction till on top. We suggest that glaciofluvial deposits acted as sticky spots onto which the subglacial traction till was deposited due to resistance to basal sliding, erosion and deformation.
- The fact that the drumlins at Fláajökull occur just proximal to the 1995 end moraine and not beyond it indicates that they were formed in a sub-marginal setting during a period of still-stand or minor re-advance from 1966-1995. If the drumlins were older, they would most likely have extended beyond the 1995 moraine.
- The drumlins formed under 'normal' low-velocity ice flow conditions during the 1966-1995 re-advance and cannot be related to any kind of fast-flow events (e.g. a surge).
- New datings of birch logs and the known age of the LIA terminal moraines suggest that the valley presently occupied by Fláajökull was ice free and carried a birch forest around 2100 cal. yr BP and that the glacier expanded thereafter to reach its maximum Holocene extent in 1894.

Acknowledgements

This study was funded by the University of Iceland Research Fund and the Icelandic Research Fund (RANNÍS) as part of our drumlin studies in Iceland. Anton Hansson at the Swedish National Laboratory for Wood Anatomy and Dendrochronology, Lund University, Sweden, is gratefully acknowledged for taking the photographs used in Fig. 14d and e. We thank Richard Waller for a highly constructive review that significantly improved the manuscript. We also thank an anonymous reviewer and the scientific editor, Chris Stokes, for useful comments.

Table 1

Drumlin no.	Length (m)	Width (m)	Height (m)	Elongation ratio
1	430	115	12	3.7
2	470	130	10	3.6
3	240	100	13	2.4
4	580	120	8	4.8
5	210	110	8	1.9
6	210	90	8	2.3
7	150	110	8	1.4
8	120	40	3	3
9	160	50	3	3.2
10	280	60	4	4.7
11	220	50	3	4.4

Figures

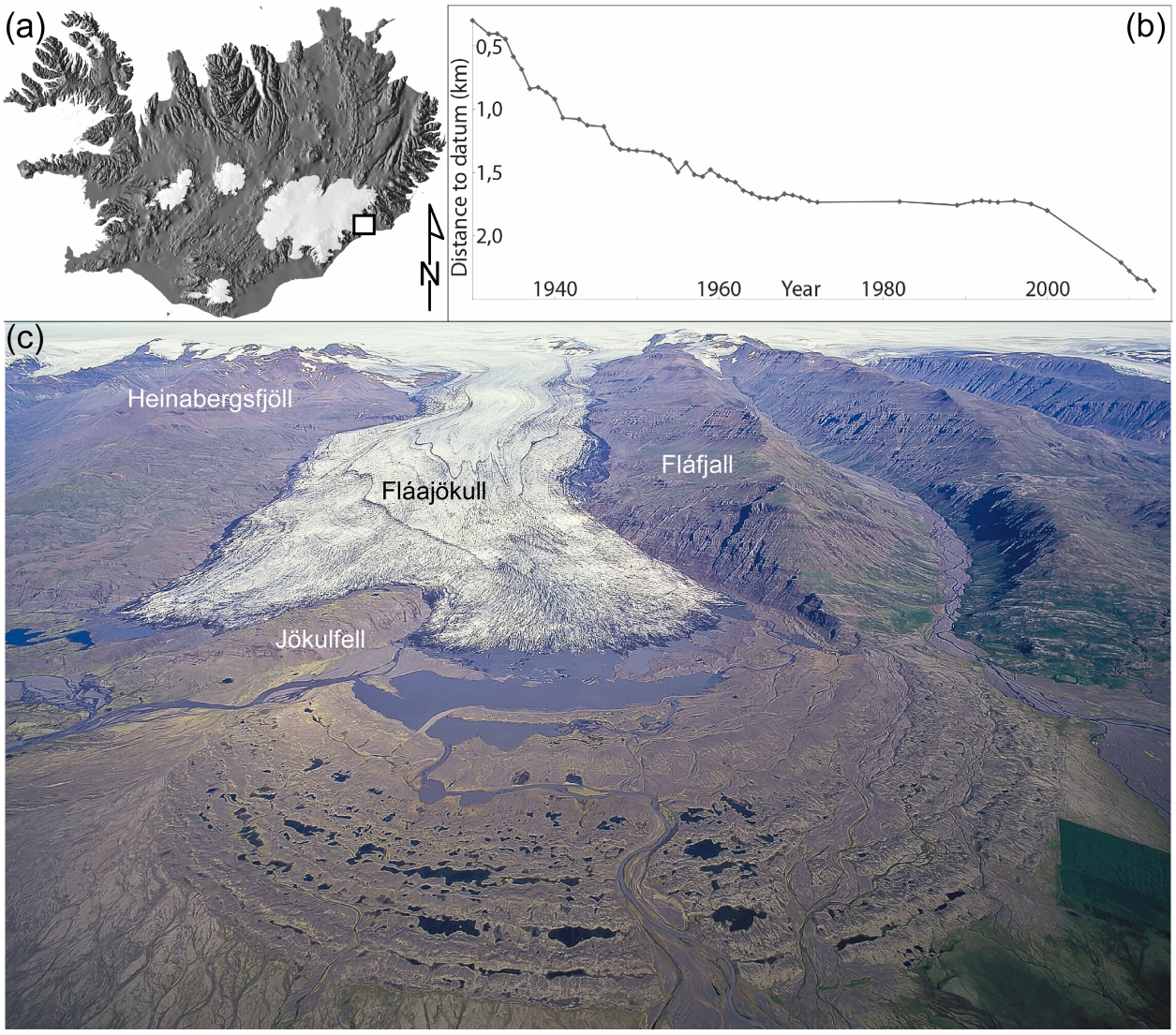

Figure 1. (a) Location of Fláajökull (square) at the south-eastern margin of the Vatnajökull ice cap. (b) Variations of the glacier snout since 1930 (data from the Icelandic Glaciological Society at spordakost.jorfi.is). Note the still-stand and minor re-advance from 1966-1995. (c) A view of Fláajökull and its forefield from the south–east in 2007. Photo courtesy of Snævarr Guðmundsson.

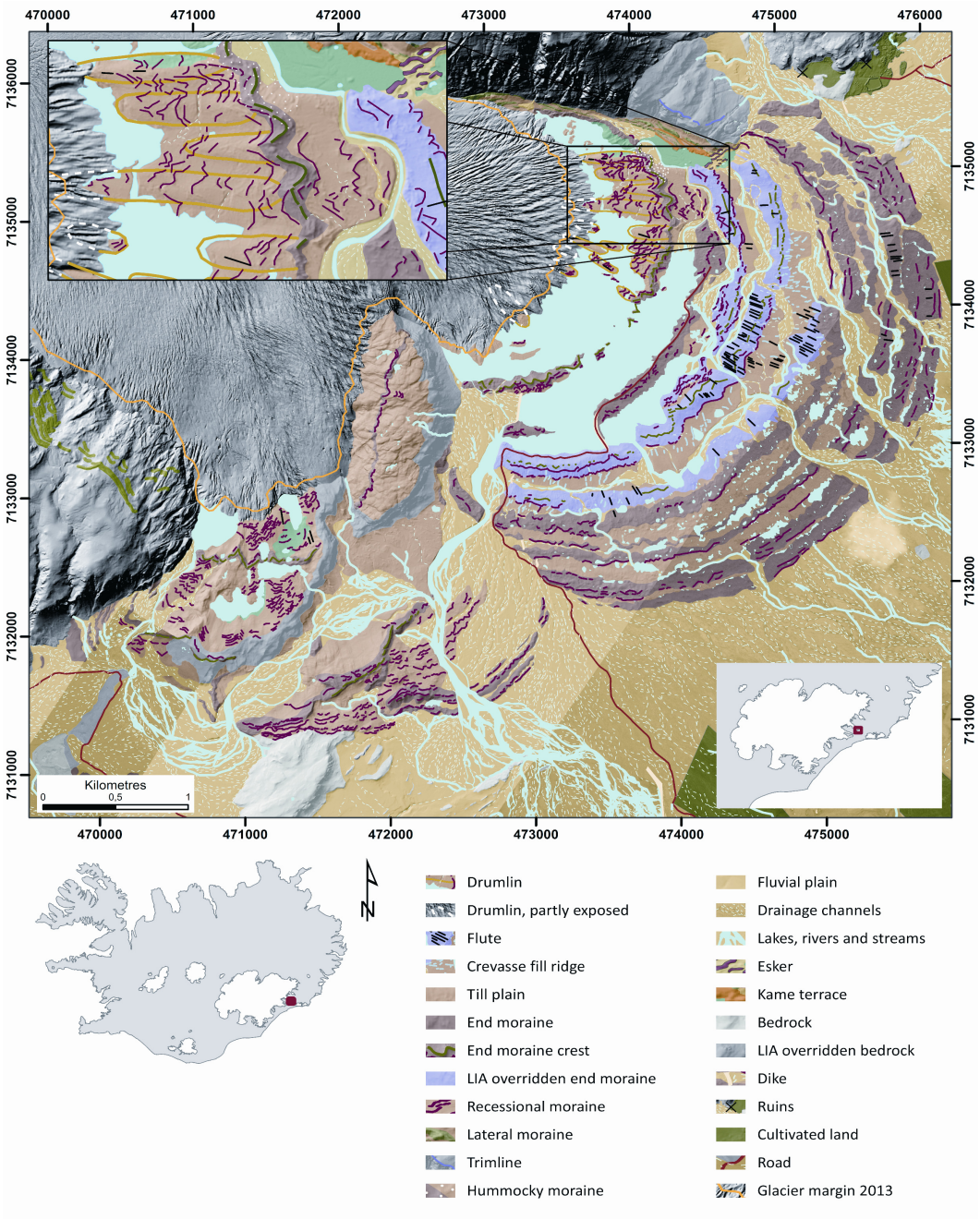

Figure 2. Geomorphological map of the Fláajökull forefield. The map is based on aerial photographs recorded in 1989 and LiDAR data from 2010. Map projection and datum: UTM 28N, WGS 84. Scale 1:32,000 on large map and 1:13,000 on insert map.

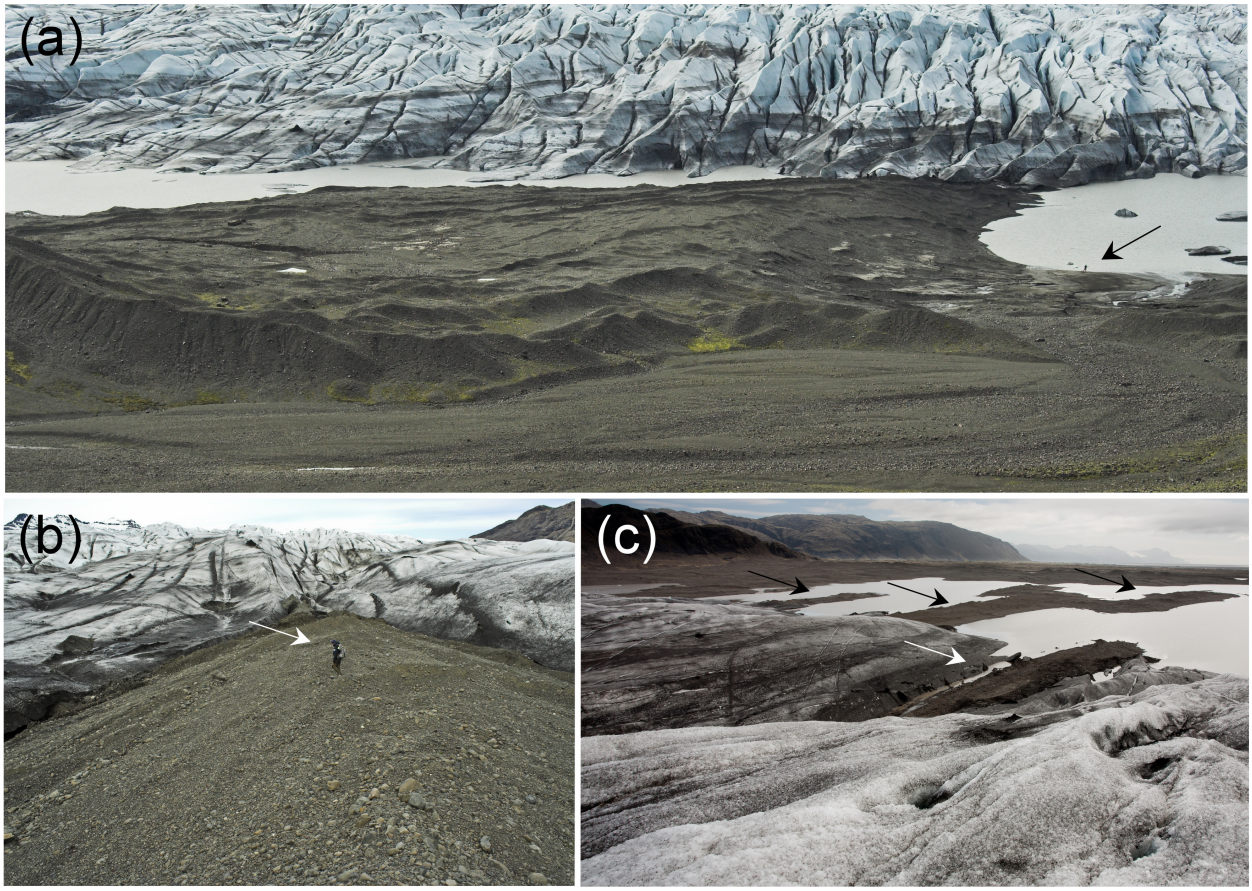

Figure 3. (a) A prominent drumlin in the northernmost part of the forefield, with recessional moraines on top. The 1995 end moraine can be seen in the foreground. Note a person for scale (arrowed). (b) A view of a sharp-crested drumlin in 2011. Note a person for scale (arrowed). (c) View from the glacier towards north-east showing partly exposed drumlin (white arrow), and few other drumlins further away (black arrows) in 2012.

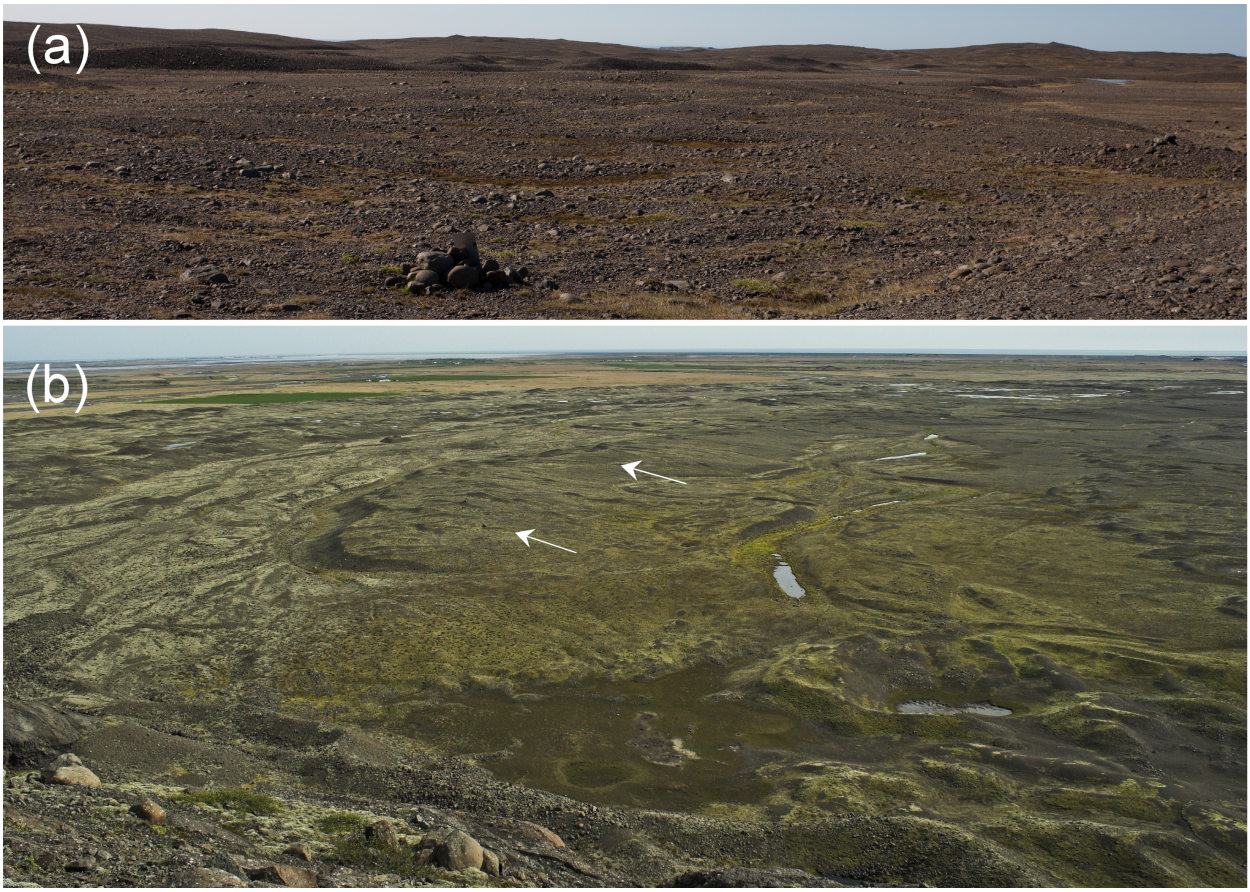

Figure 4. (a) An overridden end moraine in the central forefield. Ice flow was away from the viewer. (b) The same overridden end moraine seen from above indicated with white arrows. The distal part of the moraine has been subject to glaciofluvial erosion. Ice flow was from right to left.

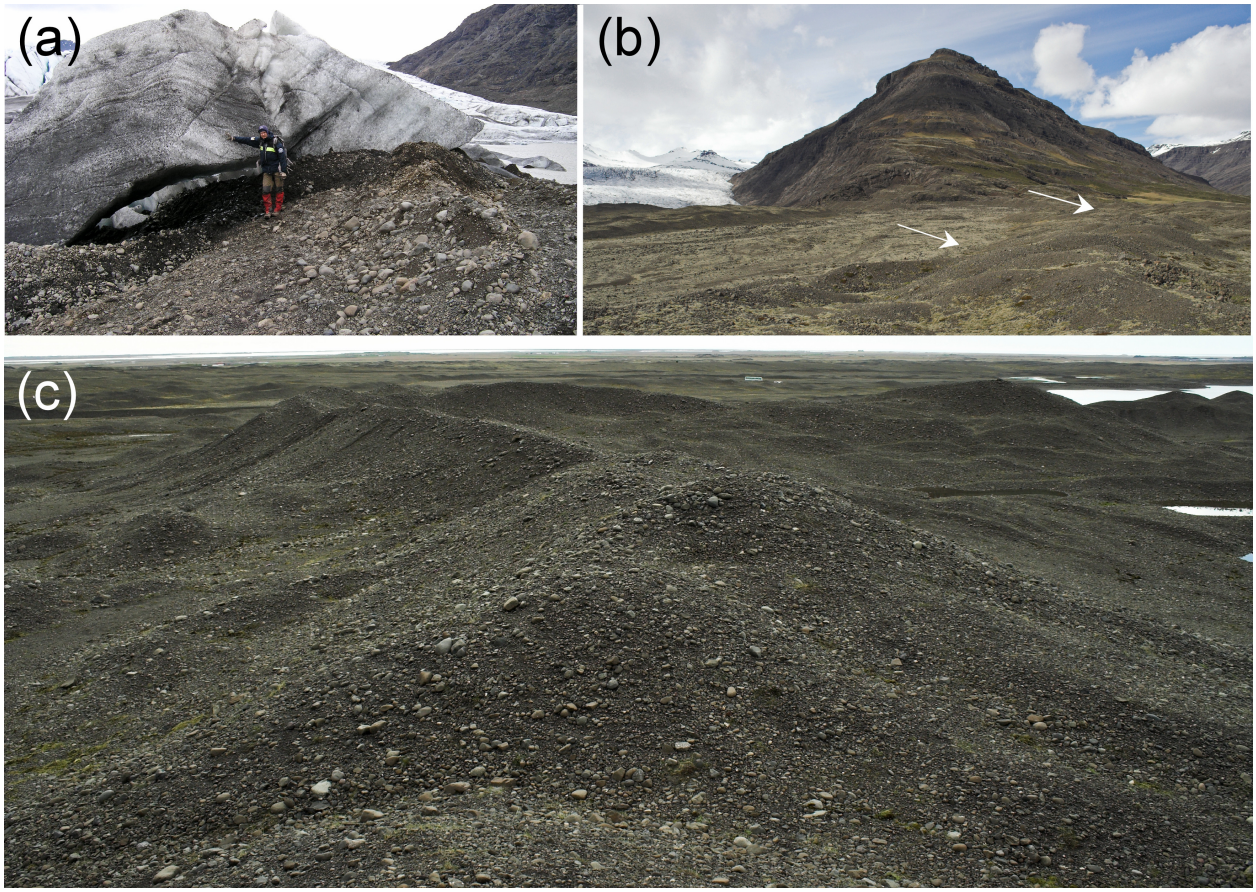

Figure 5. (a) A recessional moraine forming at the ice front in the spring of 2010. Person for scale. (b) An old end moraine in the forefield of Fláajökull (arrowed). The width of the moraine is approximately 30 m. (c) View to the West along the crest of the 1995 end moraine. Note the sawtooth shape of the moraine. Ice flow was from right to left.

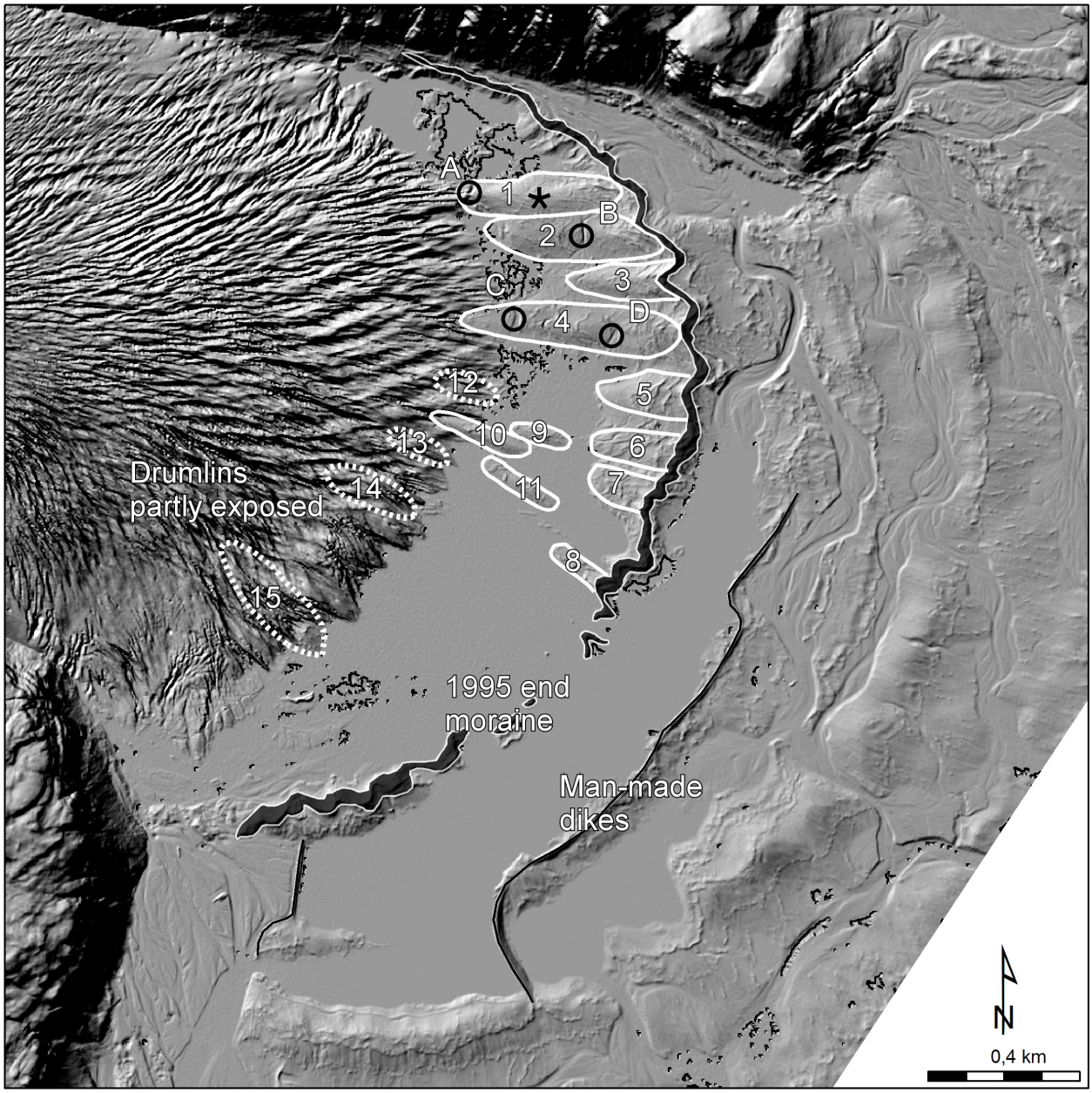

Figure 6. A LiDAR hillshade model from 2010 showing the ice margin and the drumlins (numbered 1-15). Sections A, B, C and D are marked with black circles. Fully exposed drumlins are shown with white outlines, partly exposed drumlins, which were mapped on a 2014 satellite image, with dashed white outlines. The 1995 end moraine is black with white outlines. Man-made levees and dikes are marked with black lines. The asterisk marks the location of the birch logs found in the surface deposits at drumlin 1.

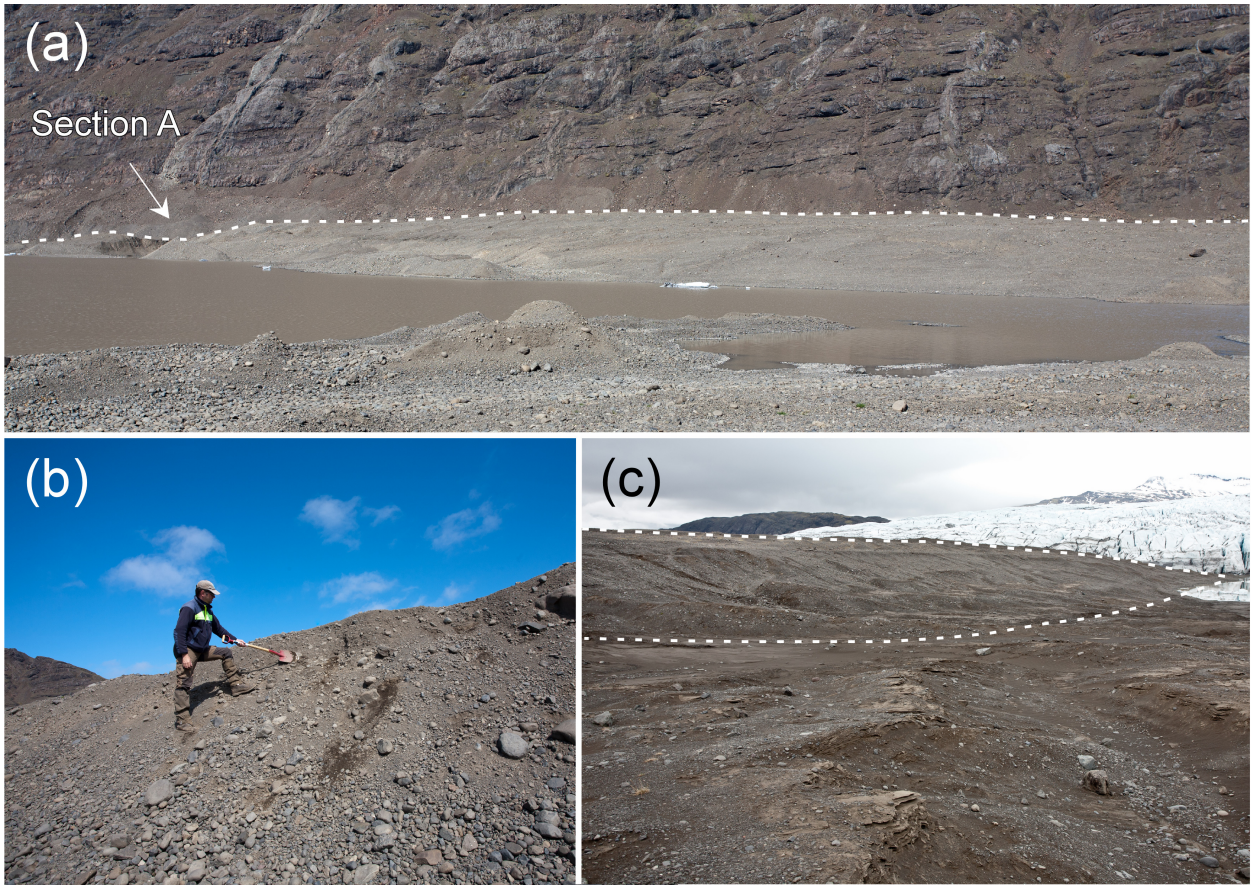

Figure 7. (a) A view from the South toward the northernmost drumlin, location of section A is indicated. (b) The top of section A. The spade is pointed at the lower boundary of the top till. (c) The northernmost drumlin in the field, view from East. Section A (not visible) is located in the far end of the drumlin. The drumlin is about 13 m high.

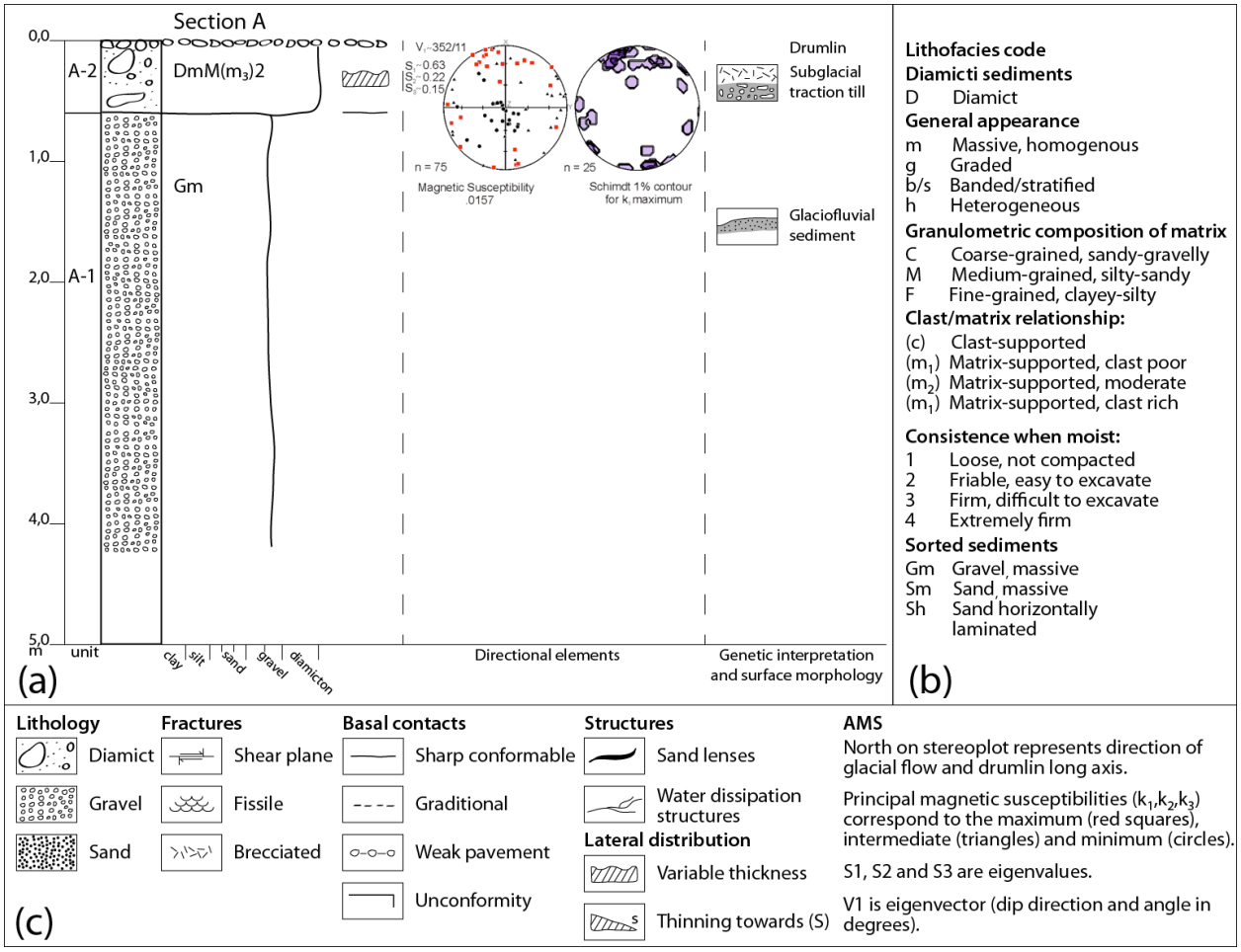

Figure 8. (a) Sedimentological log from section A. (b-c) Explanations of lithofacies codes and symbols used in this and other logs in Figs 10, 11, and 13.

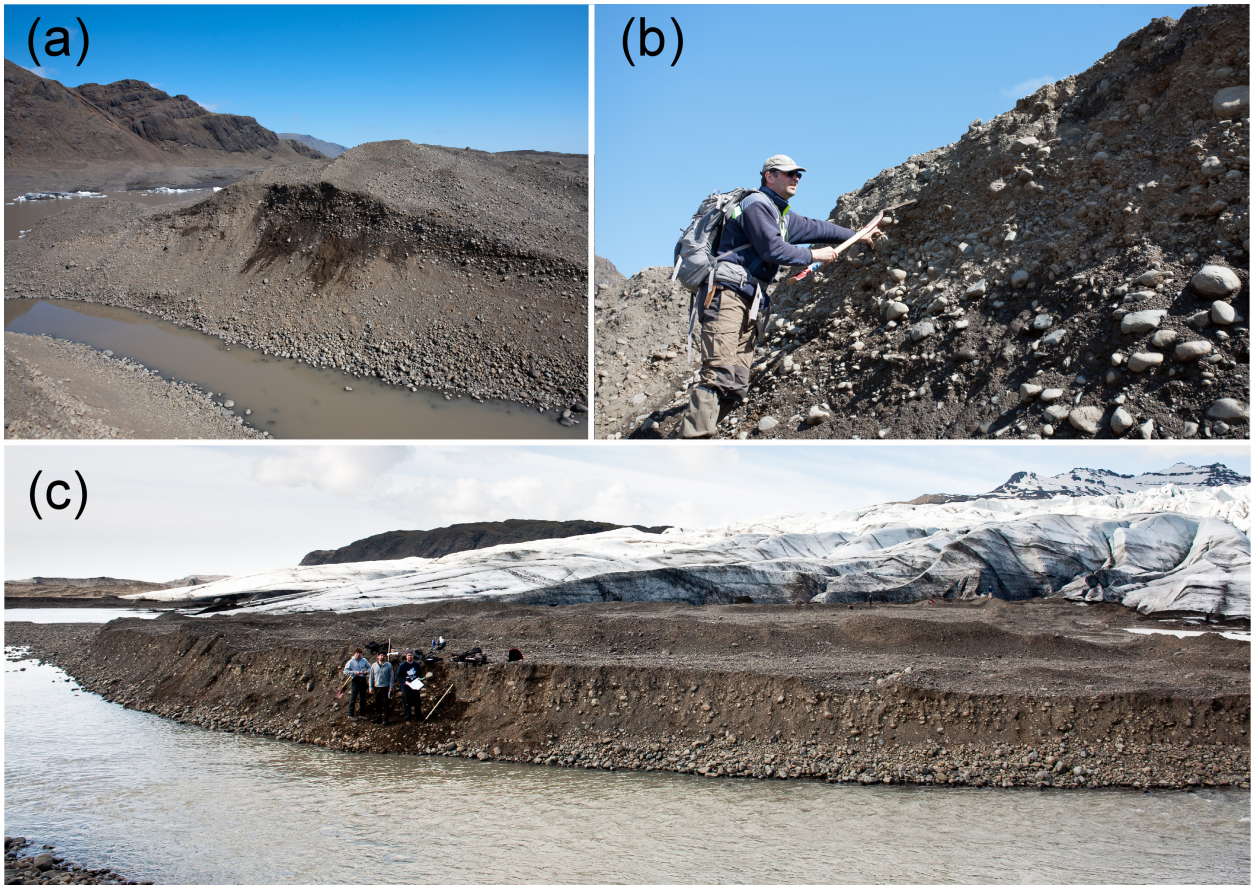

Figure 9. (a) An overview of section B looking away from the glacier. The section is about 8 m high. (b) Section B, the spade is pointed at the contact between units B-1 and B-2. (c) An overview of section C.

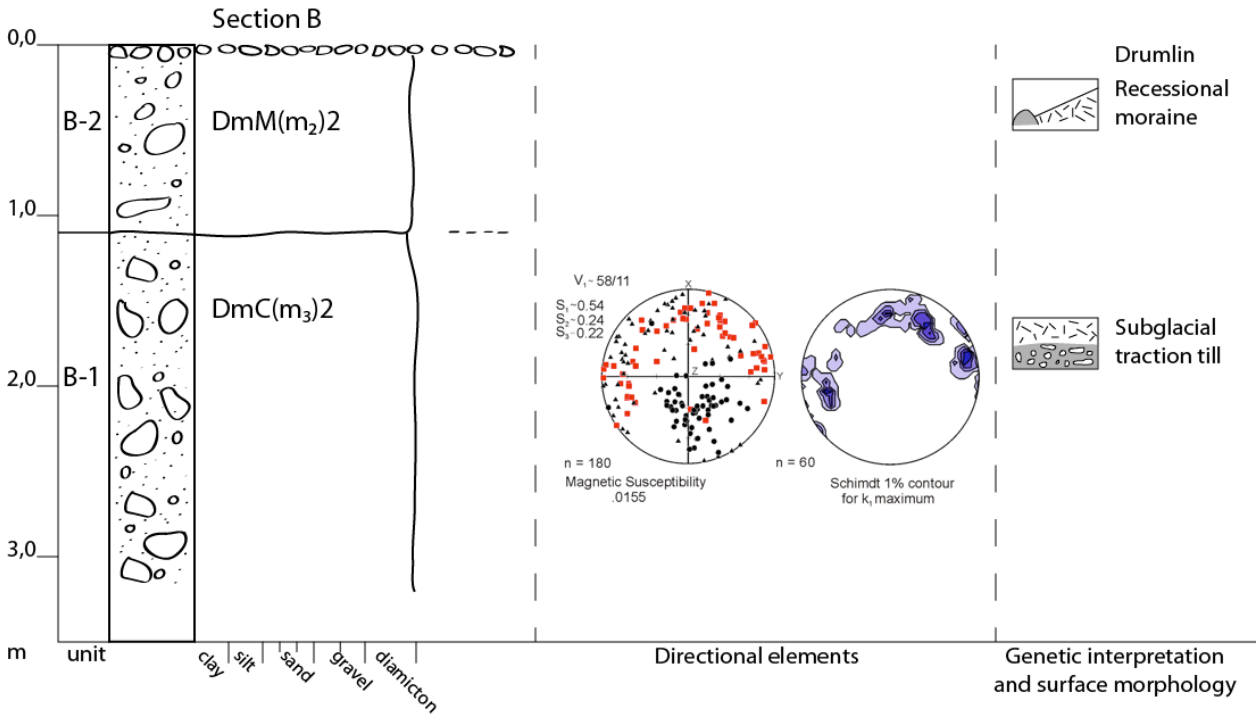

Figure 10. Sedimentological log from section B. Explanations of symbols and lithofacies codes can be seen in Fig. 8.

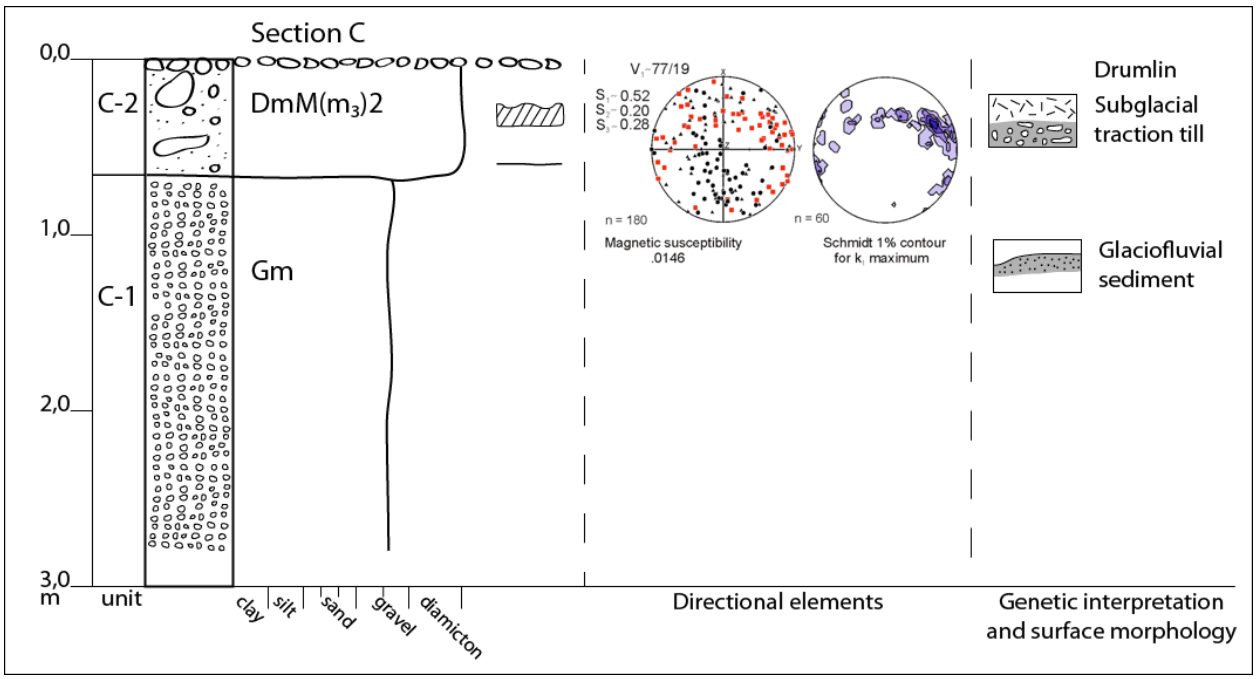

Figure 11. Sedimentological log from section C. Explanations of symbols and lithofacies codes can be seen in Fig. 8.

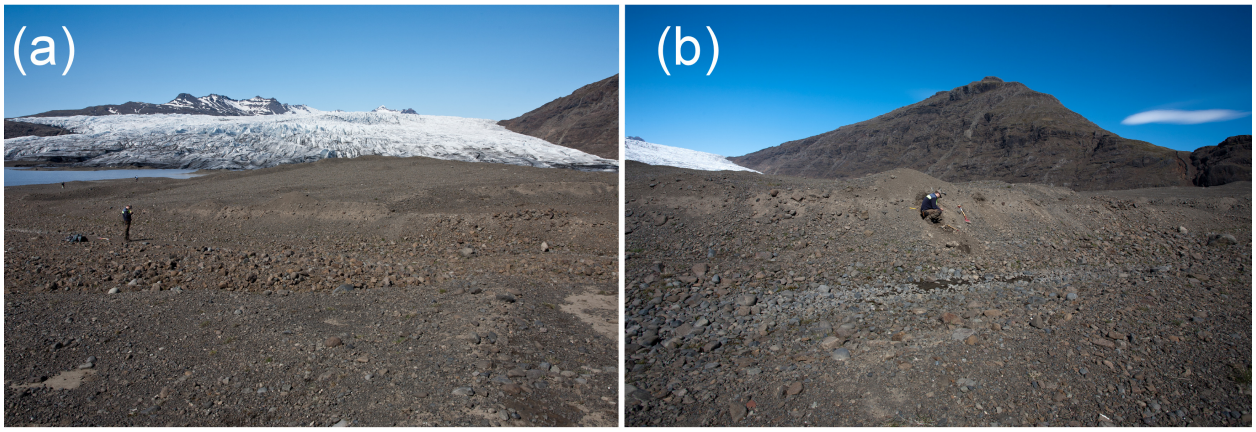

Figure 12. (a) Overview of section D. The view is towards the glacier along the long axis of the drumlin. Person for scale by the section. (b) An overview of section D along the channel in which it occurs. Person for scale.

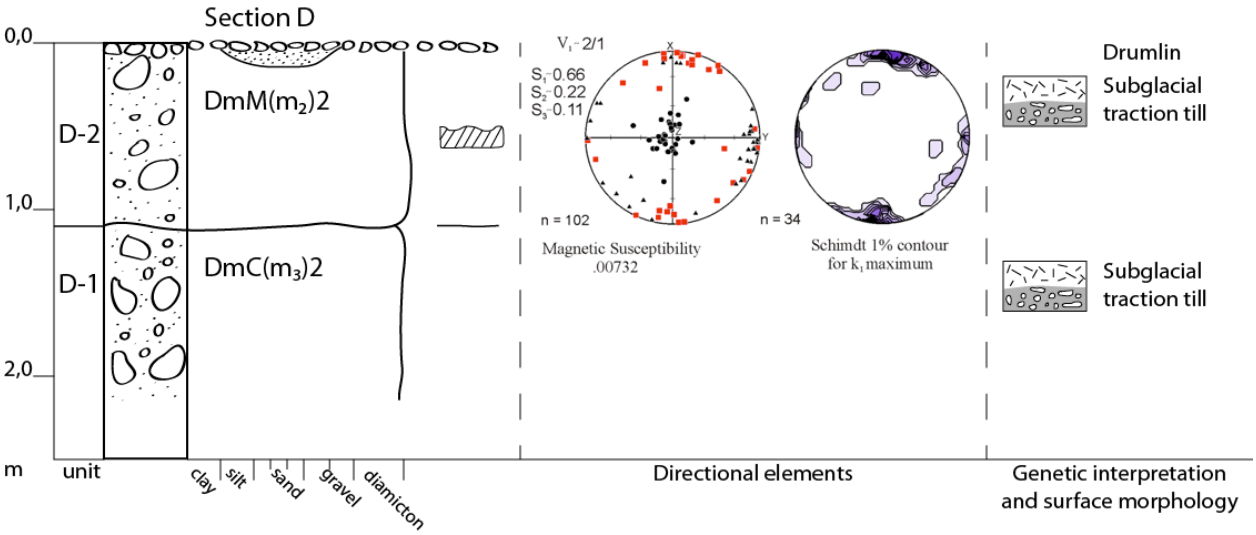

Figure 13. Sedimentological log from section D. Explanations of symbols and lithofacies codes can be seen in Fig. 8.

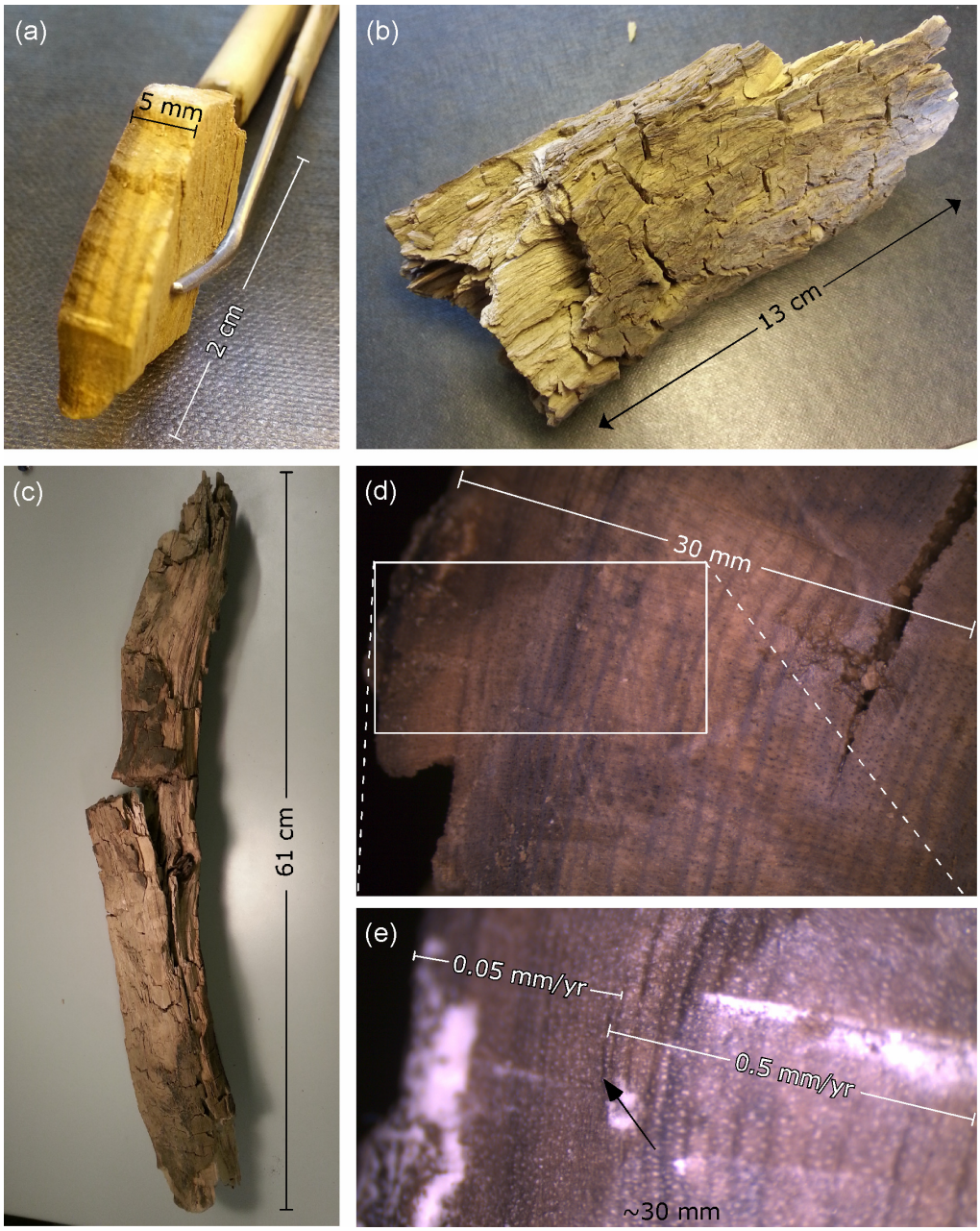

Figure 14. (a) Sample LuS 10801 dated to 2310-2055 cal. yr BP. The sample is the outermost part of a tree that was 20-30 cm in diameter, as indicated by the curvature of the sample. The width of the tree rings indicates relatively warm growing conditions and high growth rates. A pair of tweezers for scale. (b) Sample LuS 10802 dated to 2155-1990 cal. yr BP. Dendrochronological analysis indicates a live-span of 25-40 years and low growth rates (dense tree-rings). (c) Sample IS000. This sample was not dated but analysed for dendrochronology. (d) And (e) Close-ups showing the tree-rings of sample IS000 with the growth rates indicated. The arrow points at the sharp boundary between higher and lower growth rates, which probably indicates an abrupt change in climate and growing conditions.

References

Aðalgeirsdóttir, G., Guðmundsson, S., Björnsson, H., Pálsson, F., Jóhannesson, T., Hannesdóttir, H., Sigurdsson, S., Berthier, E., 2011. Modelling the 20th and 21st century evolution of Hoffellsjökull glacier, SE-Vatnajökull, Iceland. *The Cryosphere,* **5**, 961-975 (doi:10.5194/tc-5-961-2011).

Alden, W.C., 1911. Radiation in glacial flow as a factor in drumlin formation. Geological Society of America, v. 22, 733-734.

Baltrūnas, V., Waller, R.I., Kazakauskas,V., Paškauskas, S., Katinas, V., 2014. A comparative case study of subglacial bedforms in northern Lithuania and south-eastern Iceland. v. 27, 75-92 (doi: 10.5200/baltica.2014.27.18).

Aðalgeirsdóttir, G., Guðmundsson, S., Björnsson, H., Pálsson, F., Jóhannesson, T., Hannesdóttir, H., Sigurdsson, S., Berthier, E., 2011. Modelling the 20th and 21st century evolution of Hoffellsjökull glacier, SE-Vatnajökull, Iceland. The Cryosphere*,* v. 5, 961-975 (doi:10.5194/tc-5-961-2011).

Alden, W.C., 1911. Radiation in glacial flow as a factor in drumlin formation. Geological Society of America, v. 22, 733-734.

Benn, D.I., Evans, D.J., 2006. Subglacial megafloods: outrageous hypothesis or just outrageous. Glacier Science and Environmental Change. Blackwell, London, 42-46.

Björnsson, H., 2009. Jöklar á Íslandi. Forlagið, Reykjavik.

Björnsson, H., Pálsson, F., 2008. Icelandic glaciers. Jökull, v. 58, 365-386.

Boulton, G., 1987. A theory of drumlin formation by subglacial sediment deformation, n: Menzies, J. and Rose, J. (eds.), Drumlin Symposium, A.A. Balkema, Rotterdam.

Briner, J.P., 2007. Supporting evidence from the New York drumlin field that elongate subglacial bedforms indicate fast ice flow. Boreas, v. 36, 143-147 (doi: 10.1111/j.1502-3885.2007.tb01188.x).

Burki, V., Larsen, E., Fredin, O., Margreth, A., 2009. The formation of sawtooth moraine ridges in Bødalen, western Norway. Geomorphology*,* v. 105, 182-192 (doi: 10.1016/j.geomorph.2008.06.016).

Clark, C.D., Hughes, A.L.C., Greenwood, S.L., Spagnolo, M. N.g., FSL 2009. Size and shape characteristics of drumlins, derived from a large sample, and associated scaling laws. Quaternary Science Reviews, v. 28, 677-692 (doi: 10.1016/j.quascirev.2008.08.035).

Evans, D., Benn, D., (2004) A practical guide to the study of glacial sediments. Hodder Education, London.

Evans, D.J.A., Ewertowski, M.,Orthon, C., 2015. Fláajökull (north lobe), Iceland: active temperate piedmont lobe glacial landsystem, Journal of Maps, 1-13 (doi: 10.1080/17445647.2015.1073185).

Evans, D.J., Lemmen, D.S., Rea, B.R., 1999. Glacial landsystems of the southwest Laurentide Ice Sheet: modern Icelandic analogues. Journal of Quaternary Science, v. 14, 673-691 (doi: 10.1002/(SICI)1099-1417(199912)14:7<673::AID-JQS467>3.0.CO;2-#).

Evans, D.J.A., Phillips, E.R., Hiemstra, J.F., Auton, C.A., 2006. Subglacial till: Formation, sedimentary characteristics and classification. Earth-Science Reviwes, v. 78, 115-176 (doi: 10.1016/j.earscirev.2006.04.001).

Evans, D.J.A.,Twigg, D.R., 2002. The active temperate glacial landsystem: a model based on Breiðamerkurjökull and Fjallsjökull, Iceland. Quaternary Science Reviews, v. 21, 2143-2177 (doi: 10.1016/S0277-3791(02)00019-7).

Geirsdóttir, Á., Miller, G.H., Axford, Y., Ólafsdóttir, S., 2009. Holocene and latest Pleistocene climate and glacier fluctuations in Iceland. Quaternary Science Reviews, v. 28, 2107-2118 (doi: 10.1016/j.quascirev.2009.03.013).

Hannesdóttir, H., Björnsson, H., Pálsson, F., Aðalgeirsdóttir, G., Guðmundsson, S., 2014. Variations of southeast Vatnajökull ice cap (Iceland) 1650–1900 and reconstruction of the glacier surface geometry at the Little Ice Age maximum. Geografiska Annaler: Series A, Physical Geography, 1-28 (doi: 10.1111/geoa.12064).

Hart, J.K., 1995. Recent drumlins, flutes and lineations at Vestari-Hagafellsjökull, Iceland. Journal of Glaciology, v. 41, 596-606.

Hart, J.K., 1999. Identifying fast ice flow from landform assemblages in the geological record: a discussion. Annals of Glaciology, v. 28, 59-66 (doi: 10.3189/172756499781821887).

Haselton, G.M., 1966. Glacial geology of Muir Inlet, southeast Alaska. Ohio State University Institute of Polar Studies Report 18.

Jelínek, V., Kropáček, R.V., 1978. Statistical processing of anisotropy of magnetic susceptibility measured on groups of specimens. Studia geophysica et geodaetica**,** v. 22, 50-62 (doi: 10.1007/BF01613632).

Jóhannesson, T., Björnsson, H., Magnússon, E., Guðmundsson, S., Pálsson, F., Sigurðsson, O., Thorsteinsson, T., Berthier, E., 2013. Ice-volume changes, bias estimation of mass-balance measurements and changes in subglacial lakes derived by lidar mapping of the surface of Icelandic glaciers. Annals of Glaciology, v. 54, 63-74 (doi: 10.3189/2013AoG63A422).

Johnson, M.D., Schomacker, A., Benediktsson, Í.Ö., Geiger, A.J., Ferguson, A., Ingólfsson, Ó., 2010. Active drumlin field revealed at the margin of Múlajökull, Iceland: A surge-type glacier. Geology, v. 38, 943-946 (doi: 10.1130/G31371.1).

Jónsson, S.A., Schomacker, A., Benediktsson, Í.Ö., Ingólfsson, Ó., Johnson, M.D., 2014. The drumlin field and the geomorphology of the Múlajökull surge-type glacier, central Iceland. Geomorphology, v. 207, 213-220 (doi: 10.1016/j.geomorph.2013.11.007).

Kerr, M., Eyles, N., 2007. Origin of drumlins on the floor of Lake Ontario and in upper New York State. Sedimentary Geology, v. 193, 7-20 (doi: 10.1016/j.sedgeo.2005.11.025).

Kjær, K.H., Krüger, J., van der Meer, J.J.M., 2003. What causes till thickness to change over distance? Answers from Mýrdalsjökull, Iceland. Quaternary Science Reviews, v. 22, 1687-1700 (doi: 10.1016/S0277-3791(03)00162-8).

Krüger, J., 1987. Relationship of drumlin shape and distribution to drumlin stratigraphy and glacial history, Mýrdalsjökull, Iceland. In: Menzies, J. and Rose, J. (eds.), Drumlin Symposium, 257-266. A.A. Balkema, Rotterdam.

Krüger, J., 1994. Glacial processes, sediments, landforms, and stratigraphy in the terminus region of Mýrdalsjökull, Iceland. Folia Geographica Danica v. 21, 1-233.

Krüger, J., 1995. Origin, chronology and climatological significance of annual-moraine ridges at Mýrdalsjökull, Iceland. The Holocene, v. 5, 420-427 (doi: 10.1177/095968369500500404).

Krüger, J., Kjær, K.H., 1999. A data chart for field description and genetic interpretation of glacial diamicts and associated sedimentswith examples from Greenland, Iceland, and Denmark. Boreas, v. 28, 386-402 (doi: 10.1111/j.1502-3885.1999.tb00228.x).

Krüger, J., Thomsen, H.H., 1984.. Morphology, stratigraphy, and genesis of small drumlins in front of the glacier Mýrdalsjökull, South Iceland. Journal of Glaciology, v. 30, 94-105.

Maclachlan, J.C., Eyles, C.H., 2013. Quantitative geomorphological analysis of drumlins in the Peterborough drumlin field, Ontario, Canada. Geografiska Annaler: Series A, Physical Geography, v. 95, 125-144 (doi: 10.1111/geoa.12005).

Mark, D.M., 1973., Analysis of axial orientation data, including till fabrics. Geological Society of America Bulletin, v. 84, 1369-1374 (doi: 10.1130/0016

7606(1973)84<1369:AOAODI>2.0.CO;2).

Menzies, J., 1979. A review of the literature on the formation and location of drumlins. Earth-Science Reviews, v. 14, 315-359 (doi: 10.1016/0012-8252(79)90093-X).

Pálsson, F., Björnsson, H., 2000.Vatnsrennsli undan eystri hluta Fláajökuls. Raunvísindastofnun Háskólans.

Patterson, C.J., Hooke, R.L., 1995. Physical environment of drumlin formation. Journal of Glaciology, v. 41, 30-38.

Piotrowski, J.A., Larsen, N.K., Junge, F.W., 2004. Reflections of soft glacial beds as a mosaic of deformating and stable spots. Quaternary Science Reviews, v. 23, 993-1000 (doi: 10.1016/j.quascirev.2004.01.006).

Rabassa, J., 1987. Drumlins and drumlinoid forms in northern James Ross Island, Antarctic Peninsula, in: Menzies, J. (Ed.), Drumlin symposium: Rotterdam, Balkema.

Reimer, R.J., Bard, B., Bayliss, A., Beck, J.W., Blackwell, P.G., Ramsey, C.B., Buck, C.E., Cheng, H., Edwards, R.L., Friedrich, M., Grootes, P.M., Guilderson, T.P., Haflidason, H., Hajdas, I., Hatté, C., Heaton, T.J., Hoffmann, D.L., Hogg, A.G., Hughen, K.A., Kaiser, K.F., Kromer, B., Manning, S.W., Niu, M., Reimer, R.W., Richards, D.A., Scott, E.M., Southon, J.R., Staff, R.A., Turney, C.S.M., van der Plicht, J., 2013. Intcal13 and marine13 radiocarbon age calibration curves 0-50,000 years cal BP. Radiocarbon, v. 55, 1869-1887 (doi: 10.2458/azu_js_rc.55.16947).

Schomacker, A., Benediktsson, Í.Ö., Ingólfsson, Ó., Friis, B., Korsgaard, N.J., Kjær, K.H., Keiding, J.K., 2012. Late Holocene and modern glacier changes in the marginal zone of Sólheimajökull, South Iceland. Jökull, v. 62, 111-130.

Schomacker, A., Krüger, J., Kjær, K.H., 2006. Ice-cored drumlins at the surge-type glacier Brúarjökull, Iceland: a transitional-state landform. Journal of Quaternary Science, v. 21, 85-93 (doi: 10.1002/jqs.949).

Sigurdsson, O., 2003. Jöklabreytingar 1930–1960, 1960–1990 og 2001–2002. Jökull, v. 53, 55–62.

Sigurdsson, O., 2013. Jöklabreytingar 1930-1970, 1970-1995, 1995-2011 og 2011-2012. Jökull, v. 63, 118-122.

Slomka, J.M., Eyles, C.H., 2015. Architectural-landsystem analysis of a modern glacial landscape, Sólheimajökull, southern Iceland. Geomorphology, v. 230, 75-97 (doi: 10.1016/j.geomorph.2014.11.006).

Stokes, C.R., Clark, C.D., 2001. Palaeo-ice streams. Quaternary Science Reviews, v. 20, 1437-1457 (doi: 10.1016/S0277-3791(01)00003-8).

Stokes, C.R., Clark, C.D., Lian, O.B., Tulaczyk, S., 2007. Ice stream sticky spots: a review of their identification and influence beneath contemporary and palaeo-ice streams. Earth-Science Reviews, v. 81, 217-249 (doi: 10.1016/j.earscirev.2007.01.002).

Striberger, J., Björck, S., Holmgren, S., Hamerlík, L., 2012. The sediments of Lake Lögurinn–A unique proxy record of Holocene glacial meltwater variability in eastern Iceland. Quaternary Science Reviews, v. 38, 76-88 (doi: 10.1016/j.quascirev.2012.02.001).

Thorarinsson, S., 1956. On variations of Svínafellsjökull, Skaftafellsjökull and Kvíárjökull. Jökull, v. 6, 1-15.

van der Meer J., 1983. A recent drumlin with fluted surface in the Swiss Alps, Evenson, EB, Schluchter, Ch. & Rabassa, J., Till and related deposits, Proceeding of the INQUA Symposia on the Genesis and Lithology of Quaternary Deposits/USA 1981/Argentina1982, 105-109.

Waller, R.I., van DijkT.A.G.P., Knudsen, Ó., 2008. Subglacial bedforms and conditions associated with the 1991 surge of Skeiðarárjökull, Iceland. Boreas, v. 37, 179-194 (doi: 10.1111/j.1502-3885.2007.00017.x).

CURRICULUM VITAE

William R. Jacobson, Jr.

EDUCATION

2009-2015	Ph.D., Geosciences, University of Wisconsin-Milwaukee
2002-2004	M.S., Physical Science, Emporia State University-Emporia, Kansas
1997-2002	B.S., Geology, University of Wisconsin-Oshkosh

WORK EXPERIENCE

2009-2014	*Teaching & Project Assistant*, Geosciences Department, University of Wisconsin-Milwaukee
2007-2009	*Exploration Geologist*, Duluth Metals Limited, Ely, Minnesota
2006-2007	*Exploration Geologist*, Victoria Gold Corp., Reno, Nevada
2002-2004	*Graduate Teaching Assistant*, Earth Science Department, Department of Physical Sciences, Emporia State University, Kansas

RESEARCH Directed field studies in Iceland, Nevada, North Dakota, & Minnesota. Research areas include glaciology, engineering geology, and geomorphology. My research focuses on laboratory experimentation using a rotary-shear device aimed at determining the microstructural properties of sheared basal till. Additionally, I have an expertise with applying magnetic fabric methods on polar ice and measuring ice grain fabrics. These methods are used to understand deformational processes within glaciers and ice sheets.

DISSERTATION PROJECT

"Field and Laboratory Study of the Fláajökull Glacier, Iceland"

MASTER'S DEGREE PROJECT

"Glaciotectonic Analysis of Devils Lake, North Dakota"

AWARDS /RECOGNITION

2011 Geological Society of America Graduate Student Research Grant, $3050

2009-2104 University of Wisconsin-Milwaukee Geosciences Graduate Teaching & Project Assistantships

2010 UWM Chancellor Scholarship Award, $1200

"Best Thesis of the Year Nomination 2005", Emporia State University (ESU)

CONFERENCE PRESENTATIONS

Jacobson, Jr., W.R., Hooyer, T.S., Amato, J.A., & Joynt, E.K., 2014. Magnetic Fabrics and their Application to Basal Crevasse Fills, Flàajökull, Iceland, (Poster presentation): *American Geophysical Union*, Fall Meeting 2014, Abstract # C33A-0356.

Jacobson, Jr., W.R., & Hooyer, T.S., 2011. Laboratory study of fabric development in shearing till: Exploring the importance of effective normal stress and shearing rate, (Poster presentation): Minneapolis, Minnesota, *Annual Geological Society of America Meeting*.

Jacobson, W.R., (2005) Glaciotectonic Structural Analysis of Devils Lake, North Dakota, (Oral presentation): University of Wisconsin-Oshkosh, *Geology Speaker Session*.

Jacobson, W.R., Aber, J.S., & Salley, S.W., 2004. Glaciotectonic Structural Analysis of Devils Lake, North Dakota, (Oral presentation): Denver, Colorado, *Annual Geological Society of America Meeting.*

PUBLICATIONS/BOOK CREDITS

Jacobson, Jr., W.R., & Hooyer, T.S., 2015. Laboratory study of fabric development in shearing till: The importance of effective pressure and shearing rate. *Geomorphology*, v. 250, 249-257.

Jacobson, Jr., W.R., 2015. Application of magnetic fabrics in dirty ice: a new fabric proxy for ice cores? *Journal of Glaciology*, submitted.

Jacobson, Jr., W.R., & Hooyer, T.S., 2011. Laboratory study of fabric development in shearing till: Exploring the importance of effective normal stress and shearing rate: *Geological Society of America Abstract with Programs*, v. 42, no. 5, p. 453.

Jónsson S.A., Benediktsson Í. Ö., Ingólfsson Ó., Schomacker A., Bergsdóttir H.L., Jacobson Jr., W.R., & Linderson, H., 2015. Submarginal drumlin formation at Fláajökull, an active temperate glacier in southeast Iceland. *Annual of Glaciology*, Accepted.

Jacobson, Jr., W.R., 2007. Contributed to Chapter 3: Kinematic Analysis and Chapter 4: Hill-hole pair of the publication *Glaciotectonism* by Aber, J.S., & Ber, A., Series Editor: Jaap J.M. van der Meer, Elsevier, 246 p.

Jacobson, W.R., Aber, J.S., & Salley, S.W., 2004. Glaciotectonic Structural Analysis of Devils Lake, North Dakota*: Geological Society of America Abstracts with Programs*, v. 36, no. 5, p. 248.

PROFESSIONAL AFFILIATIONS

American Geophysical Union
Geological Society of America
International Glaciological Society